UNIVERSITÉ DE SHERBROOKE
Faculté de génie
Département de génie Mécanique

Caractérisation du transport fluidique et thermique dans les mousses métalliques capillaires en cuivre

Characterization of fluid and thermal transport in copper metal foam wicks

Thèse de doctorat
Spécialité: génie mécanique

Mahmood Reza Salim Shirazy

Jury: Luc. G. Fréchette (directeur)
Marcel Lacroix
Raymond Panneton
Yoav Peles

Sherbrooke (Québec) Canada Mai 2013

Your file Votre référence
ISBN: 978-0-499-00424-6

Our file Notre référence
ISBN: 978-0-499-00424-6

À ma famille et mon adorable épouse,

Sanaz

RÉSUME

La gestion thermique de l'électronique constitue un défi majeur dans la fabrication et la production de circuits électroniques de haute performance. La hausse constante de la puissance de calcul nécessite toujours plus d'énergie, qui doit ensuite être évacuée (sous forme de chaleur) de l'ordinateur. Parmi les diverses solutions, les caloducs sont proposés comme un moyen de transférer et finalement éliminer ce surplus de chaleur. La partie principale d'un caloduc typique est la mèche qui fournit un milieu pour la capillarité et l'évaporation à l'interface liquide-vapeur. Différents matériaux sont proposés comme mèche pour un caloduc et parmi eux, les mousses métalliques récemment inventées (Metafoam) présentent une performance très significative et des limites de transport élevées par rapport aux matériaux concurrents. Par une approche essentiellement expérimentale, les propriétés capillaires, de mouillage et d'évaporation des mousses métalliques en cuivre avec des porosités différentes ont été étudiées. Une étude approfondie de caractérisation de surface est effectuée sur les mousses afin d'identifier le rôle de la mouillabilité de la surface sur la performance capillaire. On a démontré pour la première fois que la perte d'hydrophilicité des matériaux poreux en cuivre exposé à l'air est provoquée par l'adsorption de composés organiques volatils et non par l'oxydation du cuivre. Il est également déduit que la raison pour la haute limite de transport des mousses par rapport à d'autres matériaux est leur microstructure unique qui a deux niveaux de porosité. Cette microstructure bi-poreuse fournit des chemins pour le transport de liquide avec de faibles pertes de charge tandis que les plus petits pores favorisent l'évaporation par couches minces et produit une haute pression capillaire. La perméabilité et le rayon effectif des pores, deux paramètres clés qui définissent la capacité de pompage, sont mesurés expérimentalement par le taux de montée de liquide. Il est constaté que le taux d'évaporation dans un matériau poreux est plus faible pendant la montée du liquide par rapport au même matériau mais complètement saturé de liquide (régime stationnaire). Cela permettra d'ignorer l'évaporation naturelle dans cette méthode et d'utiliser des modèles simplifiés pour mesurer le rayon effectif des pores et la perméabilité. Le rôle de la récession du ménisque dans le pompage capillaire et dans le taux d'évaporation est caractérisé pour la première fois et un modèle est proposé pour mesurer le rayon de pore effectif de matériaux poreux dans des conditions d'opération. Il est montré que le rayon de pore effectif peut diminuer jusqu'à 50% à cause de l'évaporation forcée. D'une perspective plus générale, les différentes expériences ont démontré qu'il existe un couplage entre la capillarité et l'évaporation. Ce couplage est établi par la variation de forme du ménisque qui affecte à la fois la capillarité et l'évaporation. Cette thèse contribue donc à faire la lumière sur la capillarité, l'évaporation et leur interdépendance dans les mèches capillaires pour les appareils biphasiques de gestion thermique.

Mots clés : capillarité, évaporation, mousse métallique, caloducs, mèche

ABSTRACT

Thermal management of electronics has become a major challenge in manufacturing and production of high performance electronic chips. Constant rise of computation power requires higher amount of energy and subsequently this energy (in the form of heat) should be transferred out of the computer. Among other solutions, heat pipes are proposed as a means to transfer and eventually remove this excess heat. The main part of a typical heat pipe is the wick which provides a medium for transport of capillary driven flow and evaporation at the vapor-liquid interface. Different materials are proposed as wick for a heat pipe and among them, recently invented Bi-porous metal foams exhibit a very significant performance improve, i.e. high transport limit in comparison with competing materials. By a mainly experimental approach, capillary, wetting and evaporation properties of copper metal foams with different porosities have been investigated. An in depth surface characterization study is done on the foams to identify the role of surface wettability on the capillary performance. It is found for the first time that the hydrophilicity loss of the copper based porous materials when exposed to air is caused by the adsorption of volatile organic compounds and not by copper oxidation. It is also inferred that the reason for high transport limit of the foams compared with other materials is their unique microstructure which has two levels of porosity. This biporous microstructure provides paths for liquid transport with low pressure drop while the smaller pores provide for thin film evaporation and produce high capillary pressure. Permeability and effective pore radius, as two key parameters defining the pumping capacity, are measured experimentally by the rate of rise method. It is also found that the evaporation rate of a rising liquid in a porous material is lower compared with that of the same material while saturated with stationary liquid. This will allow ignoring natural evaporation in the rate of rise method and using simplified models to capture permeability and effective pore radius. The role of meniscus recession in capillary pumping and evaporation rate is characterized for the first time and a model is proposed to measure the effective pore radius of porous materials in operating conditions. It is shown that the effective pore radius can decrease up to 50% due to forced evaporation. In a more general perspective, through different experiments, it is shown that there is a coupling between capillarity and evaporation. This coupling is established through variation in meniscus shape which will affect both capillarity and evaporation. The findings of this thesis will shed light on the capillarity, evaporation and their interconnected nature in the capillary wicks in two phase thermal management devices.

Key words: capillarity, evaporation, metal foam, heat pipe, wick

ACKNOWLEDEGMENTS

I am not sure how many students have the chance and opportunity in their graduate studies to work with people so influential that can profoundly change their attitude and understanding of the whole life. Fortunately I was one of them and I really wish more students have this opportunity like me! The most influential person throughout this life changing journey is my supervisor Professor Luc, G. Fréchette. I would like to extend my gratitude to him, for teaching me not only the scientific concepts and the true meaning of research but also for his human, ethical, patient and flexible attitude towards me. In my case, these qualities could mean the success or failure of my PhD. Luc acted as a true mentor and friend during my PhD and working with him was certainly a turning point in my life. I would also like to thank the committee members, Professors Marcel Lacroix, Raymond Panneton and Yoav Peles for their valuable inputs and support regarding this research.

This work could not have been completed without the help, guidance and support of Dominic Pilon, founder of Metafoam Technologies Inc. Sébastien Labbé and others in Metafoam Technologies fabricated and provided the copper metal foam samples, whom I would like to thank. I would like to thank Professor Hugues Menard for insightful discussions on the surface chemistry of the foams. I am also grateful to Sonia Blais, Irène Kelsey and Stéphane Gutierrez of the centre de caractérisation des matériaux (CCM) for their invaluable help in the characterization of the foam samples. Sonia Fortin at the department of mechanical engineering helped much by ordering and buying the many pieces required for different test setups used in this project. The help of Sébastien Rioux, Claude Dugual and Réal Dubuc in the fabrication of the different components of the test setups is highly appreciated. I would also like to thank Alexandre Landry-Blais and Louis-Simon Malo who during their internship in the Micros research group contributed to different activities related to this project.

My sincerest thanks go to all my past and present lab mates and friends, especially Selin, Mokhtar and Étienne. And last but not least, I wish to thank my parents, my brothers, and my wife Sanaz for their unconditional love and support during this journey.

TABLE OF CONTENTS

LIST OF FIGURES

LIST OF TABLES

1 INTRODUCTION

1.1 Need for thermal management

Since the first days of invention of the computing machines in the 1940s, extracting and taking out the excess heat has been an important issue [13]. The invention of transistors, integrated circuits (IC) and complentry metal-oxide semiconductor (CMOS) circuit technology to replace high heat dissipating bipolar circuit technology have not been able to satisfy the need for thermal management. Two main factors leading to ever increasing rate of heat dissipation are denser packaging and higher performance circuits, which are required steadily by the market. In 2005, the size of the market of cooling technologies for thermal management of PC's and telecom equipment was estimated to be $4.1 billion per year with the prospect of $4.8 billion [3]. At present, the heat fluxes in high end server applications are around 100W/cm^2 (around 10 times that of a household clothes iron[50]) and it is predicted to increase up to 500-1000W/cm^2 (near the ballistic re-entry heat flux of 1000W/cm^2) for the next generation of chips and electronic devices [38]. Currently the next objective for cooling technologies research is 300W/cm^2 [3].

Traditionally, air cooling using extended heat sinks (fins) and fans has been the main cooling method for electronics, but this technology is at its limits and cannot satisfy the increasing rate of dissipated heat in new chips [91]. Different technologies have been proposed to address the need for an effective cooling technology. Jet impingement, Spray cooling, single and two phase flow in micro-channels, micro-pumps, miniature flat heat pipes, transient phase change energy storage systems, thermoelectric coolers and piezoelectric fans have been studies and compared in some review papers[3, 25, 38, 85]. Among them, jet impingement [38] and boiling in micro-channels [3] have demonstrated the highest performance. However, they both face important challenges before being employed in commercial systems and currently much research is being done to better understand their physics. But as a short and medium term solution, heat pipes seem very appealing.

1.2 Heat pipes

Heat pipes are passive micro-fluidic devices that are usually designed for the thermal management of electronic components [44] . They have also been used in other applications such as the cooling of fuel cells. A heat pipe is a cavity of small thickness filled with a two-phase working fluid (Figure 1.1). A heat input source is located at one end and a heat sink is placed at the other end of the cavity with the other parts being insulated. Evaporation and condensation occur at the location of the heat source and the heat sink, respectively. The liquid returns from the condenser to the evaporator by capillary action through a porous wick structure made of meshes, sintered powder wicks or metal foams (the focus of this thesis). The vapor travels back to the condenser through the vapor core. Since the latent heat of vaporization is high, heat pipes are able to transfer high heat fluxes with small temperature gradients. Therefore, the overall thermal resistance of the device is significantly lower than a solid material of the same dimensions.

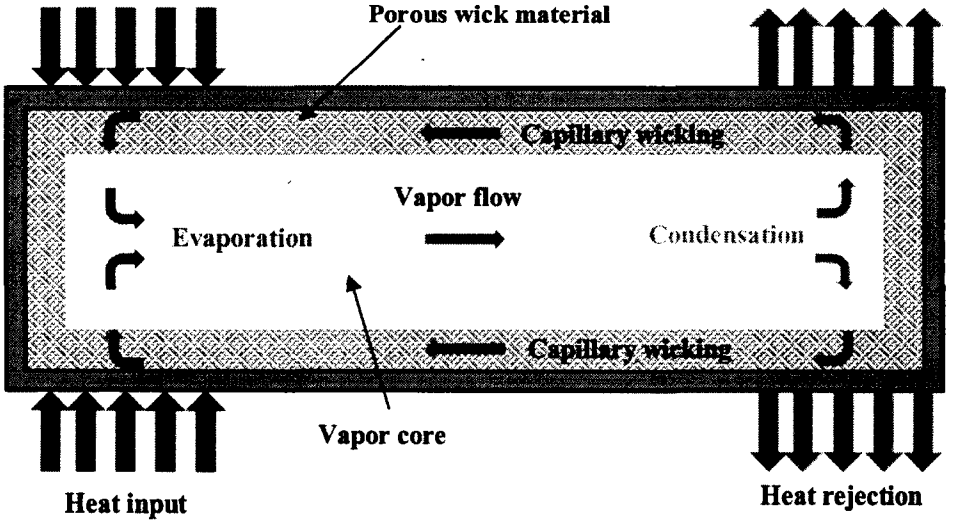

Figure 1.1 schematic drawing of an operating heat pipe

Heat pipe and heat spreaders (vapor chambers) have the same operating principle and the only difference is the location of evaporator and condenser. In heat pipes, evaporator and condenser zones are located at the extremities of the device and the objective is to transport heat with

minimum temperature drop through a relatively long distance. In heat spreaders, heat is transported from a small high density heat source to a large area heat sink. The heat transport distance in vapor chambers is smaller compared with heat pipes but occurs in two dimensions.

1.3 Copper metal foam wicks

The heat pipe design and type of wicking material are the main factors that influence the heat transfer capability of a heat pipe [79]. Open cell metal foams are proposed as wicks in heat pipes. Metal foams are a good candidate for two phase and single phase chip cooling because they are thermally conductive, light weight, have a high surface area and high porosity, and can provide good thermal contact between the heat pipe wall and the wick. Novel open cell metallic foams can be fabricated with a wide range of porosities, material composition, and microstructures, through a patented process initially developed at the National Research Council, NRC-IMI (Bourcherville, Qc, Canada) and now being manufactured and commercialized by the Canadian company Metafoam Technologies (Figure 1.2). In preliminary tests, these foams exhibit higher operating limits in a heat pipe than common wicks, suggesting high cooling rates for microelectronics applications [57].

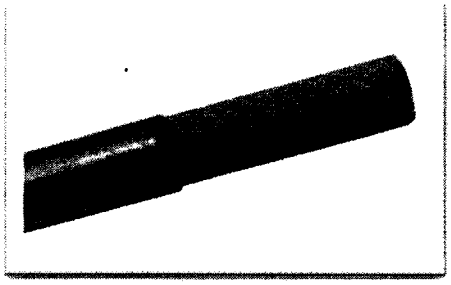

Figure 1.2 Metafoam copper foam wicks for heat pipe and vapor chambers[58]

The novel aspect of Metafoam copper foams is their particular microstructure compared with other metal foams and sintered copper powder (Figure 1.3). As it can be seen in Figure 1.3d, the foams have a spherical cluster structure (SCS) with the approximate diameter of 10-50μm and unlike other types of metal foams (Figure 1.3a and b), no ligaments as well as no polygon shape cells can be observed. Distinct pores are hard to find and several through holes are observed.

Instead, the small particles join each other to form clusters that are separated from each other to provide a large-scale porosity in the foam (Figure 1.3d). Within the clusters, we can observe a second smaller scale porosity formed between the particles. The microstructure formed by the small particles and their clusters is therefore characterized by two pore scales and a high surface area. This is very different than other porous wicks which are characterized by having only one level of porosity. This biporous microstructure may lead to interesting capillary and evaporation properties that has not yet been fully characterized.

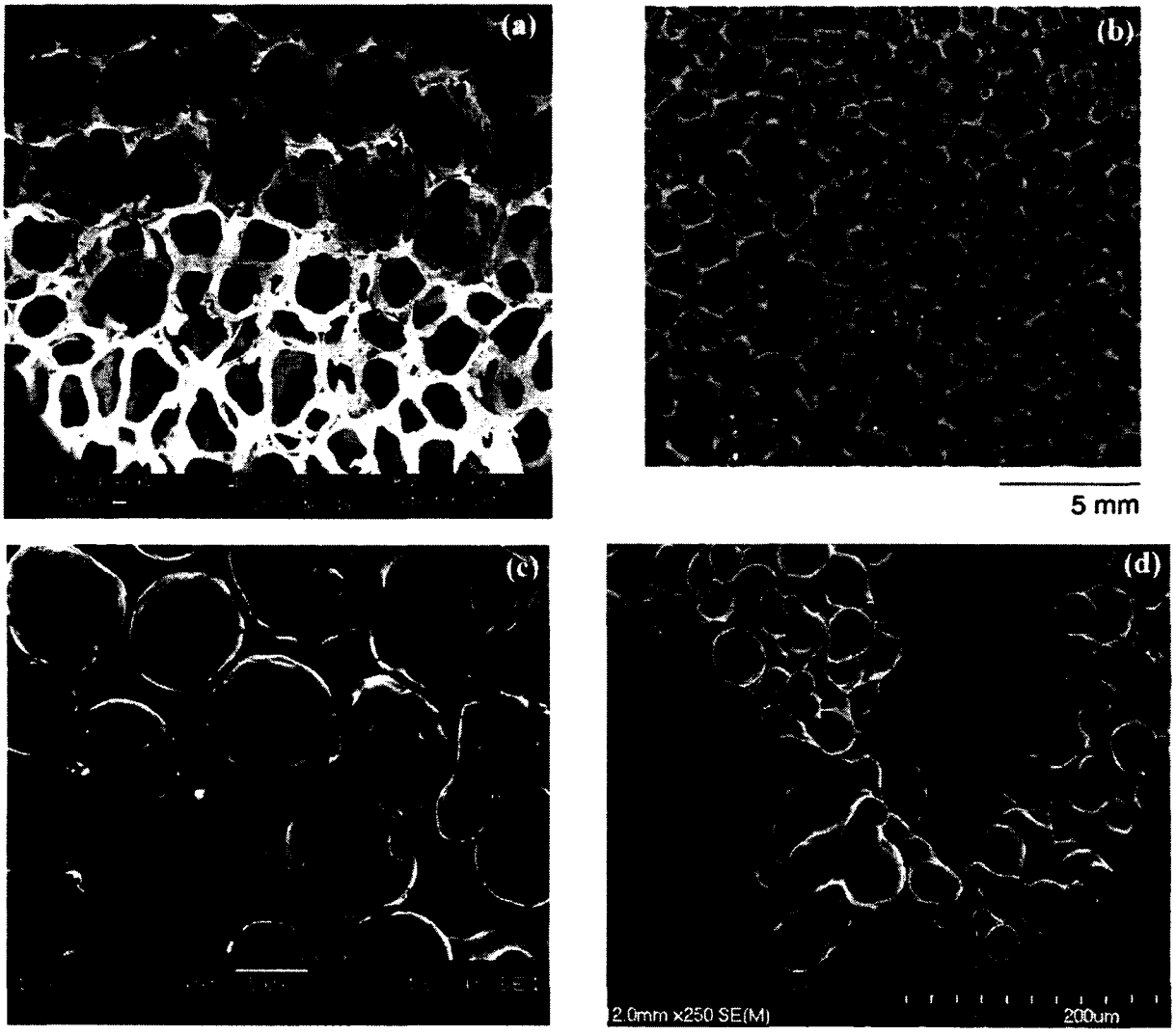

Figure 1.3 Different microstructures of (a) steel alloy metal foam [93] (b) copper metal foam [94] (c) sintered copper powder [76] (d) Metafoam copper metal foams

This project is therefore aimed at studying the mechanism of capillary driven heat and mass transfer for heat pipes employing these novel copper metal foams as wicks. The general objective in this research will be to understand the mechanism of capillarity and evaporation in wicks made of Metafoam materials and characterize the corresponding parameters. In a more general perspective, through different experiments, it will be shown that there is an interconnection between capillarity and evaporation. This interconnection is established through variations in the meniscus shape which will affect both capillarity and evaporation. This will be discussed in more detail in the future sections.

1.4 Thesis outline

This thesis includes 7 chapters. State of art is presented in chapter 2, which also includes the overall scientific notions required to understand the subsequent chapters. The project definition and objectives are also discussed in this chapter. Chapter 3 covers the results of a parametric study on the heat pipe transport limits, showing that capillary limit is the dominant limit in the performance of heat pipes using metal foams. Therefore, capillarity and evaporation as well as wettability are identified as the main transport mechanisms involved in this limit and studied in more detail in the subsequent chapters. Wettability mechanism in copper metal foams is studied in chapter 4 and a wetting and surface characterization study is presented. The reason for hydrophilicity loss of copper metal foams is explained for the first time and the double scale porosity of the foams is shown through microscopic observations. As the next step, Capillary properties of different porosity copper foams are investigated in chapter 5. The effect of evaporation on capillarity is also investigated in this chapter. Evaporation rate is varied by using partially saturated ambient and attaching external walls. Effect of natural evaporation on the rate of capillary liquid rise is evaluated and it is shown that evaporation rate from a capillary driven rising liquid in a porous media is less than that of a saturated sample. This shows a clear effect of capillarity on the evaporation occurring in a porous material. The interconnection between capillarity and evaporation can best be seen in chapter 6 and appendix 1.Chapter 6 presents the experimental setup to study the evaporation properties of foams. In this chapter, the meniscus recession effect due to forced evaporation on the capillary pumping is investigated. It will be seen

that higher evaporation rate will lead to meniscus recession which in turn will increase capillary pumping rate. The impact of meniscus recession on the wick thermal resistance is also evaluated and studied in appendix 1. Lastly, chapter 7 provides conclusions and suggestions for future work.

2 STATE OF ART

From the practical point of view and in order to choose a heat pipe or heat spreader for electronics thermal management, the device's performance should be evaluated by suitable metrics. These metrics are high heat and mass transport limits and low overall thermal resistance. The former deals mostly with capillarity whereas the latter includes mainly evaporation. These two metrics and their underlying phenomena (capillarity and evaporation) will be discussed in more detail in the following sections and the link between the present research effort and these metrics will be established.

2.1 Heat pipe transport limits

Although heat pipes are very efficient cooling systems, they are subject to a number of classical heat transfer limitations [18]: continuum flow limit, frozen start-up limit, viscous limit, sonic limit, entrainment limit, capillary limit, condenser limit and boiling limit. These phenomena limit the maximum heat input that may be transported by a heat pipe; heat rates above these limit values result in failure. The failure in this case is the sudden temperature jump in the heat pipe which will lead to overheating of the target electronic device. Viscose limit, Sonic limit, entrainement limit, capillary limit and boiling limit will be discussed in detail chapter 3. In the small heta pipes and at very low operating temperatures , the vapor flow in the heat pipe may be in the free molecular or rarified condition which limits the heat transport and is called vapor continuum limit. Condenser limit happens if condenser section of a heat pipe is in such way that it cannot transfer the amount of heat that the heat pipe is designed for. In the frozne stratup limit, the vapor from the evaporator zone to the adiabatic or condenser section may freez. Among these limits, the capillary limit is more likely to occur in heat pipes used in electronics thermal management due to the typical working fluids and temperature ranges encountered in this application.

The capillary limit occurs when the capillary pressure produced by the porous wick is not enough to overcome the combined pressure drops due to viscous effects in the wick and vapor core,

phase-change mass transfer and gravity effects. If the capillary pumping of the wicking material is not sufficient to supply water to the evaporator, it will dry out. The heat pipe temperature at the heat source will then rise since evaporation is no longer extracting the heat. Wick properties such as permeability (K) and effective pore radius (r_{eff}) are critical in defining the capillary limit of heat pipes. Permeability (K) is a parameter that shows the ease of flow movement through the porous material and is dependent only on the microstructure properties of the porous material. Effective pore radius (r_{eff}) on the other hand is dependent both on microstructure properties (pore dimension) and liquid-solid wetting properties (contact angle θ). In other words, r_{eff} is the radius of a hypothetical pore, assuming a complete wetting between the pore wall and the liquid ($\theta = 0$). This can be seen through the following equations. The capillary pressure of a wicking material P_{cap} and its dependence on pore radius r_p and effective pore radius r_{eff} can be described as:

$$P_{cap} = \frac{2\sigma}{r_{eff}} \quad and \quad r_{eff} = \frac{r_p}{\cos\theta} \tag{2.1}$$

It can be seen that as the pore radius decreases, the capillary pressure increases. Furthermore, a strongly wetting liquid-solid system (lower $\cos\theta$) will also increase the capillary pressure. Therefore a lower effective pore radius (r_{eff}) will increase the capillary pressure and will provide more liquid supply to the evaporator. However, decreasing the r_{eff} will lead to decrease of the permeability (K). Darcy's law, which shows the liquid pressure drop for 1-D flow through a porous material, is [18]:

$$\frac{dP}{dx} = -\frac{\mu_l \dot{m}_l}{\rho_l A_w K} \tag{2.2}$$

This equation shows the inverse proportionality of the liquid pressure drop in a porous material to permeability K. Therefore, it can be seen that the capillary limit of a heat pipe is a function of a trade-off between permeability and effective pore radius. As will be shown in Chapter 3, the ratio of K/r_{eff} can be used as a metric to evaluate the capillary pumping of a porous wick. A higher

K/r_{eff} will lead to a higher capillary pumping and eventually a higher dryout heat flux. Therefore, a good knowledge of these parameters and a robust method to measure them is important.

Modeling of the operation and performance of heat pipes has received a lot of attention in two main categories: 1) the numeric or analytic simulation of steady state or transient operation of heat pipes, and 2) the transport limits (mainly capillary and boiling) and dry-out lengths. Numerous studies exist on simulations of flow and heat transfer inside heat pipes [78][80], transport limits, and dry-out lengths [44, 54, 80, 87]. By analyzing the literature, it can be generally seen that steady state and transient operation of heat pipes can be predicted fairly well. These simulations should include coupled heat transfer in the wall, wick and vapor core. However, the prerequisite of these simulations is having precise values for capillarity properties including wick properties of permeability (K) and effective pore radius (r_{eff}). Although there are several analytic models to predict permeability but these models are developed for wicking materials other than biporous metal foams which are the focus of the current work. Moreover, current understanding of effective pore radius and its dependence to evaporation is very limited and there is need for models to predict this parameter in the conditions occurring in a heat pipe. Knowledge of this parameter is also critical for predicting capillary limit and dryout which is the main operating limit in heat pipes for electronics thermal management.

There are numerous studies on the foams for thermal management of electronics by single phase forced convection using different coolants [6, 17, 41, 42, 92]. In terms of electronic cooling by liquid phase change, studies done on open cell foams are much less and can be divided into two categories: non-metallic (graphite) foams such as [15] and [47] and metal foams. In case of the metal foams, Phillips [56] performed an extensive study of the permeability, capillary pressures and evaporative performance of different porous materials from square mesh screen to metal foams and felts in order to evaluate their performance as wicks in heat pipes. Peterson et al. [24], Carbajal et al. [8, 55] and Queheillalt et al. [61] have studied transient response of a multifunctional structure numerically and experimentally respectively. This structure is composed of aluminum walls, a truncated square honeycomb (cruciform) core and nickel foam as a wick which is exposed to a non uniform localized heat flux. Rather than heat pipe, this

configuration can be considered as a heat spreader consisted of smaller cells that each can be assumed as a vapor chamber. Temperature range and distribution of the heat flux in this research is different than what is encountered in electronics cooling (more than 100C in this study). Therefore, the results may not be directly applicable for thermal management of electronics. Metafoam foams have been the subject of another study in which thermal conductivity, permeability and electrochemical properties were investigated [27, 59].

From the above literature analysis, it can be seen that no significant work including wettability, capillarity and evaporation and their interconnected dependence exists on the metal foam wicks in heat pipes for two phase electronics thermal management. Moreover, the novel biporous microstructure of Metafoam foams take the complexity involved in transport phenomena one step further and requires a thorough investigation. Therefore, as a first step, it is necessary to determine and identify the dominant transport limit for the copper metal foams in typical heat pipe geometry. Consequently, this is the focus of chapter 3. Later in chapter 5, capillary properties such as permeability and effective pore radius are studied in more detail.

2.1.1 Capillary and wetting properties of wicks

In capillary-driven systems, the driving potential for the working fluid circulation is provided by the difference in the curvature of the evaporating and condensing liquid-vapour interfaces. Consequently, determining the maximum pumping capacity, and the corresponding heat transfer performance, of these systems depends strongly on the accuracy of the prediction of the shapes of the evaporating and condensing interfaces. In the heat pipes, capillarity is the driving mechanism for transporting liquid form the condenser to the evaporator. As it was stated before, capillary pressure is a function of the pore radius r_p and θ. Where, θ the apparent contact angle, is dependent on the fluid-wick material pair used. The contact angle is a measure of the degree of wettability of the liquid on the wick structure, and it will be discussed in more detail in the following sections.

2.1.1.1 Capillarity

Capillarity can be defined as the study of the interfaces between the two immiscible liquids or a liquid and air [26]. Before attempting to define wettability, we need to define the contact angle (θ). It is the angle formed at the contact point between three phases (liquid, solid and gas) and is always measured from the solid/liquid interface towards the gas/liquid interface. It can be described as [26]:

$$\cos\theta = \frac{\sigma_{SG} - \sigma_{SL}}{\sigma_{GL}} \qquad 2.3$$

where the three coefficients σ are the surface tensions at the solid/gas (σ_{SG}), solid/liquid (σ_{SL}) and gas/liquid (σ_{GL}) interfaces, respectively. The angle θ is the liquid contact angle (CA) on the flat surface, otherwise known as the Young contact angle. A surface is called hydrophilic when the contact angle of water is $\theta < 90^{o}$, and hydrophobic when $\theta > 90^{o}$. When the CA of water is larger than 150°, it is called superhydrophobic and when the CA of water is almost 0°, it is called superhydrophilic [20].

Liquid motion in a capillary path can be achieved if the dry tube has a surface energy σ_{SG} greater than the surface energy σ_{SL} of the same path when wet. An impregnation parameter I can be defined by:

$$I = \sigma_{SG} - \sigma_{SL} \qquad 2.4$$

When I is positive, the system lowers its energy if a wet surface is substituted by a dry surface and the liquid rises in the capillary path. The liquid descents if I is negative. In fact, I is the nominator of the Young relation (Eqn 2.3) and a negative I leads to $\theta_Y > 90^{o}$, i.e. a hydrophobic surface. It can be concluded that a hydrophilic liquid-solid system is the necessary condition to transport the liquid via capillarity.

2.1.1.2 Wetting

Wetting is how the liquid deposited on a surface spreads out [26]. From the engineering point of view, capillarity explains the motion of a liquid in a suitable pore or capillary path while wetting describes the spreading of that liquid on a surface of the same material. In other words, capillarity deals with fluid dynamics while wetting deals with fluid statics.

Wetting stems from the surface tension and can be dived into two groups:

- Total wetting: when the liquid has a strong affinity for the solid
- Partial wetting for the opposite case

To distinguish these two categories, a parameter can be defined as spreading parameter *S*, which measures the difference between the surface energy (per unit area) of the substrate when dry and wet [26] :

$$S = [E_{substrate}]_{dry} - [E_{substrate}]_{wet} \qquad 2.5$$

or

$$S = \sigma_{SG} - (\sigma_{SL} + \sigma_{GL}) \qquad 2.6$$

- $S > 0$: Total wetting

If the parameter S is positive, the liquid spreads completely in order to lower its surface energy ($\theta = 0$).

- $S < 0$: Partial wetting

The drop does not spread but, instead, forms a sphere resting on the substrate with a contact angle θ.

It is also evident that θ can be defined only if the spreading parameter is negative. Young contact angle increases when the liquid is non-wetting.

As it was mentioned in section 2.1.1.1, the degree of wetting of a surface has a direct effect on the capillary characteristics of the capillary structures made from the same surface. According to the Young-Laplace equation, the capillary pressure produced on the surface of the porous wick, is directly proportional to the cosine of the contact angle. Therefore, increasing the wettability i.e., decreasing the contact angle and producing a hydrophilic surface can have a significant impact on the overall performance of a heat pipe. Studying the surface properties of the copper metal foams and their microstructure is the subject of Chapter 4.

2.2 Heat pipe thermal resistance

A heat pipe acts basically as a thermal resistance which will transfer a certain heat flux with a corresponding temperature difference between the evaporator and the condenser. In order to keep the electronics temperature in an acceptable range, this resistance should be minimized which will lead to a minimized temperature difference. A simplified representation of transport in heat pipes may be described by a thermal resistance network [18]. Due to much lower values of wick and vapor core axial resistances, they are usually ignored compared with other resistances and evaporator thermal resistance is considered to be the dominant resistance [54]. Therefore, to decrease the overall thermal resistance of the heat pipe, evaporator thermal resistance should be reduced.

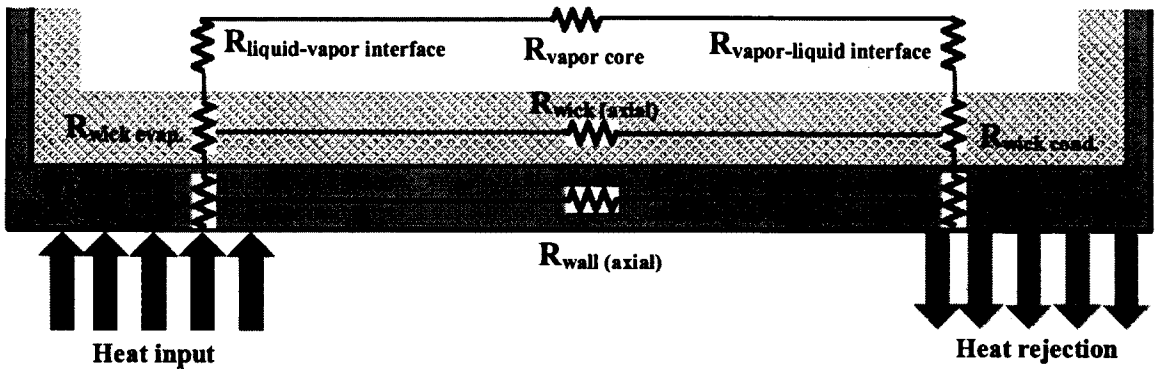

Figure 2.1 Simplified heat pipe thermal resistance network (only the lower half of the heat pipe

is depicted here)

During heat pipe operation, heat is conducted from the substrate through the saturated wick (Figure 2.2). Due to lower conductivity of the liquid, most of the heat is conducted through the wick structure to the wick surface. At the surface, heat transfer occurs mainly in the thin liquid film region of several microns thickness [49]. The liquid thickness in the thin film region is around 10 μm and it is responsible for up to 55% of the total meniscus mass transfer. This is caused mainly by the very low thermal resistance due to very thin liquid layer.

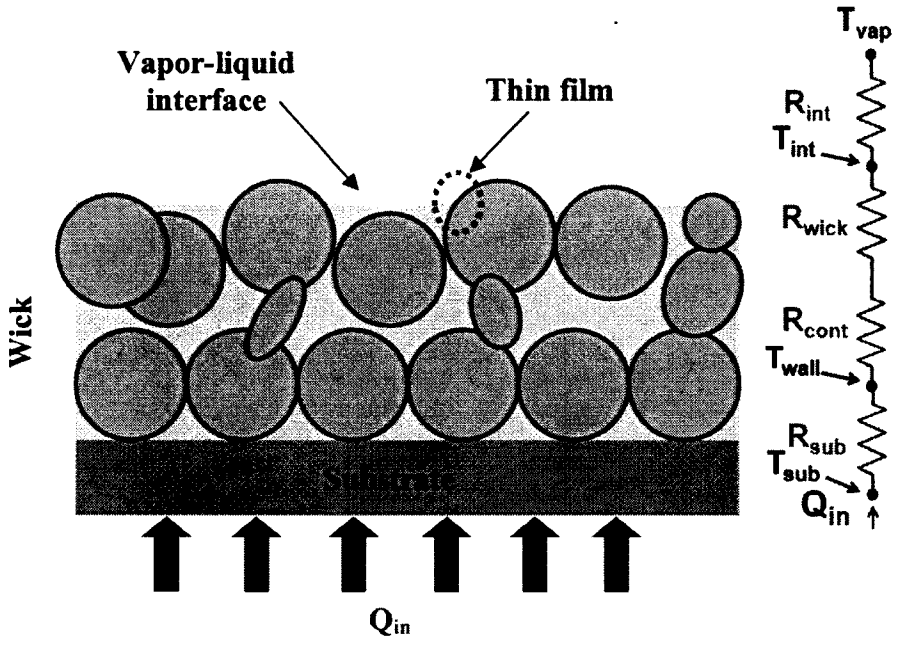

Figure 2.2 Schematic drawing of liquid saturated wick and its associated thermal resistance

The heat transfer at the surface depends on the thin film area, its thickness and also the effective conductivity of the saturated porous wick [30]. A wick with low evaporation resistance is characterized by a low thermal resistance of the saturated wick R_{wick} and the liquid-vapor interface R_{int}. However, it is shown that R_{int} is dominant only in the case of very thin wicks (~100 μm) [62]. Consequently, investigating mechanisms affecting wick thermal resistance across the wick thickness in the evaporator section such as meniscus recession is another focus of the current research which will be presented in chapter 6.

2.3 Project definition

The principal objective of the current work is to understand the heat and fluid transport in copper metal foams as heat pipe wicks and thereby improve modeling and performance capabilities. The research question can be defined as: what are the mechanisms governing the heat and mass transport in the capillary driven phase change heat transfer in metal foams used as wick in heat pipes utilizing Metafoam materials? Due to the complicated nature of transport in porous copper metal foams, an experimental approach is mainly chosen. After identifying capillarity and evaporation as the general phenomena governing heat pipe operation, experimental facilities are developed to further study these two phenomena in copper metal foams. Wetting, capillary and evaporation properties are measured which can be later used in numerical and design work.

2.4 Objectives of the thesis

Having an industrial partner in this project (Metafoam technologies), an effort was made to consider the partner's interests as well as the scientific originality and contributions required for a PhD project. The industrial partner's objectives are:

- Explanation on why heat pipes utilizing Metafoam's materials have superior performance compared to competing materials
- Characterizing the performance of metal foams for heat pipe applications
- A numerical model of heat pipe performance

To address these needs and also consider the requirements of a PhD (novelty and originality), the following objectives are defined:

2.4.1 Capillary action

- Studying the wetting properties of copper metal foams
- Characterizing the foam hydrophilicity loss in ambient air and its cause
- Measuring permeability and effective pore radius to investigate the effect of porosity and a sintered external wall

2.4.2 Evaporation

- Investigating the capillary driven evaporation phenomena
- Investigating the effect of different parameters such as porosity, and wall superheat on the rate of evaporation.
- Measuring critical heat flux and wall superheat to investigate the mechanism of heat pipe failure for different porosities

2.5 Original contribution

This project is the first work of its type in the Micros research group and the first of this type to ever investigate phase change phenomena in the porous copper metal foams as produced by Metafoam. Several original contributions of this work can be mentioned as:

- By studying the foam microstructure, two levels of porosities are identified which directly enhances thermal and fluid transport phenomena in these foams. This microstructure is unique in metal foams and is speculated to be the main cause of high performance of these foams compared with other wicking materials. Although no direct experiment is done to prove this point, it is supported by observations with other biporous (having two level of porosity) wicks in the open literature and the similarity between the two. This point is discussed in chapter 4.

- It is found for the first time that the reason for hydrophilicity loss of the copper metal foams when exposed to ambient air is the adsorption of organic material and not copper oxidation. A very common misunderstanding as to the role of the copper oxides is therefore corrected for the first time. A novel method is also developed to measure the rate of hydrophilicity loss of copper metal foams based on measuring the spreading time of a droplet on the porous foam. This is the focus of chapter 4.

- In this thesis, the first characterization of K, r_{eff}, and internal contact angle for Metafoam copper metal foams is provided and also the conditions under which the rate of rise measurements should be done for proper parameter extraction is clarified. It was found that the rate of evaporation while the liquid is rising is significantly lower than the evaporation rate of a saturated sample with stationary liquid. It was also observed that sintering copper walls has almost no effect on the capillary rise and on the evaporation rate. By combining measurements done with acetone and water, the internal contact angle of water in hydrogen treated copper foams was measured and found to be lower than on a flat plate. Chapter 5 will focus on this topic.
- A novel experimental approach is proposed to measure the evaporation rate in chapter 6. Together with an analytical model, the effect of meniscus recession on the capillary pumping of copper metal pumps is characterized for the first time. The improved values of effective pore radius found by this method can have significant impact on the prediction of the capillary limits in two phase capillary driven devices. Moreover, occurrence of minimum wick thermal resistance in the same heat flux where dryout happens and also where minimum meniscus radius exists shows the importance of meniscus recession in the capillary driven transport phenomena in porous media.

- As the overall contribution of this thesis, the interconnection between capillarity and evaporation in the porous media is shown for the first time here. This aspect is especially important because the link between the two requires the simultaneous investigation of these two phenomena in the future researchworks.

CHAPITRE 3 AVANT-PROPOS

Auteurs et affiliation:

- Mahmood R.S. Shirazy: étudiant au doctorat, Université de Sherbrooke, Faculté de génie, Département de génie mécanique.
- Luc G. Fréchette : professeur, Université de Sherbrooke, Faculté de génie, Département de génie mécanique.

Date d'acceptation: 13 mai 2010

État de l'acceptation: version finale publiée

Revue: Proceedings of ASME 2010 3rd Joint US-European Fluids Engineering Summer Meeting and 8th International Conference on Nanochannels, Microchannels, and Minichannels, FEDSM2010-ICNMM2010.

Référence: [70]

Titre français: Une étude paramétrique des limites d'opération des caloducs

Contribution au document:

Cet article contribue à la thèse en déterminant la limite d'opération dominante dans les caloducs utilisant des mousses métalliques en cuivre. Après avoir connu la limite dominante dans cette étape, qui est la limite capillaire, on peut se concentrer sur les phénomènes qui se produisent dû à cette limite. Donc, la capillarité et l'évaporation sont identifiées et sont étudiées dans les chapitres prochains.

Résumé français :

Une étude paramétrique a été réalisée pour étudier les limites d'opération des caloducs utilisant un nouveau type de mousse métallique comme mèche pour des applications de

refroidissement des puces. Ces mousses ont une microstructure unique, formée de regroupements de pores sphériques avec une surface très élevée par rapport au volume comparé aux mousses métalliques traditionnelles. Elles présentent des limites d'opérations plus élevées dans les tests préliminaires de caloducs, ce qui suggère des taux élevés de refroidissement pour des applications microélectroniques. Dans la première partie de cette étude paramétrique, les corrélations déjà connues sont utilisées pour calculer les cinq types de limites de transfert de chaleur (capillaire, ébullition, visqueuse, l'entraînement et sonore) en fonction de la température, le type de mousse, et la porosité. Les résultats montrent que la limite dominante est la plupart du temps la limite capillaire, mais pour la mousse de type de 50 pore-par-pouce (PPI), la limite d'ébullition sera dominante. En outre, les mousses de 50 et 60 PPI ont des limites supérieures de transfert de chaleur que la poudre de cuivre frittée. Dans la deuxième partie de cette étude, un modèle thermodynamique en régime permanent d'un caloduc plat a été fait pour étudier l'effet des différents paramètres sur la limite dominante (capillaire). Un nombre sans dimension a été proposé pour évaluer l'équilibre entre la perte de charge dans les phases vapeur et liquide comme un guide de conception supplémentaire pour améliorer la limite capillaire des caloducs plats.

3 A PARAMETRIC INVESTIGATION OF OPERATING LIMITS IN HEAT PIPES

3.1 Abstract

A parametric investigation has been performed to study the different operating limits of heat pipes employing a novel type of metal foam as wick for chip cooling applications. These foams have a unique spherical pore cluster microstructure with very high surface to volume ratio compared to traditional metal foams and exhibit higher operating limits in preliminary tests of heat pipes, suggesting high cooling rates for microelectronics. In the first part of this parametric study, widely used correlations are applied to calculate the five types of heat transfer limits (capillary, boiling, viscous, entrainment and sonic) as a function of temperature, type of foam, and porosity. Results show that the dominant limit is mostly the capillary limit, but for 50 pore-per-inch (PPI) foam, the boiling limit will be dominant. Also, 50 and 60 PPI foams have higher heat transfer limits than sintered copper powder. In the second part of this study, thermodynamic steady state modeling of a flat heat pipe has been done to study the effect of the different parameters on the dominant limit (capillary). A dimensionless number has been proposed to evaluate the balance between the pressure loss in the vapor and liquid phases as an additional design guideline to improve the capillary limit in flat heat pipes.

3.2 Introduction

Flat plate heat pipes (FHP) are capillary driven passive devices that are usually used for the thermal management of electronic components. A flat heat pipe is a cavity of small thickness filled with a two-phase working fluid [44]. Heat sources and heat sinks are typically located near the opposite extremities of the heat pipe with the other parts being insulated. Evaporation occurs at the location of the heat sources. The vapour travels along the heat pipe, transporting the extracted thermal energy to the heat sink zones where it condenses. The liquid returns from the condenser to the evaporator through a wick or capillary structure made of micro-

grooves, meshes, sintered powder wicks or metal foams. In the field of electronic cooling, working temperatures are in the range of 60 to 120 °C. At this temperature level, the commonly used fluids are acetone, methanol, ethanol or water.

The design and type of capillary structure are main factors that influence the heat transfer capability of a heat pipe [79]. Open cell metal foams are proposed as wicks in flat heat pipes. Metal foams are a good candidate for two phase and single phase chip cooling because they are thermally conductive, light weight, have a high surface area and can provide good thermal contact between the heat pipe wall and the wick. Novel open cell metallic foams can be fabricated with a wide range of porosities, material composition, and microstructures, through a patented process initially developed at the National Research Council, NRC-IMI (Bourcherville, Qc, Canada) and now being manufactured and commercialized by the Canadian company Metafoam Technologies . These foams have a unique spherical pore cluster microstructure with very high surface to volume ratio compared to traditional metal foams and show good performance for heat transfer applications [58]. In preliminary tests, these foams exhibit higher operating limits in a heat pipe than common wicks, suggesting high cooling rates for microelectronics applications.

Although flat heat pipes are very efficient cooling systems, they are subject to a number of classical heat transfer limitations [18]: continuum flow limit, frozen start-up limit, viscous limit, sonic limit, entrainment limit, capillary limit, condenser limit and boiling limit. These phenomena limit the maximum heat input that may be transported by a heat pipe; heat rates above these limit values result in failure. Frozen-start up limit is not usually encountered in electronics cooling applications and if the condenser is well designed and the heat pipe is free of non-condensable gases, the condenser limit is not typically encountered either.

Modeling of the operation and performance of flat heat pipes has received a lot of attention in two main categories: 1) the numeric or analytic simulation of steady state or transient operation of FHPs, and 2) the transport limits (mainly capillary and boiling) and dry-out lengths. Numerous studies exist on simulations of flow and heat transfer inside FHPs [78][80],

transport limits, and dry-out lengths [44, 54, 80, 87], but most of these studies are performed assuming a grooved wick structure.

For instance, Lips et al. [1] studied the boiling limit of a transparent flat grooved heat pipe. They showed that the onset of nucleation does not prevent the operation of the FHP and even enhances its performance. Due to experimental challenges, they cannot clearly show that the boiling limit is actually the dominant one (lower than the capillary limit). Dry-out in the evaporator is observed for heat fluxes much higher than the onset of boiling. Hanlon et al. [6] attempted to describe the evaporation process in sintered copper wicks theoretically and by doing experiments. According to them, as the bubbles appear in the wick, the thermal performance of the wick decreases. This result is opposed to [1] and is probably caused by the difference in nucleation mechanisms and bubble growth in grooves and sintered copper. It suggests that the mechanisms involved in failure of a flat heat pipe are not the same for different material wicks and depend on the topology and microstructure of the wicking material.

Only few studies have addressed the application of metal foams as wicks in heat pipes. Phillips [56] studied the permeability, capillary pressures and evaporative performance of different porous materials including high porosity metal foams in order to evaluate their performance as wicks in heat pipes. He concludes that from the capillary pumping point of view, foam wicks are most desirable, felts rank second, and screens are least desirable. But for the onset of nucleate boiling, felts are more convenient than foams. Carbajal et al. [8, 55] and Queheillalt et al. [61] have studied transient response of a large flat heat pipe structure employing nickel foam as a wick, while exposed to a non uniform localized heat flux. Studies to date on metal foams have therefore focused on the wick properties or specific applications, but the relationship between these properties and operating limits remains to be investigated. A survey of the literature does not indicate significant efforts, both at macroscopic and microscopic levels, to study the performance of metal foams in flat heat pipes for electronics cooling applications. Further understanding of phase change alongside capillary driven flow,

and also its corresponding relationship to heat pipe limits, are important for efficient flat heat pipes. The current study aims to take an initial step towards this goal.

In order to evaluate the possibility of using the available correlations for calculating the operation limits of a heat pipe with a metal foam wick, and to identify the important design parameters affecting the dominant operating limit, a parametric study has been done in two parts. In the first part, correlations commonly used in the field to calculate the heat pipe limits have been employed to determine different operating limits of a typical circular heat pipe. The circular geometry has been chosen in order to use the existing correlations for ordinary heat pipes. In the second part, thermodynamic steady state modeling of a flat heat pipe has been done to study the effect of the different parameters on the dominant limit, determined in the first part. Here, a rectangular (flat) geometry has been chosen. The main difference between the flat plate and cylindrical geometries is the vapor core cross section. It will be seen that the thickness of the vapor core has considerable impact on the general performance of a FHP. Overall, this device level study will define the research topics that are most critical to further investigate for accurate predictive modeling of FHP with metal foams.

3.3 Nomenclature

A_v	Vapour core cross section area (m^2)
A_w	Wick cross section area (m^2)
C	Constant depending on Mach number
D	Flat heat pipe width (m)
h_v	Vapor core height (m)
h_l	Wick thickness (m)
K	Permeability (m^2)
k_{eff}	Effective thermal conductivity
L_{eff}	Effective length of the heat pipe (m)
L_e	Evaporator length (m)
L_c	Condenser length (m)

L_{adi}	Adiabatic length (m)
M	Molecular weight
Ma_v	Vapour core mach number
$\dot{m}_v$	Vapor mass flow rate (kg/s.m)
$P_{c,m}$	Capillary pressure (Pa)
P_v	Vapour pressure (Pa)
P_l	Liquid pressure (Pa)
Q_{tot}	Heat power injected in the evaporator (W)
q_d	Heat flux (W/m^2)
q	Heat transfer rate (W)
R_v	Vapor constant (J/kg.K)
$\bar{R}$	Universal gas constant (J/ mol.K)
Re_v	Reynolds number
$r_{h,v}$	Vapor core radius (m)
r_c	Pore capillary radius (m)
r_n	Nucleation radius (m)
$r_{h,w}$	Surface pore hydraulic radius (m)
T_v	Vapor temperature (K)
T_v	Vapour temperature (K)
$\bar{w}_v$	Mean velocity of the vapor in the x direction (m/s)
$\bar{w}_l$	Mean velocity of liquid in the x direction (m/s)
μ_l	Liquid viscosity ($N.s/m^2$)
μ_v	Vapour viscosity ($N.s/m^2$)
v_v	Vapour kinematic viscosity (m^2/s)
v_l	Liquid kinematic viscosity (m^2/s)
γ_v	Ratio of the specific heats

λ Latent heat of vaporization (J/kg)

ρ_v Vapour density (kg/m^3)

ρ_l Liquid density (kg/m^3)

θ Contact angle (^{o})

σ Surface tension (N/m)

3.4 Operating limit correlations

3.4.1 Capillary limit

The most commonly studied limitation in flat or miniature heat pipes is the capillary limit [10, 40, 87]. The driving potential for the circulation of the working fluid is the capillary pressure difference. Capillary limit occurs if the maximum capillary pressure is not enough to overcome the sum of all pressure losses (due to liquid friction, vapor friction, and gravity) inside the heat pipe. This can be expressed as [54]:

$$\frac{2\sigma\cos\theta}{r_c} = \left(\frac{C(f_v \mathrm{Re}_v)\mu_v}{2(r_{h,v})^2 A_v \rho_v \lambda}\right) L_{eff} q + \left(\frac{\mu_l}{K A_w \lambda \rho_l}\right) L_{eff} q \qquad 3.1$$

The left-hand term is the maximum capillary pressure produced by the porous structure, where σ is the surface tension, θ is the contact angle (assumed to be zero here) and r_c is the pore capillary radius. The first term at the right side of Eqn 3.1 expresses the vapor core pressure drop, where μ_v is the vapor viscosity, $r_{h,v}$ vapor core radius, A_v vapor core cross section area, ρ_v vapor density, λ latent heat of vaporization, q is the rate of heat transferred and L_{eff} is the effective length of the heat pipe ($L_{eff} = 0.5L_e + L_{adi} + 0.5L_c$). The normal hydrostatic pressure is neglected in this equation because of the small inside diameter of the tube. The axial hydrostatic pressure can also be neglected if the heat pipe is assumed to be horizontal. The

constant C depends on the Mach number and determines the compressibility of the flow inside the vapor core. The Mach number can be defined as:

$$\mathrm{Ma}_v = \frac{q}{A_v \rho_v \lambda \left(R_v T_v \gamma_v\right)^{1/2}} \tag{3.2}$$

where R_v is the gas constant, T_v is the vapor temperature and γ_v is the ratio of the specific heats (1.33 in this case). The vapor flow regime (laminar or turbulent) can be determined by evaluating the local axial Reynolds number in the vapor. The Reynolds number appears in Eqn 3.1 as a product with the friction factor: $f_v \mathrm{Re}_v$. Reynolds number in the vapor core is defined as:

$$\mathrm{Re}_v = \frac{2(r_{h,v})q}{A_v \mu_v \lambda} \tag{3.3}$$

The values for these two parameters, C and $f_v \mathrm{Re}_v$, depend on Re_v and Ma_v, according to:

$$\begin{aligned} &\mathrm{Re}_v < 2300 \quad \& \quad \mathrm{Ma}_v < 0.2 \\ &f_v \mathrm{Re}_v = 16 \qquad\quad \mathrm{C}=1.00 \end{aligned} \tag{3.4}$$

$$\mathrm{Re}_v < 2300 \quad \& \quad \mathrm{Ma}_v > 0.2$$

$$f_v \mathrm{Re}_v = 16 \qquad \mathrm{C} = \left[1 + \left(\frac{\gamma_v - 1}{2}\right)\mathrm{Ma}_v^2\right]^{-1/2} \tag{3.5}$$

$$\mathrm{Re}_v > 2300 \quad \& \quad \mathrm{Ma}_v > 0.2$$

$$f_v \mathrm{Re}_v = 0.38\left(\frac{2(r_{h,v})q}{A_v \mu_v \lambda}\right)^{3/4} \qquad \mathrm{C}=1.00 \tag{3.6}$$

Because the equations used to evaluate both the Reynolds number and the Mach number are functions of the heat transport capacity, it is first necessary to assume the conditions of the vapor flow. Using these assumptions, an iterative procedure must be used to determine the maximum heat capacity. Once this value is known, it can be substituted into the expressions

for the vapor Reynolds number and Mach number to determine the accuracy of the original assumption.

The second term at the right side of the Eqn 3.1 is the liquid pressure drop in the wick. In this term, μ_l is the liquid viscosity, K is the wick permeability, A_w the wick cross section area, and ρ_l is the liquid density.

3.4.2 Boiling limit

The boiling limit occurs when the applied evaporator heat flux is sufficient to cause nucleate boiling in the evaporator wick. This creates vapor bubbles that partially block the liquid return and can lead to evaporator wick dry-out. They can also violate the curved meniscus interface and hence affect the capillary pumping power [18]. By using the nucleate boiling theory, the boiling limit can be found from the following equation [54]:

$$q_{b,e} = \frac{2\pi L_e k_{eff} T_v}{\lambda \rho_v \ln(r_i/r_v)} \left[\frac{2\sigma}{r_n} - P_{c,m} \right] \qquad 3.7$$

where $P_{c,m}$ is the capillary pressure in the wicking structure and k_{eff} is the effective thermal conductivity of the porous material. An important parameter is the nucleation radius r_n which can have a significant effect on the boiling limit values. This parameter should be determined experimentally and it is not available for this type of copper metal foam. It is usually in the range of 2.54×10^{-5} - 2.54×10^{-7}m [54]. In the absence of experimental data, r_n can be assumed to be 10^{-7} [18].

3.4.3 Sonic limit

The sonic limit is due to the fact that at low vapor densities, the corresponding mass flow rate in the heat pipe may result in very high vapor velocities, and the occurrence of choked flow (Ma_v reaches 1) in the vapor passage may be possible. The sonic limit can be found from the following equation [54]:

$$q_{s,m} = A_v \rho_\circ \lambda \left[\frac{\gamma_v R_v T_\circ}{2(\gamma_v + 1)} \right]^{\frac{1}{2}} \qquad 3.8$$

$T_\circ$ and $\rho_\circ$ are the temperature and density of the vapor. R_v is the vapor constant ($R_v = \bar{R}/M$).

3.4.4 Entrainment limit

The entrainment limit stems from the case of high shear forces developed as the vapor passes in the counterflow direction over the liquid saturated wick. Here, the liquid may be entrained by the vapor and returned to the condenser. This, results in insufficient liquid flow to the wick structure. The entrainment limit can be estimated using [54]:

$$q_{e,m} = A_v \lambda \left[\frac{\sigma \rho_v}{2 r_{h,w}} \right]^{1/2} \qquad 3.9$$

where $r_{h,w}$ is the surface pore hydraulic radius.

3.4.5 Viscous limit

The viscous limit occurs at low operating temperatures, where the saturation vapor pressure difference between the evaporator and the condenser region may be of the same order of magnitude as the pressure drop required for driving the vapor flow in the heat pipe. This results in an insufficient pressure available to drive the vapor. The viscous limit is sometimes called the vapor pressure limit. Finally the viscous limit can be estimated from the following equation [54]:

$$q_v = d_v^2 \lambda A_v \frac{P_v \rho_v}{4 f_v \mathrm{Re}_v L_e \mu_v} \qquad 3.10$$

where $f_v \mathrm{Re}_v$ can be found from the Eqns 3.4 to 3.6 based on the flow regime.

3.5 Transport limits for a circular heat pipe

Dimensions used for this part of the study can be seen in Table, representative of industrial applications for microelectronics. These are the dimensions of a typical tube which later is pressed and flattened in order to produce FHP for laptops. The limiting heat transfers have been calculated for three of Metafoam's metal foams (250, 60 and 50 PPI) as well as for a typical sintered copper powder wick. Table 3.2 shows the properties of these wicks [48]. The permeability to capillary radius ratios (PCR) is normalized by the PCR of sintered powders. Working fluid is water.

Table 3.1 . Dimensions of the circular heat pipe

Length(m)	Outside diameter (m)	Wall thickness (m)	Wick thickness (m)	Evaporator length (m)	Condenser length (m)
0.25	0.006	0.0003	0.0007	0.02	0.03

3.5.1 Results for different wick types

In order to determine the dominant transport limit for the 4 types of wick materials, the above limits are calculated and compared in Figure 3.1 through Figure 3.4. It can be seen in Figure 3.1 to Figure 3.1 that the capillary limit is dominant. The next most limiting phenomena are entrainment at lower temperatures and boiling at higher temperatures. In Figure 3.4 however, (50 PPI copper foam), the entrainment limit dominates until approximately 60 °C, and beyond that, the boiling limit becomes dominant.

Table 3.2 . Wick properties [48]

Material	Porosity (%)	Thermal conductivity (W/m.K)	Permeability (m^2)	Capillary radius(μm)	Normalized PCR ratio
Sintered copper Powders	30-50	40	$9.41e^{-12}$	27	1
Copper foam 250 PPI	60	30	$1.30e^{-11}$	47	0.77
Copper foam 60 PPI	70	10	$1.10e^{-10}$	89	3.44
Copper foam 50 PPI	75	7	$1.37e^{-9}$	100	40.17

Due to the high PCR of this foam, its capillary limit is higher than the capillary limit of the other wicks. In all cases, the viscous limit is the most negligible. As it was mentioned before,

while dealing with the numbers obtained for entrainment and boiling limits, one should be careful about the inaccuracies in the correlations used to calculate them.

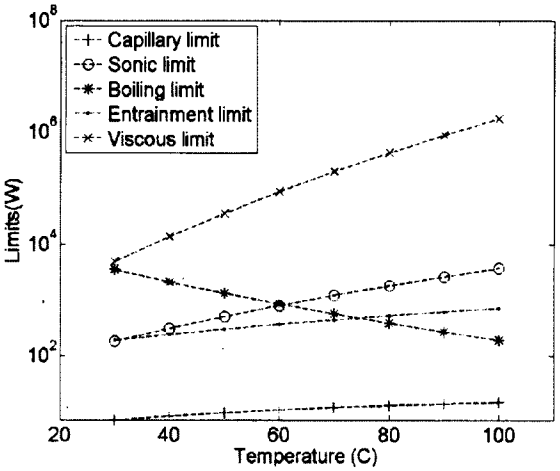

Figure 3.1 Different limits for sintered copper powder

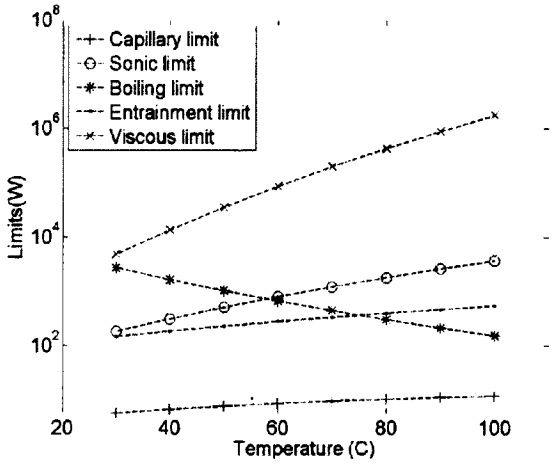

Figure 3.2 Different limits for 250 PPI copper foam

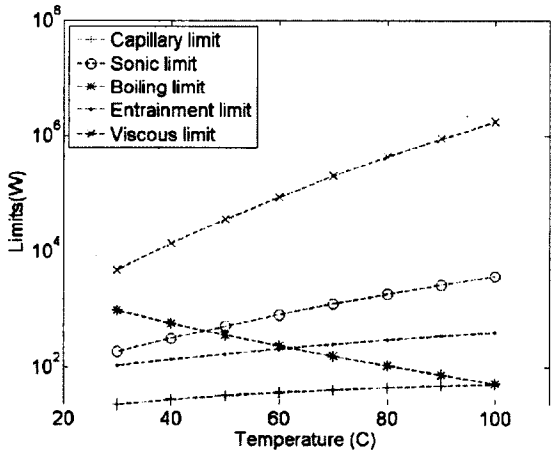

Figure 3.3 Different limits for 60 PPI copper foam

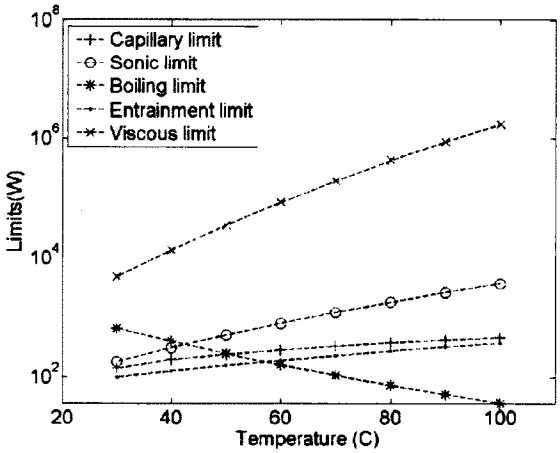

Figure 3.4 Different limits for 50 PPI copper foam

For the boiling limit, it should be noted that the nucleation radius is not determined for these materials and the value used for Figure 3.1 to Figure 3.4 is chosen to be the average of the upper and lower values of this parameter mentioned in section 3.4.2 (2.54×10^{-6}). Different values can have significant impact on the numbers obtained as the limits and it will be shown in section 3.5.3. Also, as it is shown in [44] the onset of nucleation cannot be considered as an operational limit. In fact, the correlation which is used in this study for boiling limit is

developed without considering the effect of the porous media on the bubble formation and escape. Therefore, the values obtained here should be considered only as a first order estimation and there is a need for a correlation for boiling limit in flat heat pipes using metal foams as a wick.

For the entrainment limit, the wick surface pore hydraulic radius is assumed to be equal to the capillary radius, which is not accurate. For copper mesh wicks this parameter is lower than the capillary radius. With a similar trend for the porous metal foams, then the entrainment limit would be higher than the values obtained here.

3.5.2 Results for the Capillary limit

Since the capillary limit is often dominant, the maximum heat transfer capacity of a heat pipe using each type of wick material has been calculated using Eqn 3.1 for a temperature range of 30 to 100 °C. The results are shown in Figure 3.5. Basically, they are only the capillary limits calculated in Figure 3.1 to Figure 3.4 which are plotted together to enable comparison. It can be seen that the highest heat transfer capacity occurs with 50 PPI metal foam and this can be attributed to the extremely high PCR of this material. It can be concluded that permeability is the dominant parameter in the effectiveness of theses wick materials. Although the capillary radius increases from 27 to 100 microns (leading to less capillary pumping capacity) the capillary limit increases due to increased permeability (less pressure drop in the liquid section). It implies that for the current geometry and dimensions, the main pressure drop is in the wick (liquid section) and not in the vapor core.

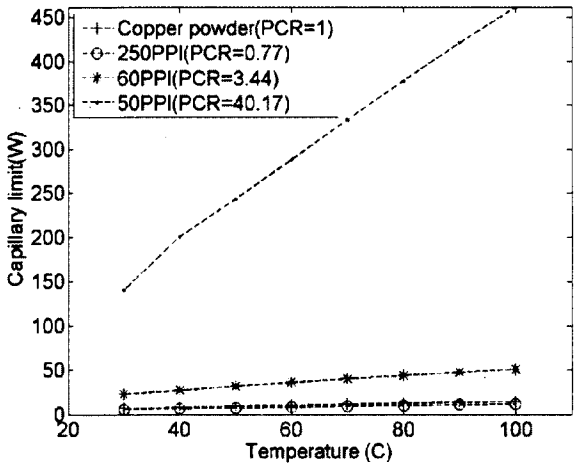

Figure 3.5 Capillary limit for different wicking materials

3.5.3 Results for the boiling limit

As it was mentioned above, according to the Eqn 3.7, the results for the boiling limit are heavily dependent on the values of r_n. To better see this dependency, a sensitivity study has been done for the 50 PPI foam and the results are shown in Figure 3.6. The values chosen for the sensitivity study are the upper and lower range suggested by Peterson [54] which are 2.54×10^{-5} and 2.54×10^{-7}m and the r_n suggested by Faghri [18] which is 10^{-7}. It can be seen that the limits differ up to two orders of magnitude which further implies the importance of the precise knowledge of this parameter.

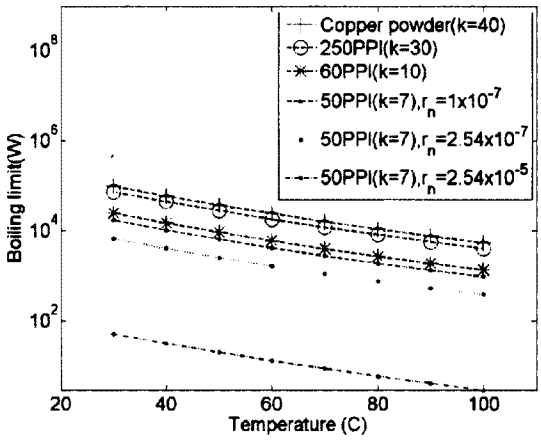

Figure 3.6 effect of the different values of nucleation radius r_n on the boiling limit for the 50 PPI foam

3.6 Parametric study of capillary limit in a flat heat pipe

As it was observed in the previous part, the dominant limit is mostly capillary limit; therefore it was decided to perform a parametric study to investigate the effect of different parameters on the maximum capillary limit of a flat heat pipe. This study is different from the previous one in section 3.5, in the sense that the geometry here is a flat rectangular heat pipe and the vapor core thickness is much smaller than the circular one. The equations and correlations used for this study are the 1-D form of the equations presented in [37], as presented in the following section.

3.6.1 Mathematical model

3.6.1.1 Assumptions

This parametric study is done under the following conditions and assumptions:

- Steady state
- Darcy flow in the wick
- Laminar and incompressible flow in the vapor core
- Working fluid is water
- Axial heat conduction in the wall is ignored

3.6.1.2 Capillary pressure

To estimate the limit, the vapor and the liquid pressure distributions within the device are needed [37]. In this study, evaporation and condensation heat transfer coefficients are not calculated, but instead, all the physics are expressed in terms of the mass and momentum conservation for the two phases, assuming saturation conditions in the phase change zones.

During the normal operation of the heat pipe, the working fluid is constantly flowing from the evaporator to the condenser in vapor state and from the condenser to the evaporator in liquid state. During this path, there are pressure drops in the liquid and vapor phase which should be

overcome by the capillary pressure produced at the vapor-liquid interface. The capillary pressure can be expressed as:

$$\Delta P_{cap} = \frac{2\sigma \cos\theta}{r_c} \tag{3.11}$$

3.6.1.3 Vapor phase

We will derive the vapor pressure from the mass rate balance during evaporation and condensation, as shown in Figure 3.7. The conservation law is applied to a control volume and simplifications are made to do the calculations. The control volume is chosen with the height of the vapor core h_v and the length dx.

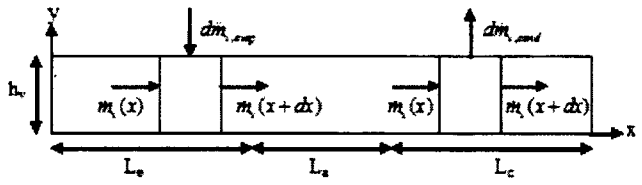

Figure 3.7 Vapor core modeling and its corresponding control volumes

3.6.1.4 Evaporation

The pressure distribution inside the vapor core can be calculated from the velocity change due to evaporation and condensation. During the evaporation, as shown in Figure 3.7, the absorbed heat can be expressed by the mass flow rate $d\dot{m}_{v,evap}$ entering the vapor control volume D.dx.h_v. The mass conservation law in this case for the control volume is expressed with Eqn 3.12:

$$\dot{m}_v(x) + d\dot{m}_{v,evap} = \dot{m}_v(x+dx) \tag{3.12}$$

The mass flow rate $\dot{m}_v(x)$ could relate to the vapor average velocities in x direction, $\bar{w}_v(x)$, by Eqn 3.13:

$$\dot{m}_v(x) = \rho_v h_v D \bar{w}_v(x) \tag{3.13}$$

where, ρ_v is the vapor density, D flat heat pipe width and h_v is the vapor core height. Replacing Eqn 3.13 in Eqn 3.12 and simplifying gives the velocity of the vapor phase:

$$\frac{d\bar{w}_v}{dx} = \frac{d\dot{m}_{v,evap}}{\rho_v h_v D dx} \tag{3.14}$$

The mass flow rate can be expressed by the total heat power, introduced to the evaporator:

$$\frac{d\dot{m}_{v,evap}}{dx} = \frac{\dot{m}_{v,evap}}{L_e D} = \frac{Q_{tot}}{L_e D \lambda} \tag{3.15}$$

where Q_{tot} is the heat power injected in the evaporator, L_e evaporator length, D flat heat pipe width and λ is the heat of vaporization.

3.6.1.5 Condensation

Using the same argumentation and procedure, the following equations will be derived for the vapor velocity in the condenser section:

$$\frac{d\bar{w}_v}{dx} = -\frac{d\dot{m}_{v,cond}}{\rho_v h_v D dx} \tag{3.16}$$

And the heat dissipated in the condenser is expressed by:

$$\frac{d\dot{m}_{v,cond}}{dx} = \frac{\dot{m}_{v,cond}}{L_c D} = \frac{Q_{tot}}{L_c D \lambda} \tag{3.17}$$

where, L_c is the condenser length. Using the Poiseuille Flow equations to express the laminar flow between the parallel plates, the vapor average velocity is:

$$\bar{w}_v = -\frac{h_v^2}{12\mu_v}\frac{dP_v}{dx} \tag{3.18}$$

where, P_v is the vapor pressure and μ_v is the vapor dynamic viscosity. Replacing Eqn 3.18 in Eqns 3.17 and 3.16 will lead to the following relation for vapor pressure distribution:

$$\frac{d^2P_v}{dx^2} = -\frac{12\mu_v}{\rho_v h_v^3 \lambda} q_d \tag{3.19}$$

where q_d is the heat flux density expressed in Eqn 3.20 for the three sections of the heat pipe:

$$q_d = \begin{cases} \dfrac{Q_{tot}}{L_e D} & \text{evaporator} \\ 0 & \text{adiabatic zone} \\ -\dfrac{Q_{tot}}{L_c D} & \text{condenser} \end{cases} \tag{3.20}$$

To have an isolated flow system, where no fluid enters or exits the device, no-flow boundary conditions must be specified:

$$\left.\frac{dP_v}{dx}\right|_{x=0} = \left.\frac{dP_v}{dx}\right|_{x=L} = 0 \tag{3.21}$$

3.6.1.6 Liquid phase

The liquid flow velocity and pressure distribution in the wick is obtained by the same method as in the case of the vapor velocity. Once again the conservation laws are applied to a liquid control volume during evaporation and condensation:

$$\frac{d\bar{w}_l}{dx} = -\frac{q_d}{\rho_l h_l \lambda} \tag{3.22}$$

The average axial velocity $\bar{w}_l$ is obtained from the Darcy's law for the liquid flow in porous media:

$$\bar{w}_l = -\frac{K}{\mu_l}\frac{dP_l}{dx} \tag{3.23}$$

where, K is the wick permeability, μ_l is the liquid dynamic viscosity, ρ_l the liquid density, h_l the wick thickness, and P_l the liquid pressure. The liquid pressure distribution is:

$$\frac{d^2P_l}{dx^2} = \frac{\mu_l}{K\rho_l h_l \lambda} q_d \tag{3.24}$$

Again, to have an isolated flow system where no fluid enters or exits the device, no-flow boundary conditions must be specified:

$$\left.\frac{dP_l}{dx}\right|_{x=0} = \left.\frac{dP_l}{dx}\right|_{x=L} = 0 \tag{3.25}$$

To solve the set of differential equations, a pressure at some point of the system should be assumed to be known. Therefore, the pressure at the end of the condenser section is assumed to be the saturation temperature of the steam at the working temperature.

3.6.2 Heat pipe and wick dimensions

This is a parametric study, in the sense that some of the parameters including the heat pipe and wick properties are changed to see the effect on the capillary limit. Table presents the nominal values that are assumed while changing others. The nominal wick material is the Metafoam 250 PPI foam (Table 3.2) and the operating temperature is chosen to be 60°C which is the typical operating temperature in practice [58]. The configuration consists of a flat rectangular cross section with wicking layers on both the top and bottom surfaces (total wick material thickness is double the value shown in Table).

Table 3.3. Dimensions and properties of the nominal FHP

Permeability (m^2)	Capillary radius (μm)	FHP length (m)	Evap. length (m)	Cond. Length (m)	Wick thickness (m)	Vapor core thickness (m)	FHP Width (m)
1.30e-11	47	0.1	0.02	0.02	.0007	0.0003	0.03

3.6.3 Results of the parametric study of the capillary limit

3.6.3.1 Effect of FHP length

The length of the FHP has a direct effect on the vapor and liquid pressure drops and hence, affects the capillary limit. The effect of the length is depicted in Figure 3.8 and as expected, the maximum heat capacity of the device reduces as the length of the heat pipe is increased. It should be noted that the capillary limit for very short heat pipes reach 80-90 watts, which is probably unrealistic because other limits (boiling for instance) can happen before that. Also, when the length is too short (5 cm in this example); the axial heat conduction along the heat pipe can have a considerable effect on the performance and limits of the heat pipe which is not considered in the current modeling.

3.6.3.2 Effect of permeability

Increasing the permeability can lead to a lower flow resistance and increase the capillary limit. This can be observed in Figure 3.9. The typical permeability of sintered copper powder is in the order of 10^{-12} and that of metal foams ranges from 10^{-11} to 10^{-9} (Table 3.2). It can be seen that for permeabilities up to 10^{-10} m^2, increasing the permeability of the wick significantly increases the capillary heat transfer limit, but the effect is insignificant above 10^{-10} m^2. For instance, an increase of two orders of magnitude of the permeability (10^{-10} to 10^{-8}) leads to only 10% increase of the limiting heat rate.

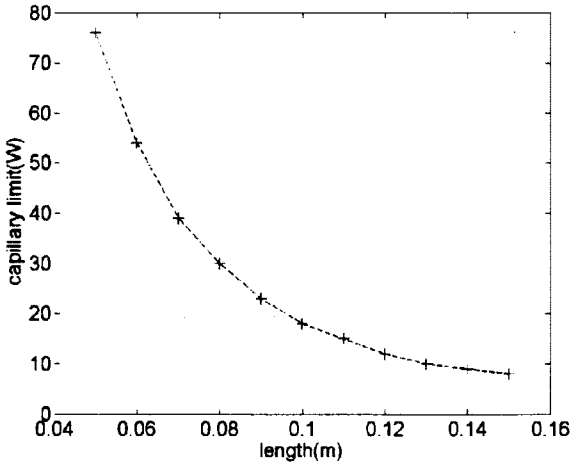

Figure 3.8 Effect of FHP length on the capillary limit

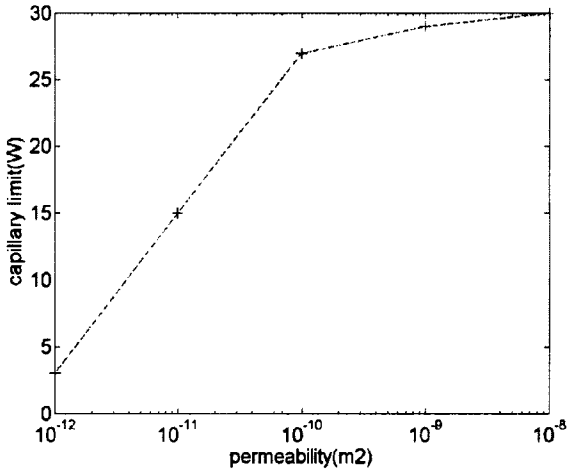

Figure 3.9 Effect of permeability on the capillary limit

3.6.3.3 Effect of vapor core thickness

Effect of increasing the vapor core thickness can be seen in Figure 3.10. As shown, increasing the vapor core thickness significantly increases the capillary limit. This implies that most of the pressure drop occurs in the vapor phase and not in the wick. Wick thickness is therefore not a limiting parameter in the thermal performance of the FHP configuration studied here. One can suppose that after a certain vapor core thickness, the pressure drops in both phases would have the same order of magnitude and their relative effects would be similar. This can justify the decreasing slope of the graph in the high values of the vapor core thickness. It should be noted that having a high pressure drop in the vapor core leads to a high temperature difference between the condenser and the evaporator, at saturation conditions. This leads to higher overall thermal resistance of the heat pipe.

3.6.3.4 Effect of pore radius

The pore radius has a direct effect on the capillary pumping potential, as a small pore radius will lead to a higher capillary pressure. It can be seen in Figure 3.11, that after a pore radius of approximately 100 microns, the effect of this parameter is not that significant.

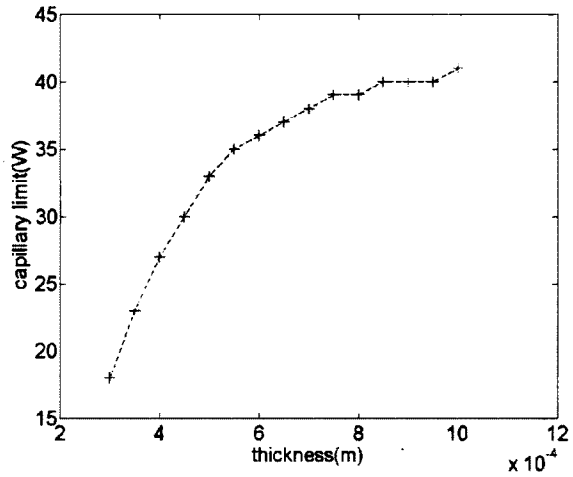

Figure 3.10 Effect of vapor core thickness on the capillary limit

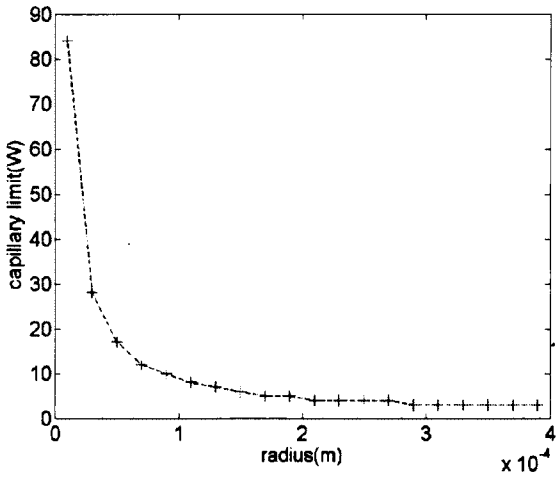

Figure 3.11 Effect of pore radius on the capillary limit

3.7 A non-dimensional parameter for capillary limit

By observing Figure 3.8 to Figure 3.11, it can be inferred that there should be a parameter that shows the relative importance of the pressure drop in the vapor core to the pressure drop in the wick. It can lead to a design parameter that helps the designer know if he should increase the core or wick thickness and up to what point it is useful. This can be achieved by defining a parameter that includes the ratio of the pressure drop in the vapor core and the pressure drop in the wick. Assuming that $q_c = q_e$, the ratio of Eqn 3.19 to Eqn 3.24 will lead to:

$$\frac{\Delta P_v}{\Delta P_l} = 12K \frac{\nu_v}{\nu_l} \frac{h_l}{h_v^3} \qquad 3.26$$

which combines the effects of the fluid properties (kinematic viscosity ratios), and the geometry at the macroscopic (wick and vapor core dimensions) and microscopic (permeability of the wick) scales. The length and width are the same for both liquid and vapor flow paths and therefore cancel out. A value of 1 for this parameter can be an adequate compromise between both losses. For instance, a value largely over 1 means higher weight of the pressure loss in the vapor core. In this case, the designer can either use a wicking material with a lower

permeability, since it's not the limiting parameter (without exceeding the maximum design capillary limit), or change the heat pipe geometry to decrease the vapor pressure drop.

Figure 3.12 to Figure 3.14 show the variation of the dimensionless pressure drop ratio (Eqn 3.25) versus geometrical parameters for the nominal FHP presented in Table. Assuming water as the working fluid and an operating temperature of 60°C, this ratio is 1.35 (for the 250 PPI Metal foam) which suggests a balance between liquid and vapor pressure drops.

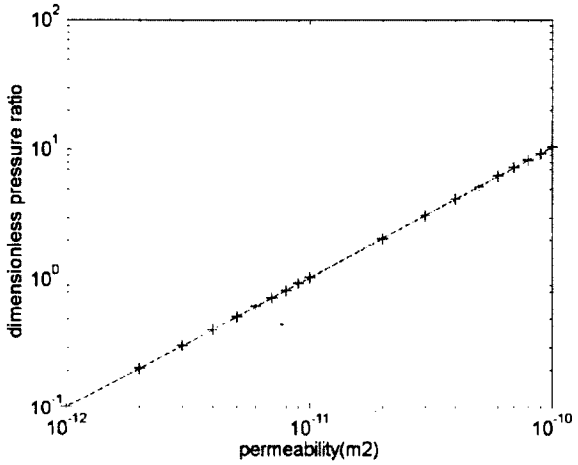

Figure 3.12 Effect of permeability on the dimensionless pressure drop ratio

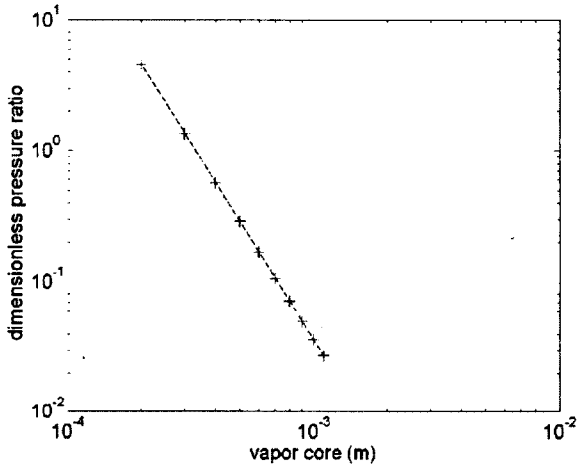

Figure 3.13 Effect of vapor core thickness on the dimensionless pressure drop ratio

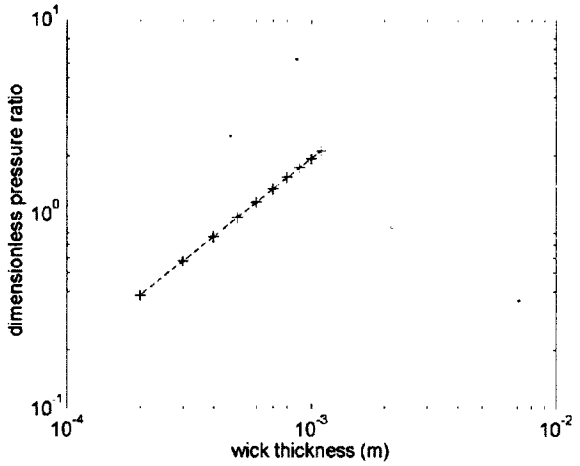

Figure 3.14 Effect of wick thickness on the dimensionless pressure drop ratio

In Figure 3.12, it is obvious that the balanced value for permeability with the current configuration is around 10^{-11}. Hence, values higher than this leads to a dominant pressure drop

in the vapor core. This is consistent with results in Figure 3.9. The same conclusions can be made about the results in Figure 3.13 to Figure 3.14, showing the relative importance of the vapor core and wick thickness on the pressure drops in the flat heat pipe. By estimating the values of permeability or vapor core thickness that have a noticeable impact on the limit, we can state that there is no more benefit in increasing permeability if the dimensionless pressure ratio is much greater than 1, or in increasing the vapor core thickness if the dimensionless pressure ratio is much smaller than 1.

3.8 Design metrics for FHP

Capillary limit occurs when there is not sufficient driving pressure to overcome the losses in the vapor and liquid regions. Therefore, a well-designed FHP is the result of an effective wicking material, to produce driving pressure, and geometry with minimal flow resistance. In order to evaluate the driving pressure of the wick, PCR can be considered as a good measure. It shows the relative importance of the permeability (wick flow resistance) to capillary radius (driving pressure source). But PCR alone is not enough as criteria to judge a well-designed FHP. As it was shown above, when the vapor core is thin, the main pressure loss will happen in the vapor region and this will require a metric to evaluate and choose a pressure balanced geometry. Hence, dimensionless pressure ratio can be used to further judge the pressure losses in the wick and the vapor core. Values much higher and much lower than 1 represent dominant vapor core and wick pressure loss respectively. It can help the designer judge his choice of dimensions and make sure that neither the wicking material nor the vapor core overly dominate the pressure losses. Once again, it should be stressed that the current discussion concerns only the capillary limit and that the boiling limit (the second most important limit in electronics cooling applications) is not considered here.

3.9 Discussion and Conclusion

Common correlations are used to calculate the dominant limit for circular heat pipes in the conditions usually encountered in electronics cooling applications. Three types of novel metal

foams and a typical sintered copper powder have been used as the wicking material in a typical heat pipe configuration. Five types of operating limits have been calculated and the dominant limits were determined, mostly capillary. In the second part of the paper, the capillary limit has been studied in more detail for a flat heat pipe. Finally, a dimensionless parameter has been proposed as a guideline for heat pipe design to evaluate the importance of the pressure losses in vapor and liquid flows.

The conclusions can be summarized as follows:

- The results in the first part (transport limits for a circular heat pipe) confirm the common belief that capillary and boiling limits are the dominant ones in the temperature ranges used in electronics cooling. Entrainment may however become limiting in lower temperature ranges. Also, the theories concerning the boiling limits need to be revised in order to account for the bubble formation in a porous structure.

- The results in the second part of the study (Parametric study of the capillary limit for a FHP) clearly show that the capillary limit is a general function of the wick properties (permeability and pore capillary radius) and geometrical specifications (vapor core thickness, wick thickness, FHP length), assuming a given working fluid. Therefore, designing an effective FHP, i.e. having a high value of heat transfer limit, requires an optimum choice of the geometrical aspects in addition to the transport properties of the wick. A dimensionless number has been proposed to address this issue. Values around 1 represent a balanced pressure loss in wick and vapor core. A good flat heat pipe design should consider both the PCR and this dimensionless pressure loss parameter to keep the balance between the driving force and losses in both liquid and vapor regions.

- Due to the uncertainties that exists in the correlations used in both parts of this study, these first order results are mostly valid to give a preliminary insight into the importance of the different parameters as opposed to providing quantitative predictions. More research is required to establish correlations for capillary and boiling limits, especially for the novel metal foams considered here.

3.10 Acknowledgments

This research was jointly funded by NSERC Canada and Metafoam Technologies Inc., with the grateful support and guidance of Mr. Dominic Pilon.

CHAPITRE 4 AVANT-PROPOS

Auteurs et affiliation:

- Mahmood R.S. Shirazy: étudiant au doctorat, Université de Sherbrooke, Faculté de génie, Département de génie mécanique.
- Sonia Blais : Agente de caractérisation des matériaux, Centre de caractérisation des matériaux (CCM), Université de Sherbrooke.
- Luc G. Fréchette : professeur, Université de Sherbrooke, Faculté de génie, Département de génie mécanique.

Date d'acceptation: 13 mars 2012

État de l'acceptation: version finale publiée

Revue: Journal of Applied Surface Science

Référence: [71]

Titre français: Mécanisme de transition de mouillabilité dans les mousses métalliques en cuivre: de superhydrophilic à hydrophobique

Contribution au document:

Cet article contribue à la thèse en déterminant la cause de changement de comportement de mouillabilité des mousses métalliques quand elles sont exposées à l'air. Une étude approfondie de caractérisation de surface est effectuée sur les mousses afin d'identifier le rôle de la mouillabilité de la surface sur la performance capillaire. Il est également déduit que la raison pour la haute limite de transport des mousses par rapport à d'autres matériaux est leur microstructure unique qui a deux niveaux de porosité. Cet article résume des efforts pour couvrir l'aspect de mouillabilité qui est suivi par une étude de capillarité dans le prochain article.

Résumé français :

L'hydrophilicité est une condition nécessaire pour les mousses métalliques en cuivre utilisés dans les caloducs. Malheureusement, les mousses métalliques hydrophiles en cuivre deviennent hydrophobes lorsqu'ils sont exposés à l'air ambiant. Cette transition de mouillabilité est généralement expliquée par la formation d'oxydes de cuivre sur la surface, mais les oxydes de cuivre sont aussi connus pour être hydrophiles. Une étude expérimentale est menée pour expliquer cette controverse. L'effet des atmosphères différents sur le taux de perte d'hydrophilicité est étudié par une approche originale qui consiste à mesurer le temps de propagation des gouttelettes sur la surface de la mousse. De plus, les techniques de caractérisation de surface telles qu'analyse chimique par spectroscopie d'électrons (ESCA ou XPS) et spectrométrie de masse des ions secondaires en temps de vol (TOF-SIMS) sont utilisées pour caractériser l'impact en fonction du temps de l'air ambiant sur la composition chimique et de la morphologie des mousses métalliques en cuivre. Le mécanisme d'hydrophobicité de mousses métalliques en cuivre se trouve être dominé par la chimie de surface et non pas sa morphologie (type Wenzel). Les résultats montrent que l'oxydation n'est pas la raison de ce changement d'hydrophile à hydrophobe, mais plutôt, l'adsorption de composés organiques volatils (COV) à la surface de la mousse de cuivre. Cette explication est confirmée par l'observation du changement de mouillabilité vers hydrophobicité en immergeant les mousses métalliques de cuivre hydrophiles dans un liquide COV (α-pinène).

4 MECHANISM OF WETTABILITY TRANSITION IN COPPER METAL FOAMS: FROM SUPERHYDROPHILIC TO HYDROPHOBIC

4.1 Abstract

Hydrophilicity is a necessary condition for wicking materials such as copper metal foams used in heat pipes. Unfortunately hydrophilic copper metal foams become hydrophobic when exposed to room ambient air. This wettability transition is commonly explained by the formation of copper oxides on the surface; however copper oxides are known to be hydrophilic. An experimental study is conducted to explain this controversy. Effect of different atmospheres on the rate of hydrophilicity loss is studied by a novel approach which is to measure the spreading time of droplet on the foam surface. Also, surface characterization techniques such as XPS and TOF-SIMS are used to characterize the time dependent impact of the ambient air on the morphology and chemical composition of the copper metal foams. The hydrophobicity mechanism of copper metal foams is found to be dominated by surface chemistry and not its morphology (Wenzel type). Results show that oxidation is not the reason for this hydrophilic to hydrophobic change but rather, adsorption of volatile organic compounds (VOCs) on the copper foam's surface. This explanation is further supported by observing the same wettability change towards hydrophobicity when immersing hydrophilic copper metal foams in a liquid VOC (α-Pinene).

4.2 Introduction

Wetting property of a porous material is a key property to determine the suitability of the material as a wicking element. A hydrophilic wick system is necessary to transport water in capillary-driven systems such as heat pipes and heat spreaders increasingly used for

electronics cooling [26]. When one end of a heat pipe is connected to a heat source, such as a hot microprocessor, heat is removed by evaporating water enclosed in the pipe. The vapor travels to the other end of the heat pipe where it condenses [54]. The water is pumped back to the hot end by the capillary action of the wicking material inserted in the pipe. It is shown that low wettability of the wicking material directly reduces the critical heat load that can be carried by a heat pipe[88]. The degree of wettability of a flat surface by a specific liquid can be shown by measuring the contact angle (CA) of a droplet of that liquid on the surface. For water as the liquid, a surface is called hydrophilic when CA < 90°, and hydrophobic when CA > 90°. When the CA of water is larger than 150°, it is called superhydrophobic and when the CA of water is almost 0°, it is called superhydrophilic [20].

Among different materials used in engineering, copper is widely used in many industrial applications. Due to its high thermal conductivity, moderate cost and good thermal contact, copper is a major candidate to make thermal management components for electronics cooling. Copper based porous materials such as sintered copper powder, have been used as the heat transfer medium in capillary driven systems such as flat heat pipes and vapor chambers for electronic cooling [83, 86]. Copper open cell metal foams are among more recent copper based porous materials which offer a high permeability, high surface area and high capillary pumping capacity. These properties make them interesting candidates as the wicking material in flat heat pipes and thermal spreaders [70].

Copper metal foams are superhydrophilic as they leave the production line. The high surface wettability combined with their porous structure yields high capillary forces which is favorable for a wicking material. A water droplet spreads on their surface immediately and is pulled into their porous structure due to high capillary forces. But after exposure to room ambient air, they gradually lose their superhydrophilic property and eventually turn into hydrophobic surfaces; a water droplet remains on the surface and does not penetrate inside the foam. Moreover, the measured contact angle is more than 90° (~136°) for a copper metal foam left in the room ambient for several days. A contact angle of more than 90° implies a hydrophobic surface which is not favorable for heat pipe applications. The same phenomenon

also happens for sintered copper powder wicks while exposed to ambient air. In order to restore the hydrophilicity of the foams and use them as wicking material, a hydrogen reduction process is typically done on the foams right before inserting them in the heat pipes. Then, the heat pipe container is evacuated, water is added inside, and the end of the heat pipe is sealed.

The widely accepted reason for the loss of hydrophilicity in the heat pipe industry is oxidation [58]. According to this common belief, often found in the literature, copper oxides form on the surface of the foam and they change the surface energy of the copper, making it hydrophobic. Faghri [18] states that copper oxides can reduce the wetting characteristics of a surface. He has also suggested methods to remove the copper oxides by immersion of the wick in the deoxidizing agents. Iverson et al. [34], although implying the role of the organic contaminants, use a hydrogen-rich reducing atmosphere to reduce any oxide present on the surface of the sintered copper powder wicks. Weibel et al. [86] have treated the sintered copper powder wicks by diluted Piranha solution (H_2SO_4 and H_2O_2) and deionized (DI) water to remove any grease contamination and surface oxidation. Recently, Wong and Lin[88] implied the role of 'hydrophobic Cu_2O' formation with time on the copper surface, for the hydrophilicity loss of copper mesh wicks.

Copper has three different oxidation states [9]: Cu(0) (metallic copper), Cu(I) (cuprous oxide, Cu_2O), Cu(II) (Cupric oxide, CuO). When exposed to air, a mixed film of cuprous oxide (Cu_2O), cupric oxide (CuO), cupric hydroxide ($Cu(OH)_2$), chemisorbed water, and carboxylate species is formed. Water with dissolved oxygen can produce the following reactions with the copper surface:

$$\begin{aligned} 2Cu + H_2O &\rightarrow Cu_2O + H_2 \\ Cu + H_2O &\rightarrow CuO + H_2 \\ Cu + 2H_2O &\rightarrow Cu(OH)_2 + H_2 \end{aligned} \qquad 4.1$$

Any of these three oxidation products can be present, provided that no kinetic limitations exist. Previous studies have identified that Copper oxides can have different microscopic morphologies and chemistry, and therefore, different wetting properties. Interestingly, there is

a relatively vast body of knowledge in the literature that clearly proves that copper oxides are hydrophilic in the as prepared state and hydrophobicity is assigned to them by using different chemicals (Teflon for instance) to lower their surface energy [11, 12, 45, 46, 52, 82, 89]. For instance, Hong et al. [32] have measured the contact angle on the nonoxidized and oxidized copper plate and concluded that water contact angle is lower on the oxidized copper surface.

Furthermore, in some studies on heat pipes, oxidation has been employed to render a copper based porous material hydrophilic. Hwang et al. [33] have used thermal oxidation to change the wettability of sintered copper wick form hydrophobicity (CA~94°) to hydrophilic (CA~43°). Nam and Ju [53] have employed chemical oxidation to grow CuO nanostructures on the non-wetting cupper post wicks to make them superhydrophilic. Popova et al. [60] have also used a thin layer (~3 μm) of CuO to enhance the wetting of a sintered copper wick of a thin flat heat pipe. We also observed the same hydrophobic to hydrophilic wettability change by growing CuO copper oxides on the surface of the foams via a thermal scheme. To explain this, Salmeron et al. [66] clearly show the important role of the dangling H-bonds at the surface for the subsequent growth of the wetting water films. For the oxides like TiO_2, Cu_2O and Si_2O, the presence of a small amount of O vacancies leads to the formation of OH groups. These surface hydroxyls will nucleate the subsequent growth of the molecular water [26].

It can be seen that there is an obvious controversy in the literature as to whether copper oxidation is the cause of hydrophobicity of copper porous materials or rather, a means to render these materials hydrophilic. We will show that volatile organic compounds (VOC) adsorbed on the copper surface are the reason for the hydrophobicity of foams. In fact, the profound effect of the adsorption of even a very thin film of the greasy material in air on a solid surface has been known for a long time [1, 2]. Yin et al. [90] have shown that volatile organic contaminations are the main reason for the loss of hydrophilicity in the superhydrophilic TiO_2 layer. Smith [77] has investigated the surface of the clean gold and has concluded that the hydrophilic surface of clean gold can become hydrophobic in the ambient air due to the formation of a carbon monolayer. The hydrophobic effect of the adsorption of

organic contaminations on the silicon wafers exposed to air is also well known in the silicon wafer industry [24, 35, 63].

The purpose of this paper is to shed light on the fact that volatile organic contaminations are responsible for hydrophilic to hydrophobic behavior change of copper metal foams when exposed to ambient air, and not oxidation. Although here we have presented the results for copper metal foams, but we believe that the same explanation can be given for the same hydrophilic to hydrophobic transition occurring in sintered copper or copper mesh wicking materials. In this work, the mechanism of hydrophobicity of copper metal foams is first discussed by comparing CA on metal foams and copper plates. Then, the effect of room ambient air, extra dry pure air and nitrogen atmosphere on the rate of hydrophilicity loss of copper metal foams is investigated by a novel method based on measuring the spreading time of a droplet on the porous foam. The time variation of chemical composition on the surface is studied by surface characterization techniques such as XPS and TOF-SIMS. Finally, the effect of a volatile organic compound (α-pinene) on the hydrophilic copper metal foam is also studied.

4.3 Experimental Methods

4.3.1 Sample preparation

Copper plates (99.9% purity, 0.8mm thickness) are used to compare CA measurement with the results of the copper foam samples. Each copper plate is polished with 100, 180, 240, 400 grit sandpapers. The copper plate samples were dried in a nitrogen flow. Copper metal foams with 75 pores per inch (PPI) and 80% porosity in the form of 15 × 15 × 0.7mm pieces were provided by Metafoam Technologies, Inc and were used in this study. No cleaning process was performed on the copper foam samples. As it can be seen in Figure 4.1 (a) and (b), the foams have a spherical cluster structure (SCS) with the approximate diameter of 10-50μm and unlike other types of metal foams, no ligaments can be observed. This morphology is also different than other types of foams which usually have cells shaped as polygons and resembles

more to sintered copper powder. Distinct pores are hard to find and several through holes are observed.

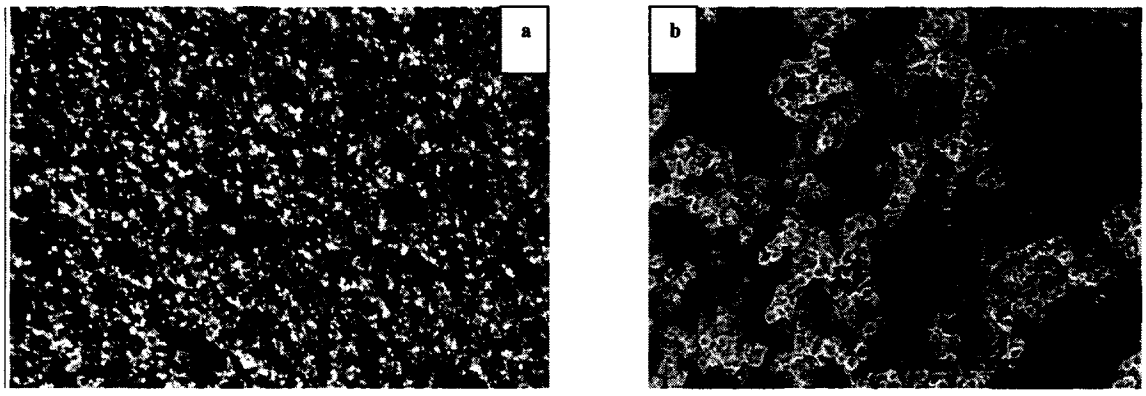

Figure 4.1. Morphology of the 75 PPI copper metal foams: (a) optical image of the copper foam surface (b) low magnification SEM (×70) of the foam structure.

4.3.2 Reduction process by hydrogen

Hydrogen reduction is based on the reduction of the oxygen on the surface to render a pure copper alloy surface. This can be explained by

$$\begin{aligned} CuO + H_2 &\rightarrow Cu + H_2O \\ Cu_2O + H_2 &\rightarrow 2Cu + H_2O \end{aligned} \qquad 4.2$$

In order to restore the lost hydrophilicity of copper metal foams, a hydrogen reduction process is done on the foam samples. A gas mixture of 7% Hydrogen (99.9999% purity) and 93% nitrogen (99.9999% purity) with a total volume flow rate of 150mL/min is injected into a tube furnace. The heating process is composed of a ramp from room temperature (~20 °C) to 600 °C in 2 hours and followed by a 2 hours plateau at 600 °C. Then the heat is shut off and the sample is left to cool gradually under the gas mixture. This method was found to be very effective to make the foams hydrophilic as will be demonstrated in section 4.4.

4.3.3 Time-of-spreading test setup

For smooth surfaces, contact angle measurement can be used as a tool to quantify the hydrophilicity loss in time. But the major difficulty to measure hydrophilicity loss rate for porous materials is that, unlike a flat surface, it's not possible to measure the contact angle on a porous hydrophilic material since the water droplet is simply absorbed and disappears. To overcome this problem, a test method is developed to measure the time-of-spreading of a droplet on a porous surface, using the setup schematically shown in Figure 4.2. A micro syringe (Microfil®, model MF 28G-5) is connected to a syringe pump (Harvard apparatus® model PHD 2000). The syringe pump is used to inject a controlled volume of DI water through the syringe. The target volume of the micro pump is set to 8μL and the infuse rate is 20 μL/min. The time for the droplet to spread on the foam's surface is measured by observing the photos taken by a high speed camera (pco®) connected to a zoom lens (Navitar® model zoom 6000) and a computer. The exposure time of the camera is 1μs.

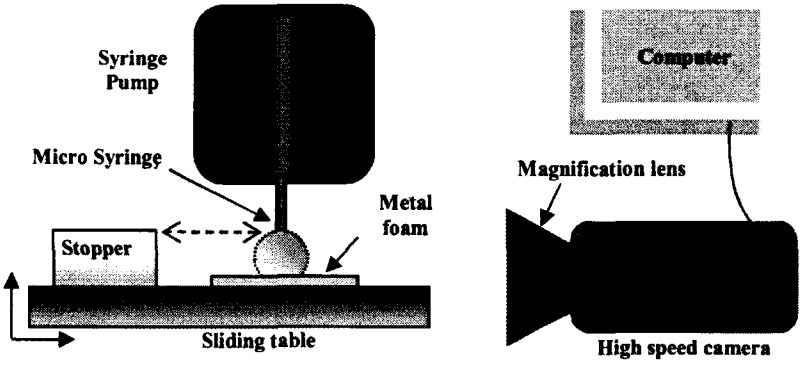

Figure 4.2. Sketch of the time-of-spreading setup

To do each set of measurements, the tip of the micro syringe is initially leveled with the stopper to make sure that the height between the copper metal foam and the tip of the micro syringe is the same for all the samples. By having the same distance from the foam's surface to the tip of the syringe, the maximum droplet volume can be more precisely controlled. A sphere with an approximate volume of 8 μL can be obtained for a stopper thickness of 3.2 mm and a 0.7 mm thick copper metal foam. As the droplet is approaching the surface of the foam, the camera starts recording the pictures and stops when the droplet has disappeared. The

results for a typical hydrophilic foam sample are presented in Figure 4.3, after the reduction process and 3 hours in nitrogen atmosphere. By observing the photos taken visually, the *time-of-spreading* is defined as the duration between the initial deformation of the droplet (as it starts to be absorbed in the foam) until the droplet totally disappears.

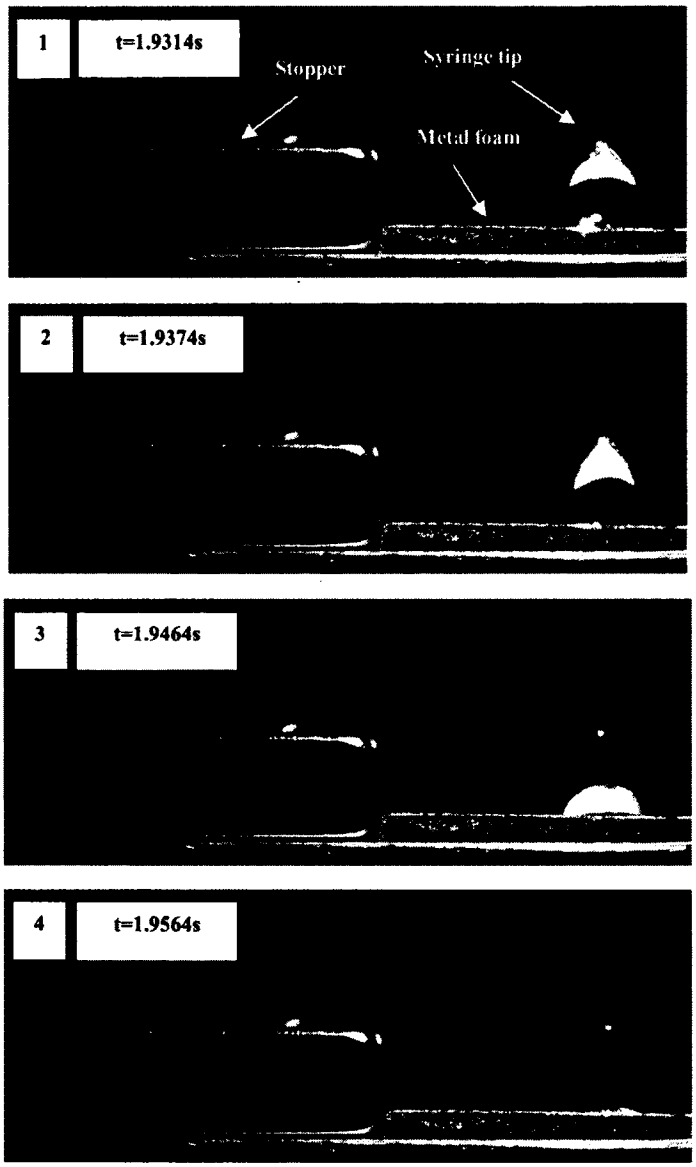

Figure 4.3. Different steps of spreading a water droplet on the surface of a hydrophilic copper foam in 0.025 s

The standard deviation and the average error for the time-of-spreading measurements are estimated to be 9 ms and 28% respectively. The main source of error in this method is the

locally non uniform porosity of the copper metal foams. As it was shown in the SEM photo, the pore diameters are not the same over the entire surface of the foam and hence, depending on where the droplet is deposited on the surface, different capillary forces will act on it.

4.3.4 Characterization techniques

Morphology and microstructures of the foams were observed using a scanning electron microscope (SEM, S-4700, HITACHI, Japan). Surface compositions of the sample were analyzed by an Axis Ultra DLD X-ray photoelectron spectroscope, XPS (Kratos Analytical Ltd., UK), equipped with a standard monochromator Al/ Ka source (hv = 1486.6 eV)) used at 15kV and 15mA and, an analyzer pass energy of 20 eV and 160 eV for the high resolution and survey scan respectively. The analysis area (700 μm x 300 μm) was defined by an aperture in the transfer lens column. The Kratos charge neutralizer system was used on all samples and no correction of charging effect was performed. Spectra were analysed using CasaXPS software (version 2.3.15). Time-of-Flight Secondary Ion Mass Spectrometry (TOF-SIMS) is another surface characterization method with the penetration depth which is only the outermost (1-2) atomic layers of the sample surface. TOF-SIMS studies were performed on a TOF-SIMS IV (Munster, Germany), with an operating pressure of approximately 2×10−8 Torr. Samples were bombarded with a source of Bi3++ at an energy level of 25 KeV. The gun operated with a pulse width of 19ns and, 0.3 pA pulsed ion current over a frame area of 10 μm × 10 μm for a dosage below the threshold level of 5×10^{11} ions/cm^2 for static SIMS.

4.4 Hydrophobicity mechanism

Wettability of a surface can be manipulated by two general methods, either by changing the surface free energy or texturing it to alter surface geometrical structure. The relation between the surface energy and wetting could be described by the Young equation [26]:

$$\cos\theta_Y = \frac{\gamma_{SG} - \gamma_{SL}}{\gamma_{GL}} \qquad 4.3$$

where θ_Y is the contact angle (CA) and is dependent on the liquid-solid pair used. The three coefficients γ are the surface tensions at the solid/gas (γ_{SG}), solid/liquid (γ_{SL}) and gas/liquid (γ_{GL}) interfaces, respectively. Liquid motion in a capillary path can be achieved if the dry tube has a surface energy γ_{SG} greater than the surface energy γ_{SL} of the same path when wet.[26] Generally, surfaces with high γ_{SG} (~500-5000mN/m) are called high energy surfaces on which almost all liquids spread. Clean metallic surfaces are considered as high energy surfaces.

For a given surface chemistry, the degree of wettability of a surface can be controlled by enhancing the material's roughness. Increasing the roughness will make a hydrophilic surface more hydrophilic while a hydrophobic surface will become more hydrophobic. There are two well-known models to describe the effect of roughness on the wettability. If the roughness scale is much smaller than the size of the drop, the complete penetration of the liquid on a chemically homogenous surface can be described by the Wenzel theory [26, 95]:

$$\cos\theta_w = r\cos\theta_Y \tag{4.4}$$

where θ_w is the Wenzel contact angle and $r > 1$ is the roughness, i.e. the actual area of the textured surface projected on the plane of the solid. It can be seen that since r > 1, roughness effect will always augment the original state of wettability. However, if the liquid is not completely filling the nooks and crannies of the surface then some air or vapor is trapped beneath the liquid drop. To describe the wetting of this chemically heterogeneous surface another model is proposed which is called Cassie-Baxter:

$$\cos\theta_{CB} = r_f f\cos\theta_Y + f - 1 \tag{4.5}$$

where θ_{CB} is the Cassie–Baxter contact angle, f is the relative fraction of the projected solid surface that is wetted by the liquid, and r_f is the roughness ratio of the wet area. When $f = 1$ and $r_f = r$, Eqn. 4.5 turns into the Wenzel equation.

In Figure 4.4, the impact of the hydrogen reduction process on copper metal foams and copper plates is compared to determine the hydrophobicity mechanism of copper metal foams. Figure

4.4 (a) and (b) show the CA of a droplet of water (8μl) before the hydrogen reduction on copper metal foam and copper plate, respectively. It can be seen that although both materials are hydrophobic (CA>90°), the CA on copper metal foam (CA~136°) is higher compared with the copper plate (CA~96°). After the hydrogen reduction process (Figure 4.4(c) and (d)), both materials become hydrophilic but the copper metal foam acts superhydrophilically while the CA on the copper plate is ~47°. After the hydrogen reduction process, the copper plate is clean, exhibits the highest surface energy and is thus hydrophilic. Due to the porous structure of the copper metal foam, the hydrophilic surface will yield high capillary forces and the foam therefore draws the water in almost instantly. It can be proposed that the adsorption of the organic contamination on the copper surface when exposed to ambient air, the surface energy lowers to the point that copper plate becomes hydrophobic. The same effect occurs on the copper foam surface and the droplet remains on the foam's surface. The pores and roughness of the foam intensifies the hydrophobicity and the CA on the foam's surface is higher compared with the copper plate. These results, suggest that the hydrophobicity in copper metal foams is Wenzel type because roughness simply enhances the already hydrophilic or hydrophobic behavior of the foams. Open cell foams provide exit paths for the trapped air under droplets and hence, the hydrophobicity mechanism does not follow the Cassie–Baxter model. This further implies that the roughness, although important in intensifying the wetting state of foams, has no effect on the transition from hydrophilic to hydrophobic behavior studied here. Therefore, the wettability transition should be explained by the change in the surface chemistry and consequently energy surface of the metal foams while exposed to air. This will be shown in more detail in section 4.5. First, quantitative measurements for wettability will be presented for hydrophilic copper foams using a transient method.

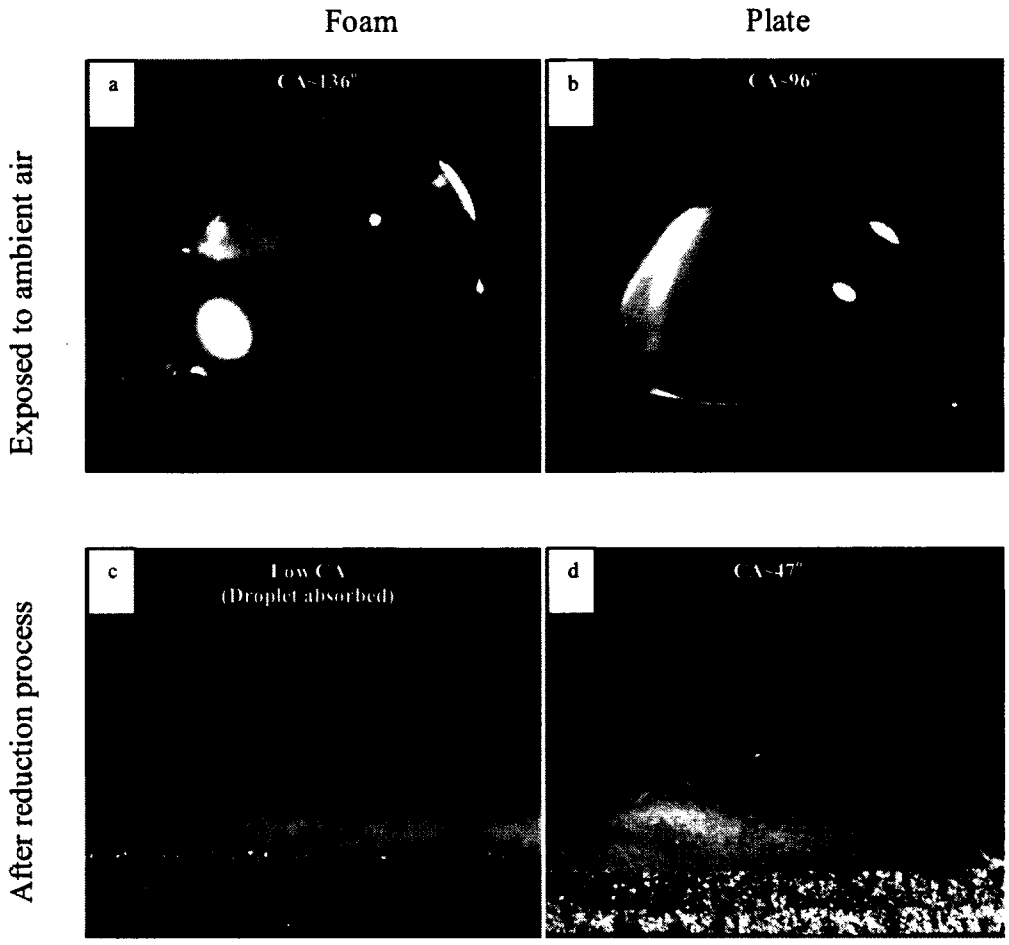

Figure 4.4. Effect of the hydrogen reduction process on the (a) copper metal foam sample exposed to air and before hydrogen reduction , CA~136° (b) copper plate sample exposed to air and before hydrogen reduction , CA~96° (c) copper metal foam after hydrogen reduction , apparent CA~0° (droplet absorbed in the foam) (d) copper plate sample after hydrogen reduction , CA~47°

4.5 Experimental Results

4.5.1 Effect of ambient atmosphere on the time-of-spreading

In order to compare the effect of ambient atmosphere on the surface chemistry and wettability of the foam surface, time-of-spreading of the droplet is obtained and compared for identical copper foam samples under the effect of ambient air, nitrogen and extra dry pure air. First, hydrogen reduction is done on the foams to make them hydrophilic. Then, hydrophilic copper

foam samples are exposed to different gas atmospheres (room air, extra dry pure air, and nitrogen) and the effect of gas atmosphere on the time-of-spreading of a water droplet is investigated. Three identical foam samples are used for each measurement and the spreading time of the droplet on the foam's surfaces is averaged over these 3 samples. The tests are done immediately after the hydrogen reduction treatment (0h), then after 3, 6, 9, 24, 48, and 96 hours, and the results can be seen in Figure 4.5(a) and (b). The samples in the ambient air were left uncovered in the laboratory during the tests while samples under nitrogen and extra dry pure air were kept in a closed desiccator filled with the corresponding gases. During the handling and setup of the samples, gloves were worn to prevent contamination. The time that the samples were left in ambient air for each time-of-spreading measurement is estimated to be no more than 10 minutes. It can be seen that in ambient air, the samples become hydrophobic after 48 hours while samples exposed to nitrogen and clean air remain hydrophilic even after 96 hours. In fact, purified air and ambient air both contain oxygen and would both cause oxidation on the surface of the foam. The higher rate of hydrophilicity loss for the samples exposed to ambient may be attributed to the adsorption of the volatile organic compounds (VOC) in the ambient air while VOCs are not present in the purified gases. Also, results suggest that the time-of-spreading is practically the same when the samples are exposed to nitrogen or purified air atmospheres, supporting that oxidation is not a plausible cause.

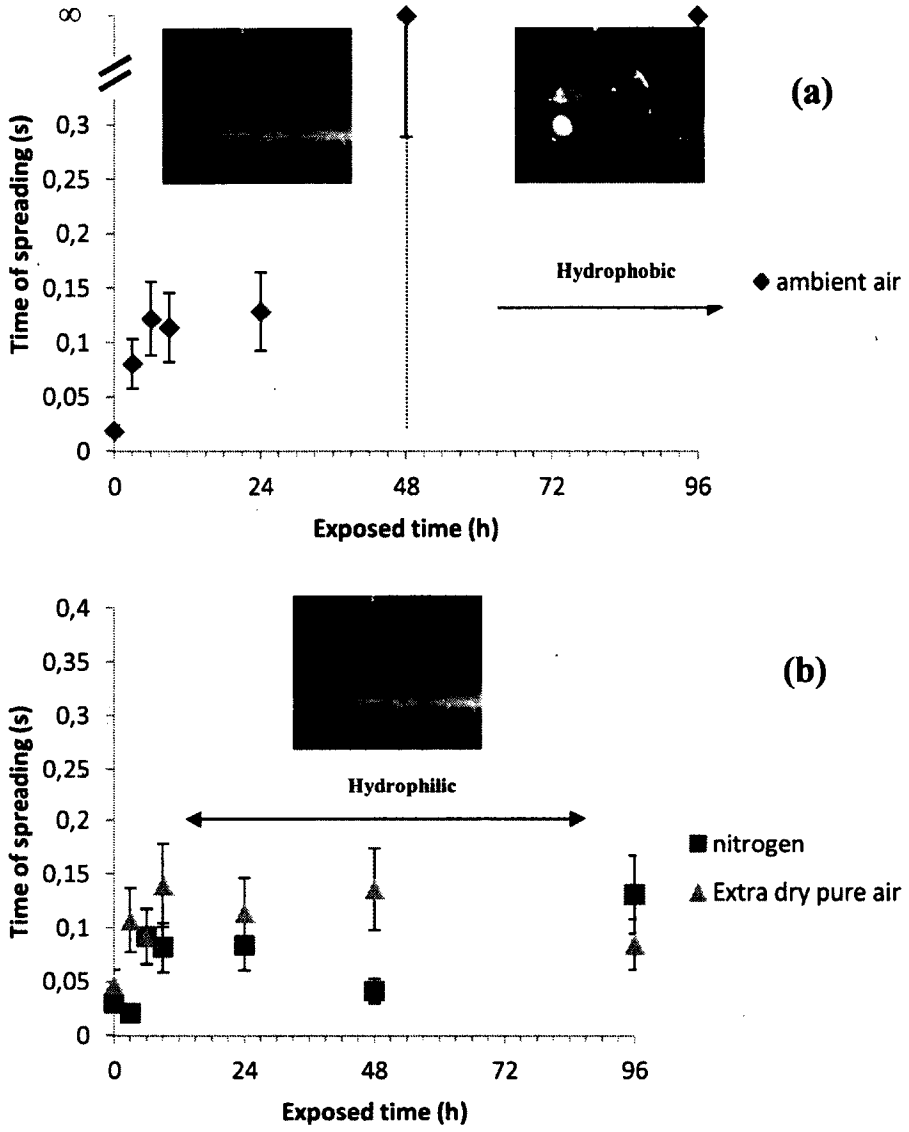

Figure 4.5. Variation of the time-of-spreading for the copper metal foams in (a) ambient air, showing hydrophobic transition; (b) nitrogen and extra dry pure air that remains hydrophilic.

4.5.2 XPS

The effect of ambient air on the surface chemical compositions of three identical copper metal foam samples are analyzed by XPS in the time intervals of 0h (after hydrogen reduction treatment), 3 hours, 6 hours and 48 hours and the results for sample 3 are presented in this section. Other samples show the same trends, so their results are not presented here.

Quantification of elemental composition was done using the survey scan, and, an example is shown in Figure 4.6 for sample 3 at 0h. It can be seen that different elements, essentially copper, carbon, oxygen and tin exist on the surface of the foam. Although the time from taking out the samples from the reducing furnace and then putting it in the vacuum chamber of the XPS is estimated to be less than 5 minutes, there is still 35.1% of C present on the surface. Scheuerlein and Taborelli [81] have shown that even a 1 minute exposure of a clean metallic Cu surface to air will cause at least 20% carbon surface atomic concentration. Therefore, XPS will always indicate at least such an amount of carbon after transferring the samples to the device through ambient air.

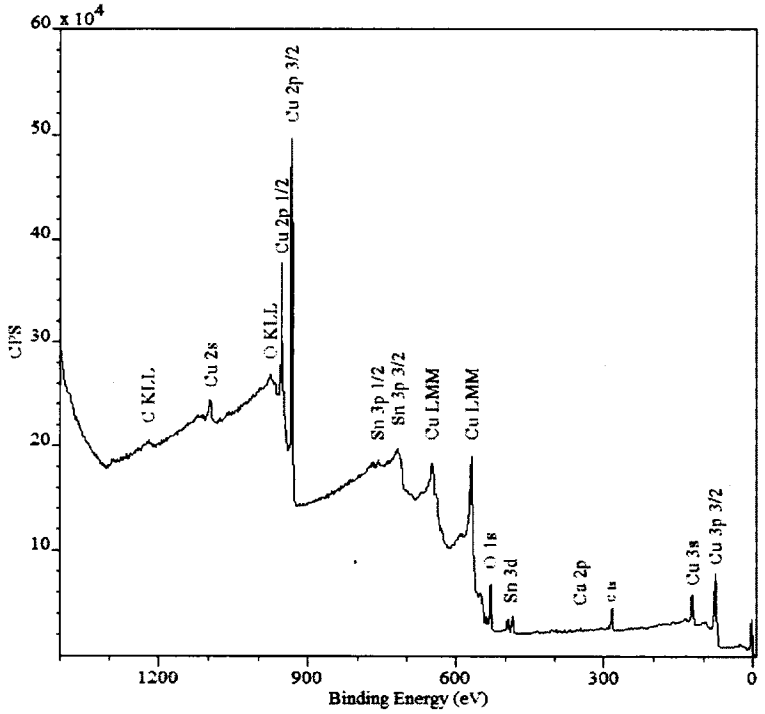

Figure 4.6. Typical XPS survey spectrum of the copper metal foam surface (sample 3) after hydrogen reduction (0h)

Figure 4.7 shows the XPS C 1s spectral signature of the copper metal foams at different stored times in ambient air. The peaks at 284.6 and 288 eV binding energies are attributed to the C-C and O-C=O correspondingly [65]. It can be seen that the carbon content is non zero at the 0h (after hydrogen reduction) and increases with time. After 48 hours it reaches the maximum amount. The increase in time of surface concentration of C (carbon content) on the foam

sample is also shown in Table 4.1. This increase suggests the adsorption of volatile organic contaminations on the copper metal foam surface. Carbon content at 3 hours is slightly higher than 6 hours which is not expected. It can be explained by non uniform contamination of the copper foams while exposed to air and the small analysis surface area in XPS.

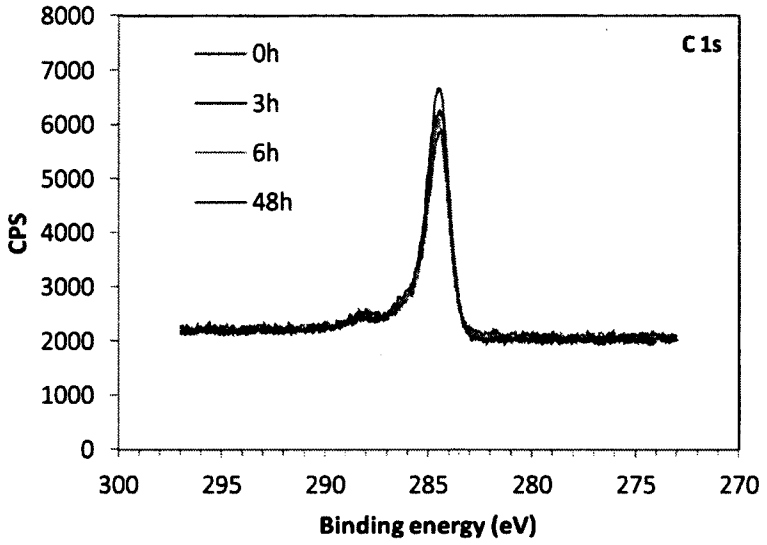

Figure 4.7. XPS C 1s spectra for copper metal foam showing the increase in carbon content with aging time.

In Figure 4.8, the time dependence of the Cu 2p spectra and Cu $L_3M_{4,5}M_{4,5}$ Auger spectra is showed for 0h to 48h. According to the curve fitting based on the model developed by Biesinger and al [5], the Auger spectra and the O 1s spectra (Figure 4.9), the two major species of the sample are Cu metal and Cu_2O. There is some CuO and $Cu(OH)_2$ but in a very small amount. The inspection of the spectra at 0h, 3h, 6h and 48h reveals that the surface concentration of Cu_2O, and $Cu(OH)_2$ increase slightly and CuO decreases very slightly, as shown in Table 4.1. But the major difference is the large decrease of Cu metal content. In fact, Auger spectra show that there is a significant change in the amount of the Cu metal while the amount of the copper oxides does not change significantly. It is probably due to the formation of a layer of volatile organic compounds on the surface of the foams.

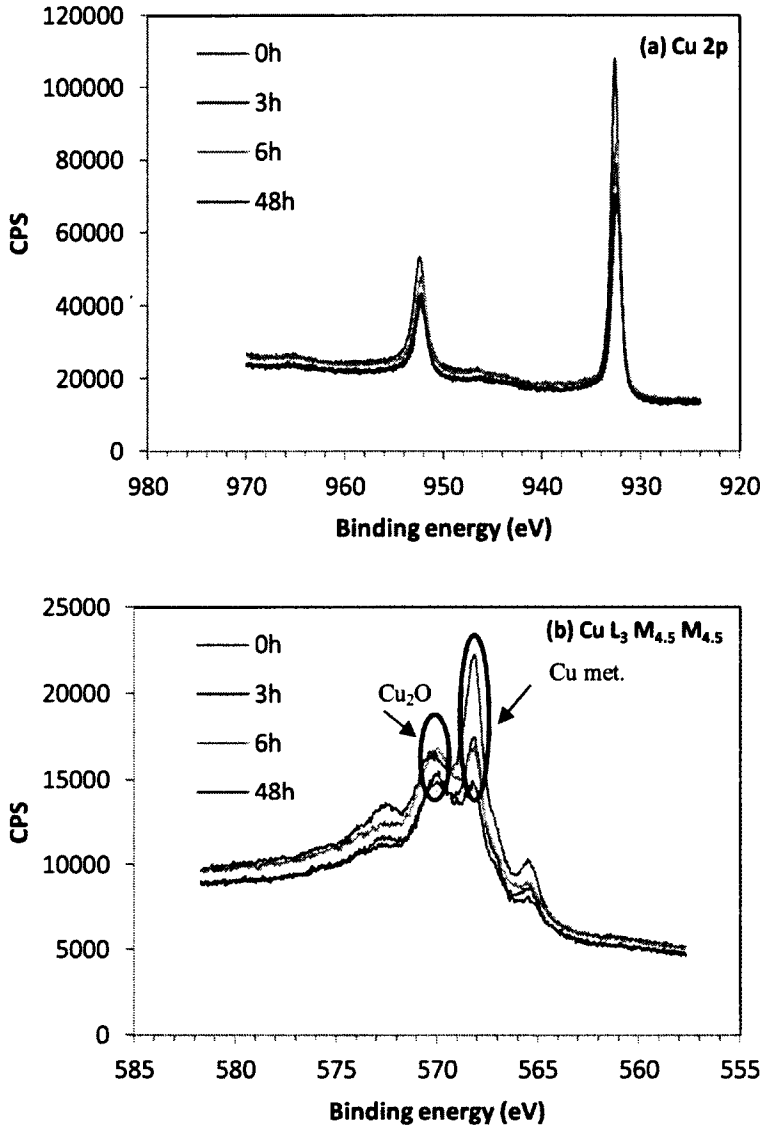

Figure 4.8. Dependence of (a) XPS Cu 2p and (b) Auger Cu $L_3M_{4.5}M_{4.5}$ spectra on time for copper metal foam

The variation of the O 1s core level spectra in time is shown in Figure 4.9. At 0h, core level peak at the binding energy of 530.4eV confirms the existence of Cu_2O. A slight widening at the shoulder of the peaks (at 531.4eV) appears when the samples are exposed to air and it increases as the time goes on. It can be attributed to a small increase in the concentration of $Cu(OH)_2$. The average surface concentration of oxygen increases slightly over time, as it can

be seen in Table 4.1. It is possibly due to the formation of chemical bonds between the oxygen and the adsorbed carbons and to the formation of $Cu(OH)_2$ and Cu_2O.

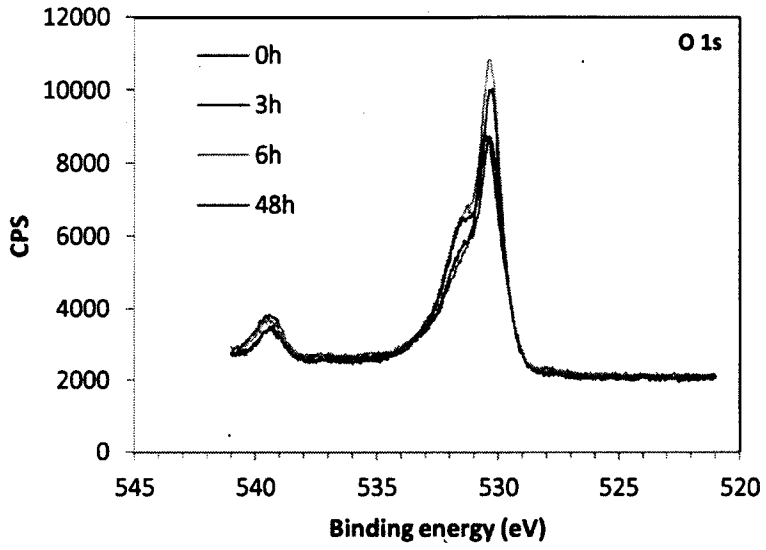

Figure 4.9. Time variation of the XPS O 1s spectra for copper metal foam.

Table 4.1. Percent (%) surface Atomic concentration

	C 1s	Cu 2p				O 1s	Ca 2p/ Sn 3d
		Cu met.	Cu_2O	$Cu(OH)_2$	CuO		
0h	35.1	29.3	7.7	2.8	1.4	22.1	2.1
3h	38.6	19.6	8.3	3.1	1.4	25.6	2
6h	34.7 41.7	17.8	10.1	4.4	1.2	28 26.6	1.5 1.4
48h		13.5	10	5.4	0		

4.5.3 TOF-SIMS

The impact of the ambient air on the copper metal foam surface is also investigated by TOF-SIMS. Two identical copper metal foam samples (with the hydrogen reduction done by Metafoam Company) are used in this test and the results for one sample are presented here. After opening the airtight packaging, both of the samples are analyzed by TOF-SIMS. The samples are then left in the lab ambient for 3 hours and the analysis is performed again. Figure

4.10 shows the positive ion TOF-SIMS spectra (left) and negative TOF-SIMS spectra (right) for the sample after opening the package and then after being exposed to air for 3 hours. It can be seen that room ambient air has a clear effect on the compositions of the foam surface. To quantify this effect, peak intensities are normalized with respect to copper (^{63}Cu) at 100%.

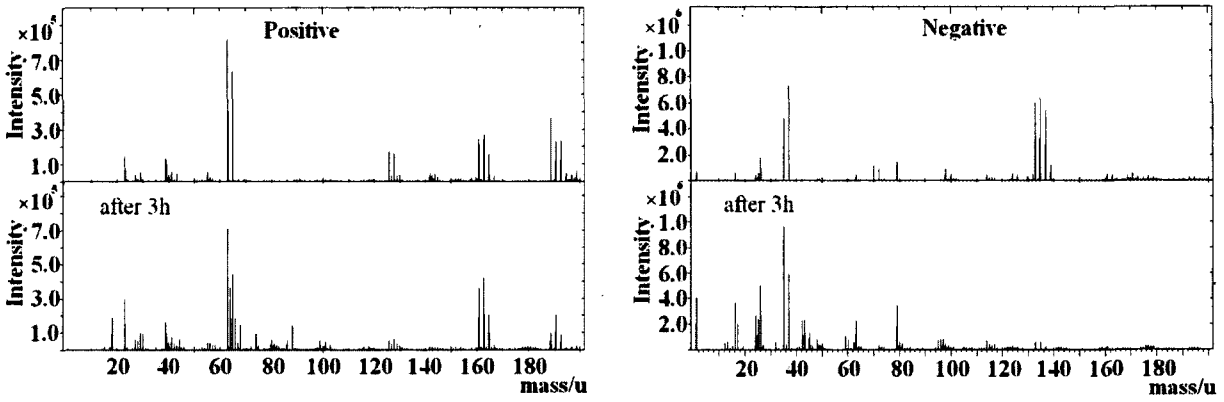

Figure 4.10. Positive ion TOF-SIMS spectra (left) and negative TOF-SIMS spectra (right) for two identical samples

Table 4.2. Positive ions with the most significant increase after 3 hours exposure to room ambient air (peak intensities normalized with respect to the copper at 100%)

Ion group	Ion	Ion mass	0h	After 3h
C_xH_y	CH_3	15	0.5%	1.8%
	C_2H_2	26	0.3%	0.8%
	C_2H_3	27	4%	7 %
	C_2H_5	29	5.3%	10.3%
	C_4H_6	54	0.3%	0.8%
	C_6H_8	80	0.07%	0.17%
C_xH_yO	C_3H_5O	57	0.1%	0.33%
C_xH_yNO	C_2H_5NO	59	0.03%	0.2%
	C_2H_6NO	60	0.01%	0.12%
	C_3H_6NO	72	0.05%	0.3%
	C_3H_7NO	73	0.06%	0.3%
	C_4H_7NO	85	0.01%	0.2%
C_xH_yN	$C_5H_{12}N$	86	0.9%	4.18%

The ions with the most significant increase after 3 hours exposure to air are presented in

Table 4.2 and Table 4.3 for positive and negative ions respectively. It can be seen that, after being exposed to air, in the positive polarity the ions with the most significant increase are: CxHy, CxHyO, CxHyNO and CxHyN. In the negative polarity, the ions with the most significant increase are: CxHyO, CuOxH, CuCHxO and C2F2. These results, confirm the XPS

results as they show an increase in the carbon content and also copper hydroxide on the foam surface. Although, not presented in the tables, but the ions having the chemical formula of Cu_xCl_y and CPO decreased after being exposed to air for 3 hours. Because Na, Cl and PO_x are present on all samples, they possibly stem from the contamination while manipulating the samples.

Table 4.3. Negative ions with the most significant increase after 3 hours exposure to room ambient air (peak intensities normalized with respect to the copper at 100%)

Ion group	Ion	Ion mass	0h	After 3h
C_xH_yO	$C_2H_2O_2$	58	5%	14%
	$C_2H_3O_2$	59	9%	316%
C_2F_2	C_2F_2	62	7.4%	124%
CuO_xH	CuOH	80	8.41%	50.5%
	CuO_2H	96	7.8%	96%
$CuCH_xO$	$CuCH_3O$	94	1.06%	21.6%

4.6 Discussion on wettability of the foams and the carbon content

As it was mentioned in section 4.5.1, the initially superhydrophilic foam samples become hydrophobic after 48 hours being exposed to room ambient air while the samples in the pure air and nitrogen remain hydrophilic even after 96 hours. Given that oxygen and oxidation occurs at both cases, the wettability change should be explained by a reason other than oxidation of the surface. In addition, as it was stated in section 4.5.2, XPS results in Table 4.1 show that copper oxides content on the surface does not change significantly during 48 hours (Cu_2O as the most abundant oxide increases form 7.7% to 10%) whereas metallic copper reduces significantly from 29.3% to 13.5%. In fact, during 48 hours, the metallic surface is covered by a molecular layer and this layer, obviously is not an oxide. The same layer is also responsible for the hydrophobic behavior of the foams. To explain this, it can be seen in Table 4.1 that the average carbon content is 35.1% in the 0h and it increases until reaching 41.7% at 48h. To clarify this point, Figure 4.11 shows the variation of surface atomic concentration of total carbon content (based on XPS results in Table 1) and two of its species versus the time-of-spreading of water for a sample left in room ambient over time. Results in different time intervals are obtained by performing one rate-of-rise test and one XPS analysis for each time interval and C-C and O-C=O data points are extracted from the original C 1s curve by

deconvolution. It can be seen that as the time of spreading increases (sample becomes more hydrophobic), more carbon content is detected on the surface. As it was explained before, the unexpected decrease in the carbon content of the sample after 6h can be attributed to the non uniform contamination of copper foam. Furthermore, TOF-SIMS results show an increase in the carbon based compositions after 3 hours. These results suggest that after the hydrogen reduction, the adsorbed volatile organic compounds accumulate on the active metallic copper foam's surface as a layer and they decrease the energy surface of the foams. In fact, the reduction process renders a highly clean and active surface by removing the copper oxides but at the same time desorption of the organic contamination. After exposure to air, volatile organic contamination adsorbs on the surface and lowers the energy surface and eventually will lead to a hydrophobic surface. The same phenomenon is expected to occur at other copper based wicking materials such as sintered copper powder and copper mesh.

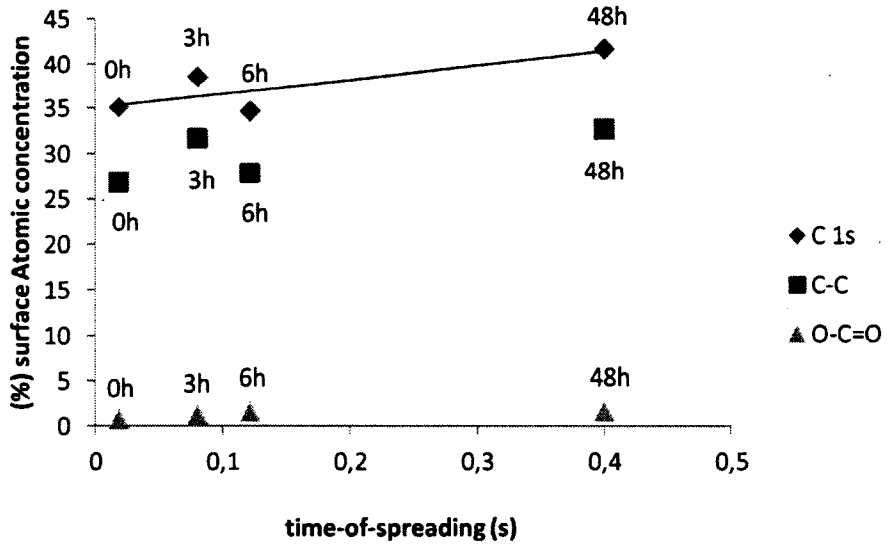

Figure 4.11. Percentage of surface atomic concentration of total carbon content (C 1s) and other carbon species with the water time-of-spreading for a copper metal foam left in room ambient air over time

4.6.1 Effect of an organic compound, α-Pinene

To simulate the effect of an organic compound on the wettability of copper metal foams, samples were exposed to α-Pinene ($C_{10}H_{16}$, Sigma aldrich, 97%). α-Pinene is a hydrophobic

organic compound with a low solubility in water (maximum water solubility of 5-10 mg/l) that is naturally present in softwoods [51]. Hydrogen treated foam samples (initially hydrophilic) were dipped in the α-Pinene solution and then dried with nitrogen flow. The contact angle was measured and it was observed that the foams were superhydrophobic. This further confirms that organic contamination can be responsible for the behavior change of copper metal foams from hydrophilic to hydrophobic.

4.7 Conclusions

The reason for the hydrophilicity loss of copper metal foams in the ambient air was investigated in this work. Analysis of driving mechanisms was conducted, considering surface chemistry and morphology. A novel approach was employed to quantify the loss of hydrophilicity rate by measuring the spreading time of a droplet on the foam's surface by using a high speed camera. The time dependence of the chemical composition of the foam's surface was investigated by using XPS and TOF-SIMS. The proposed explanation for the hydrophilicity loss was tested by using an organic compound and the proposed hypothesis was confirmed. The key findings of this study include:

- By comparing the CA on the hydrophilic and hydrophobic copper metal foams and copper plate, it can be concluded that the hydrophobicity mechanism is of Wenzel-type and not Cassie–Baxter. Therefore, it can be concluded that the surface chemistry is the main reason to alter the wettability properties of the foam and while surface roughness intensifies the present state of wettability, it has no role for the wettability transition in ambient air.

- Contrary to a common belief in the heat pipe community, the adsorption of volatile organic compounds (VOC) and not the oxidation is the reason for the loss of hydrophilicity in metal foams. Foam samples kept under extra dry pure air remain hydrophilic even after 96 hours while samples kept in the room ambient become hydrophobic after 48 hours.

- Time dependent XPS and TOF-SIMS results show that carbon content on the foam's surface increases. On the other hand, XPS results reveal that the copper oxide content does not change significantly while metallic copper reduces significantly. It can be concluded that the adsorption of the volatile organic compounds on the active surface of metallic copper reduces the metallic Cu and lowers the surface energy of the copper metal foams. It will eventually lead to a hydrophobic surface.

- Low amounts of carbon do not affect the wettability of copper metal foams and only reaching to a certain point of contamination (41.7% of carbon content in this case) will result in hydrophobicity. The impact of high amounts of carbon content on the hydrophobicity of foams is further confirmed by applying an organic contamination (α-Pinene) on the hydrophilic foam, which turned it into a hydrophobic material.

4.8 Acknowledgments

This research was jointly funded by NSERC Canada and Metafoam Technologies Inc. We are grateful for the support and guidance of Dominic Pilon, Sébastien Labbé and Ian Benoit of Metafoam Technologies Inc. and Hugues Ménard of Université de Sherbrooke. TOF-SIMS measurements and data analysis were conducted by Suzie Poulin from École polytechnique de Montreal.

CHAPITRE 5 AVANT-PROPOS

Auteurs et affiliation:

- Mahmood R.S. Shirazy: étudiant au doctorat, Université de Sherbrooke, Faculté de génie, Département de génie mécanique.
- Luc G. Fréchette : professeur, Université de Sherbrooke, Faculté de génie, Département de génie mécanique.

Date d'acceptation: 8 Novembre 2012

État de l'acceptation: version finale publiée

Revue: International Journal of heat and mass transfer

Référence: [72]

Titre français: Propriétés de capillarité et de mouillage des mousses métalliques en cuivre en présence d'évaporation et de murs frittés

Contribution au document:

Cet article contribue à la thèse en déterminant les propriétés capillaires par le taux de montée de liquide dans un matériau poreux. La perméabilité et le rayon effectif des pores, deux paramètres clés qui définissent la capacité de pompage, sont mesurés expérimentalement. Cet article résume des efforts pour couvrir l'aspect de capillarité de cette thèse et il sert comme une étape initiale avant le chapitre suivant sur l'évaporation.

Résumé français :

Une étude expérimentale a été faite pour définir les caractéristiques de mouillage et de capillarité d'un nouveau type de mousse métallique de cuivre qui doit être utilisé comme une mèche à caloducs plats pour le refroidissement électronique. Contrairement à d'autres mousses

métalliques, une microstructure comprenant des particules d'échelle microscopique et les grands chemins capillaires peuvent être observés dans ce type de mousse métallique en cuivre. En raison de l'importance considérable des propriétés telles que la perméabilité capillaire (K) et le rayon de pore effectif (r_{eff}) pour définir la limite capillaire de caloducs, la méthode de taux de montée de liquide basé sur la masse mesurée est utilisée pour extraire ces paramètres. Des mousses de porosités différentes (68% à 85%) ont été entièrement caractérisés avec plusieurs fluides (eau, l'acétone et l'éthanol). Le ratio K/r_{eff} trouvé est près de 5 fois plus grand que celui de la poudre de cuivre fritté, un matériau de mèche commun dans les caloducs. L'impact de l'évaporation et des parois frittées sur une face ou sur les deux côtés de bandes de mousse a été étudié dans l'air ambiant et partiellement saturé. Le taux d'évaporation en cours de montée de liquide a été mesuré en soustrayant la masse de liquide stocké dans la mousse de la masse totale. Il a été constaté que le taux d'évaporation pendant que le liquide est en monté est nettement plus faible que le taux d'évaporation d'un échantillon saturé avec un liquide stationnaire. On a également observé que les murs de cuivre frittés n'a presque aucun effet sur la montée capillaire et sur le taux d'évaporation. En combinant les mesures effectuées avec de l'acétone et de l'eau, l'angle de contact interne de l'eau dans les mousses de cuivre traitées à l'hydrogène s'est avéré plus faible que sur une plaque plate et varie de 10° à 37° en fonction de la porosité des mousses. Ce travail fournit donc la première caractérisation de K, r_{eff}, et l'angle de contact interne pour ces nouvelles mousses métalliques, mais précises également les conditions dans lesquelles des mesures de taux de montée de liquide devraient être prises pour l'extraction de paramètres appropriés.

5 CAPILLARY AND WETTING PROPERTIES OF COPPER METAL FOAMS IN THE PRESENCE OF EVAPORATION AND SINTERED WALLS

5.1 Abstract

An experimental study has been done to define the capillary and wetting characteristics of a novel type of copper metal foam which is to be used as a wick in flat heat pipes for electronic cooling. Unlike other metal foams, a microstructure including micro scale particles and larger capillary paths can be observed in this type of copper metal foam. Due to the significant importance of the capillary properties such as permeability (K) and effective pore radius (r_{eff}) in defining the capillary limit of heat pipes, the rate of rise method based on the measured mass was used to extract these parameters. Foams of different porosities (68% to 85%) were fully characterized with multiple fluids (water, acetone, and ethanol). The ratio K/ r_{eff} was found to be almost 5 times larger than that reported for sintered copper powder, a common wicking material in heat pipes. The impact of evaporation and walls sintered on one side or on both sides of foam strips has been studied in open and partially saturated ambient. The evaporation rate during wicking was measured by subtracting the stored mass of liquid in the foam from the total wicked mass. It was found that the rate of evaporation while the liquid is rising is significantly lower than the evaporation rate of a saturated sample with stationary liquid. It was also observed that sintering copper walls has almost no effect on the capillary rise and on the evaporation rate. By combining measurements done with acetone and water, the internal contact angle of water in hydrogen treated copper foams was found to be lower than on a flat plate and varies from 10° to 37° depending on the foams porosity. This work therefore provides the first characterization of K, r_{eff}, and internal contact angle for these novel metal foams, but also clarifies the conditions under which the rate of rise measurements should be done for proper parameter extraction.

5.2 Nomenclature

g	Gravity, m/s^2
h	Liquid height, m
K	Permeability, m^2
m	Liquid mass, kg
$\dot{m}$	Liquid mass flow rate, kg/s
$\dot{m}_e$	Evaporation flux from the surface, kg/m^2 s
m_{evp}	Evaporated liquid mass, kg
m_{st}	Stored liquid mass in the foam, kg
m_{tot}	Total wicked liquid mass, kg
P	Periphery, m
r	Pore radius, m
r_{eff}	Effective pore radius, m
t	Time, s
T	Foam thickness, m
W	Foam width, m
Greek symbols	
φ	Porosity
μ	Viscosity, Pa s
ρ	Liquid density, kg/m^3
Θ	Contact angle, deg.

5.3 Introduction

Wicking materials are the main part of two phase cooling devices increasingly used for thermal management of electronics, such as flat heat pipes and heat spreaders. Due to their capillarity and open pore structure, they carry liquid from the condenser side to the evaporator side in heat pipes or heat spreaders. When one end of a heat pipe is connected to a heat source,

such as a hot microprocessor, heat is removed by the evaporation of the liquid enclosed in the pipe. The vapor travels to the other end of the heat pipe where it condenses [54]. The liquid is pumped back to the hot end by the capillary action of the wicking material inserted in the pipe or chamber. The operating range of heat pipes is subjected to several physical limits. For the case of a flat heat pipe utilizing copper metal foam as wicking material, the dominant limit will be capillary limit [70]. This limit is reached when the capillary pumping of the wicking material is not sufficient to supply the required rate of liquid to evaporator and hence, the evaporator will dry out. Therefore, the pumping capacity of the wicking material is a key parameter in the performance of heat pipes. Typical wicking materials include sintered copper powders, copper meshes and more recently copper metal foams. These wicking materials are characterized by their permeability, pore size, porosity, and thermal conductivity. Copper metal foams used in this research (made by Metafoam technologies Inc.) have shown promising results in heat pipes [57] but their wicking performance has not yet been fully characterized.

Capillary properties of a wicking material such as permeability (K) and effective pore radius (r_{eff}) are critical in defining the capillary limit of heat pipes, because their ratio (K/ r_{eff}) is a measure of pumping capacity of the wicking material [18]. Permeability can be defined as the porous material resistance against the liquid passing through it. A high permeability will result in a lower liquid pressure drop. Permeability is a pure function of the porous material microstructure and does not depend on the liquid used. Effective pore radius on the other hand, depends on the wetting properties of the liquid in the porous structure. The meniscus profile formed at the liquid-vapor interface of each pore is a function of the pore structure and also liquid contact angle on the porous material. Therefore, effective pore radius is rather used instead of geometrical pore radius to account for the effect of liquid contact angle. According to the definition of the effective pore radius, it is related to the actual pore radius of a porous material, r, by the liquid contact angle on that material:

$$r_{eff} = \frac{r}{\cos\theta} \qquad 5.1$$

Effective pore radius is inversely proportional to the liquid contact angle on the solid surface. Hence, a lower liquid contact angle will result in a lower effective pore radius which in turn will increase the K/r_{eff}. Wetting property of a liquid-solid system is defined by measuring the contact angle of the liquid droplet on the solid surface. In the case of water, wettability is expressed by hydrophilic (contact angle less than 90°) and hydrophobic (contact angle more than 90°). It can be concluded that in capillary driven systems such as heat pipes and heat spreaders using water, a hydrophilic wick system is necessary to transport water [26]. It is shown that low wettability of the wicking material directly reduces the critical heat load that can be carried by a heat pipe[88]. Therefore, a good knowledge of these capillary and wetting parameters and a robust method to measure them is important.

The wetting property of a material is commonly determined by measuring the external contact angle of a droplet of liquid on that material (Sessile drop test). This method is not suitable for porous materials since the liquid wicks and disappears under the surface. Furthermore, relating the contact angle on a flat surface to a porous media of the same material can be misleading [28]. The meniscus inside the porous media experiences a complicated 3-D structure which is significantly different from the uniform roughness assumption done in the Sessile drop test. For porous media, a series of methods are available to measure capillary parameters, such as pressure drop measurement for permeability [4, 59], or bubble test and rising meniscus for the effective pore radius [18]. One major drawback in these methods is their inability to deliver both K and r_{eff} parameters at the same time and in one test [31].

A potentially more informative method is based on measuring the transient rate of rise of a liquid in a porous medium by measuring its height visually or the increasing mass with a balance [39]. Unlike the rising meniscus which is a static method based on measuring the maximum height of the liquid in a sample, rate of rise method is a dynamic and time dependent method. By fitting a suitable mathematical model to the rate of rise measurements, one can extract both permeability and effective pore radius, or their ratio. This method can also be used to characterize wetting properties of a porous material (internal contact angle) by doing this test with liquids of different surface tension [23, 28, 29]. The rate of rise method

will therefore be used in this work to extract the permeability, effective pore radius and internal contact angle.

When dealing with the transient movement of a liquid in a porous media rising against gravity (vertical sample), a balance between capillary forces wicking the liquid upwards and the opposing inertial, gravity, viscosity and evaporation-induced forces should be considered. Given the complexity of the physics involved, simplified models were initially developed to characterize wicking properties of porous media. By only balancing the viscous pressure drop with the capillary force, and neglecting the other effects, the widely used Lucas-Washburn equation will be obtained [67]. With this method, K and r_{eff} will be obtained as a ratio. To find the values of K and r_{eff} independently, one needs to find the maximum attainable height or mass. This requires fabrication of long samples which may be impractical in many cases. By adding gravitational effects to the Lucas-Washburn equation, Holley and Faghri [31] developed a different equation which permits the extraction of both K and r_{eff} directly (without finding the maximum height or mass). Evaporation taking place on the surface of the porous material will lead to a higher liquid flow rate to accommodate for the evaporated liquid. By assuming a uniform rate of evaporation over the wetted area of their samples, Fries et al [22] developed a fully implicit solution for all the effects except for inertia, but their experimental results show a 20% difference from their modeling results. Rogacs et al [64] considered the effects of capillarity, viscosity and evaporation for their thin (~10μm) silicon nanowire array and obtained the K/ r_{eff} ratio and internal contact angle for this porous structure. Ideally, a suitable model should include the effects of capillarity, viscosity, gravity to extract K, r_{eff}, and internal contact angle, but may also need to account for evaporation in realistic conditions.

Although ignoring the evaporation is useful to simplify the extraction of K and r_{eff}, its omission or the uncertainty on evaporation rate measurements can falsify the results. Understanding the role of evaporation in the rate of rise method is specifically important while dealing with highly volatile liquids like acetone and ethanol. These liquids, due to their low surface tensions, rise easily in copper metal foams in room ambient without the need for any surface treatment. This can alleviate the problem of rapid loss of hydrophilicity in copper-

based porous materials when exposed to room ambient. Our tests show that leaving the samples more than 3 minutes in ambient air has quantifiable effects on the rate of rise of water in these foams. To restore the hydrophilicity, a high temperature hydrogen treatment that may take up to 7 hours should be done on the samples, which is not necessary with acetone and ethanol.

Another overlooked aspect is the role of attached walls in the capillary behavior of the porous materials. In practical applications, wicking materials are not used alone and are sintered to a wall to form a two-phase cooling device such as a heat pipe or a heat spreader. A wall can change the flow pattern in the adjacent foams and hence affect the values of permeability. Moreover, the sintered wall effectively covers the foam surfaces and can alter the evaporation rate from the foam.

Due to the novelty of these copper metal foams, capillary and wicking properties have not been fully understood. This work therefore aims to characterize K, r_{eff}, and internal contact angle of these foams as a measure of their wicking capacity. However, we first need to clarify the role of evaporation and the presence of adjacent walls to ensure the measurement accuracy with the rate of rise method. In this work, copper metal foams with porosities of 68%, 75% and 82%, using DI water, ethanol and acetone as test fluids will be used. To evaluate the effect of adjacent walls, the rate of rise tests have been performed on bare foam strips (no walls) as well as samples with walls sintered on one side or on both sides of the foam strip. To clarify the evaporation effect, high volatility liquids (acetone and ethanol) were used in the open air ambient and in a nearly saturated ambient. Although the rate of evaporation is much lower in saturated ambient, results will show that the capillary rise behavior is not significantly affected by evaporation, simplifying the extraction of K and r_{eff}. In fact, our results will show that the evaporation rate of a rising liquid in copper metal foams is lower than stationary liquid inside a saturated sample. The method developed herein will be used to fully characterize these novel copper foams including K, r_{eff}, and their internal contact angle with water.

5.4 Governing equations and models

A complete momentum equation for rise of liquid in a wick should include the capillary pressure, hydrostatic force of the liquid column, viscous friction force in the porous media, inertia of the liquid and the effect of evaporation. Applying force balance on the volume averaged flow, the momentum equation can be written as [22]:

$$\frac{2\sigma}{r_{eff}} = \frac{g}{TW\phi}.m + \frac{\mu}{K\phi(TW\rho)^2}.m.\frac{dm}{dt} + \frac{1}{\rho(\phi TW)^2}\frac{d}{dt}(m.\dot{m}) + \frac{\mu\dot{m}_e(W+T)}{K\rho^3(TW)^3\phi^2}.m^2 \qquad 5.2$$

The term on the left-hand side is the capillary pressure in which σ is the surface tension (N/m) and r_{eff} is the effective pore radius (m) of the porous material. Capillary pressure is generated by the curvature of the meniscus formed in the pore at the liquid-vapor interface. On the right-hand side, the first term is the hydrostatic pressure of the liquid column in the foam strip in which g is the gravity (m/s^2), T is the foam thickness (m), W is foam width (m) , φ is foam porosity, and m is liquid mass in the foam (kg). Friction in the form of a pressure drop is expressed by Darcy's law, as shown by the second term, expressed here in terms of mass. It is a function of viscosity, μ (Pa s), liquid density, ρ (kg/m^3), permeability, K (m^2), and time, t (s). The third term represents the inertial force, expressed in terms of the liquid mass flow rate, $\dot{m}$ (kg/s). It is generally accepted that inertial effects can be ignored compared to other effects [22, 31]. Evaporation from the foam surface requires an additional mass flow rate through the foam that should be considered in the governing equation. This extra mass flow rate due to evaporation will induce an additional pressure drop along the foam due to the viscous friction forces. To consider this effect of evaporation, the last term on the right-hand side is added which acts as an extra pressure drop term. The complete derivation of this term was presented by Freis *et al.* [22], but briefly, it accounts for a non-uniform pressure drop along the foam, assuming a uniform and constant evaporation rate $\dot{m}_e$ over the wetted surface. This evaporation rate per unit area (kg/m^2 s) should be measured separately for each combination of porous material, liquid and surrounding ambient.

Ignoring the inertial effects and solving for the rate of change in mass will lead to the following equation:

$$\frac{dm}{dt} = \frac{2\sigma K\phi(TW\rho)^2}{\mu r_{eff}} \cdot \frac{1}{m} - \frac{\dot{m}_e(W+T)}{\rho TW\phi} \cdot m - \frac{KgTW\rho^2}{\mu} \qquad 5.3$$

which can be expressed in the simplified form:

$$\frac{dm}{dt} = \frac{A}{m} - B.m - D \qquad 5.4$$

where:

$$A = \frac{2\sigma K\phi(TW\rho)^2}{\mu r_{eff}}, \quad B = \frac{\dot{m}_e(W+T)}{\rho TW\phi}, \quad D = \frac{KgTW\rho^2}{\mu} \qquad 5.5$$

Freis et al. [22] have presented a fully implicit solution for this equation when it is a function of height *h(t)*. Solution for other limiting cases as a function of *h(t)* are also available in literature [21, 64, 67]. By relating mass to the wicking height according to the following equation

$$m = hTW\phi\rho \qquad 5.6$$

one can readily obtain all the solutions for the mass case (Eq. 5.4). Table 5.1 shows these solutions for the four limiting cases. It can be seen that only models 2 and 4 can directly lead to two parameters K and r_{eff} separately, as opposed to their ratio. If it can be shown that the effect of evaporation is negligible, model 2 may be more appropriate because it is simpler and there is no need to know the rate of evaporation.

Table 5.1. Mass uptake rate for four limiting cases

Mathematical models	solutions
1.Negligible gravitational and evaporation effects (Lucas-Washburn), B=D=0	$m(t)=\sqrt{2At}$
2. Negligible evaporation effects, B=0	$m(t)=\frac{A}{D}[1+W(-e^{-1-\frac{D^2t}{A}})]$
3. Negligible gravitational effects, D=0	$m(t)=\sqrt{\frac{A}{B}(1-e^{-2Bt})}$
4.Complete equation (full implicit solution)	$\psi=-4AD-B^2$ $t=\frac{1}{2D}[-\ln(\frac{-Dm^2-Bm+A}{A})]$ $-\frac{B}{2D\sqrt{-\psi}}\times\ln[\frac{(-2Dm-B-\sqrt{-\psi})(-B+\sqrt{-\psi})}{(-2Dm-B+\sqrt{-\psi})(-B-\sqrt{-\psi})}]$

5.5 Materials and methods

The copper metal foams used in this study consist of 16 × 160 × 0.7 mm strips with 68%, 75% and 82% porosity, provided by Metafoam Technologies, Inc (Figure 5.1.a). As it can be seen in Figure 5.1.b and c, the foams have a spherical cluster structure (SCS) with the approximate particle diameter of 10-50μm, and unlike other types of metal foams, no ligaments can be observed. This morphology is also different than other types of foams which usually have cells shaped as polygons. Instead, the small particles join each other to form clusters that are separated from each other to provide a large-scale porosity in the foam. Within the clusters, we can observe a second smaller scale porosity formed between the particles. The microstructure formed by the small particles and their clusters is therefore characterized by two pore scales and a high surface area.

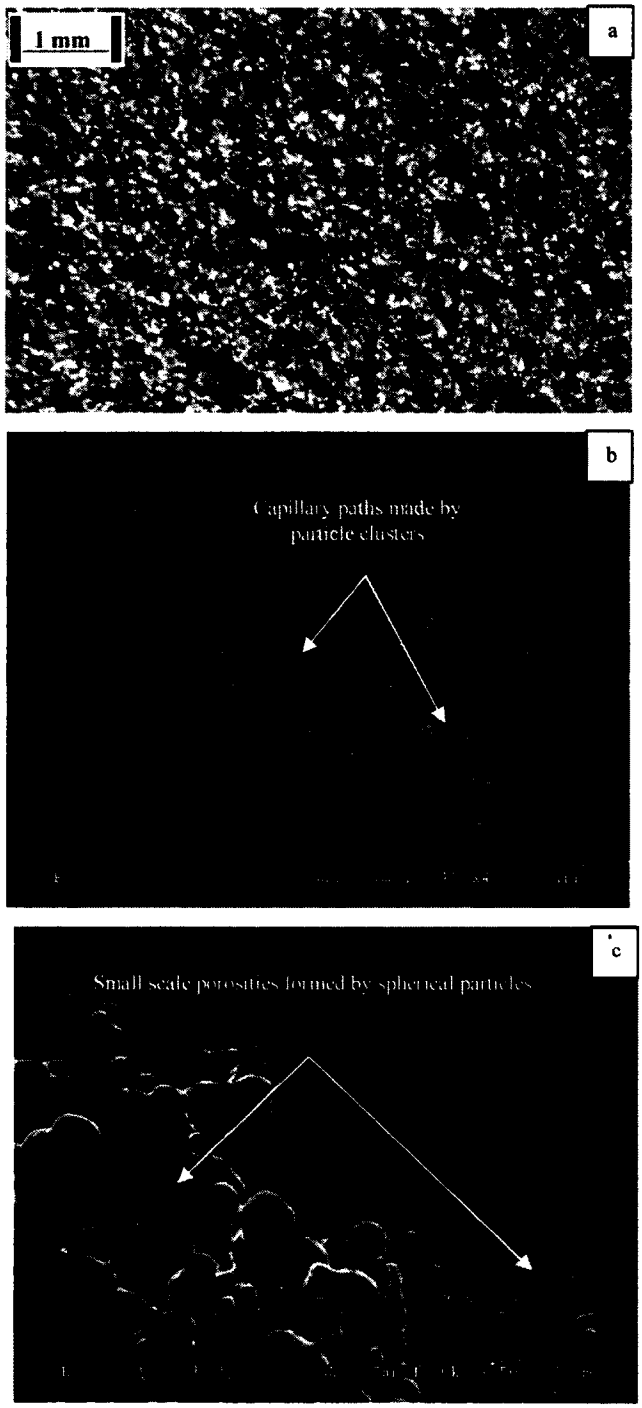

Figure 5.1. Morphology of the 75% porosity copper metal foams: (a) A macroscopic view of the copper metal foam (b) capillary paths made by clusters of the spherical particles; (c) Small scale porosities formed between the spherical particles

As a working fluid, water is a logical choice because of its interesting thermal and fluid properties and since it is commonly used in real heat pipes. To better characterize the effect of evaporation and to check the repeatability of the results, acetone and ethanol were also used as test fluids. Copper based porous materials become hydrophobic when exposed to ambient air and a time consuming hydrogen treatment is required to make them hydrophilic again. But unlike water, a low surface energy liquid like acetone (with almost zero contact angle on copper), allows the rate of rise tests to be done without hydrogen treatment because it already imbibes the copper foam samples easily. Moreover, its higher rate of evaporation compared to water makes it easier to characterize the effect of evaporation. Table 5.2 shows the properties of the liquids used in the experiments.

Table 5.2. Properties of the liquids used in the experiments, 20 °C [2]

	Acetone	Ethanol	Water
Viscosity (Pa s)	0.32e-3	1.17e-3	1e-3
Surface Tension (N/m)	0.023	0.022	0.072
Density (kg/m3)	791.2	788.8	1002

No cleaning process was performed on the copper foam samples. In order to restore the lost hydrophilicity of copper metal foams, a hydrogen reduction process is however done on the foam samples. A gas mixture of 7% Hydrogen (99.9999% purity) and 93% nitrogen (99.9999% purity) with a total volume flow rate of 150mL/min is injected into a tube furnace. The heating process is composed of a ramp from room temperature to 600°C in 2 hours and followed by a 2 hours plateau at 600°C. Then the heat is shut off and the sample is left to cool gradually under the gas mixture. This method was found to be very effective to make the foams hydrophilic and therefore, water was absorbed and could rise in the foams very well.

To evaluate the effect of a wall and evaporation barriers, copper plates (99.9% purity, 0.8mm thickness) are sintered once on one side and then on the both sides of copper foam samples. Before the sintering process, copper plates are washed with acetone, methanol and IPA to remove all organic contamination. External pressure is applied on the foam and copper plate by a fixture made of two stainless steel plates held by nuts and bolts. Then, the whole package is heated with the same procedure explained above except for the hydrogen concentration

which is increased to 20%. This concentration increase is necessary so that hydrogen can better penetrate through the external fixture and reach all the foam pores.

The measurement setups for the rate of rise test based on mass are depicted in Figure 5.2. A high precision analytical balance (A&D® model HR-120) with a precision of 0.1mg is connected to a computer and is used to measure liquid mass uptake in the foam. To measure the stored mass of the liquid (m_{st}) as a function of time (configuration I), the balance is placed on a support so that the foam sample can be mounted vertically from the hook under the balance (Figure 5.2.a and b). The liquid container placed on the moving stage under the foam sample is raised gradually until the tip of the sample touches the liquid surface. The mass increase is measured in 0.5s intervals and the measurement is stopped when the measured mass becomes constant (a plateau in the rising liquid graph above ~100s). In all tests, this plateau is reached when the wetted height is less than the maximum height of the sample (160 mm). The time period between taking out the sample from furnace and starting the test is less than 3 minutes for all tests with water. For tests with acetone and ethanol, the same procedure but without the hydrogen treatment was employed since their surface energy is low and they easily imbibe the foams.

To evaluate the effect of evaporation of acetone and ethanol, tests were also done under a partially saturated ambient created by a semi-closed transparent container (30 cm height). A small opening (7mm diameter) was made at the top of the container to attach the samples to the balance. A partially saturated ambient was created by allowing some of the volatile liquid inside the container to evaporate and displace the air, since the vapor density of both acetone and ethanol are greater than that of air. As will be discussed later, this will act as a partially saturated atmosphere and consequently decrease the evaporation rate of acetone and ethanol at the surface of the foam during rate of rise tests. By observing the liquid rise of a test sample, it was found that waiting more than 30 min has no quantifiable effect on the rate of liquid rise and hence, all tests were performed after 30 min of leaving a sample in the container.

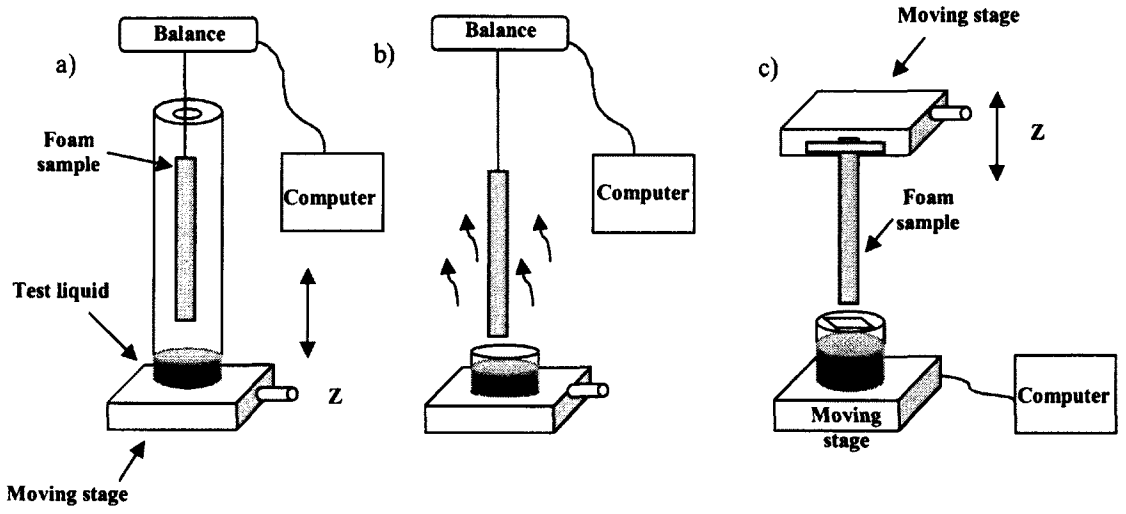

Figure 5.2. Different configurations of the experimental setup to measure the rate of rise of a liquid based on mass, done in: a) semi-closed container for the partially saturated atmosphere; b) open container for free convection with the ambient; c) container directly on the balance to measure the sum of capillary forces and evaporated mass from the foam.

In order to measure the total wicked mass of liquid in the foam (m_{tot}), the configuration in Figure 5.2.c is used (configuration II). Total wicked mass is the sum of the stored mass (m_{st}) and the mass evaporated from the foam surface (m_{evp}). In this configuration, the liquid container is placed directly on the balance and the sample is connected directly to the moving stage. Therefore, the measured liquid mass at each moment is the sum of stored mass due to capillary and also evaporation from the foam ($m_{tot} = m_{st} + m_{evp}$). To minimize the errors resulting from the evaporation of the liquid in the container, its top is covered and only a slot large enough to insert the sample is left open to ambient. The liquid level inside the container is kept to the maximum so that only the tip of the foam (~2mm) needs to enter the container. This will ensure that the exposed foam surface is the same as the first configuration (Figure 5.2.a and b), with minimal impact on the evaporation rate. For configuration II, only ethanol was used as the test liquid because of a stability problem of the balance due to high rate of acetone evaporation. In fact, acetone evaporated so fast from the liquid surface in the container that the balance could not stabilize to provide a starting point. To measure the evaporation rate from saturated suspended foam strips (16 × 50 × 0.7mm), a number of bare samples and samples with walls sintered to one side (backed) or both sides (double backed) of the strip

were tested. They were brought in contact with the liquid, left to become saturated and then detached from the liquid surface. Weight decrease due to evaporation is then recorded in 3s intervals until the sample is fully dry.

5.5.1 Corrections on the raw data

5.5.1.1 Side meniscus effect

As the foam sample touches the liquid surface, a macroscopic meniscus is formed around the end of the sample. This meniscus applies a pulling force to the samples due to the liquid surface tension. The weight measured by the balance is therefore the sum of the actual weight of liquid inside the foam and this pulling force. A simple estimate of this pulling force can be done based on the equation $F=\sigma.P$, where σ is the liquid surface tension and P sample perimeter. For water at 20 °C, a pulling force up to 0.24 g can be expected, which is 20-25% of the whole mass uptake of the foams. Such a significant effect cannot be neglected in the analysis of the results and should be subtracted from the mass uptake. This is done by detaching the sample from the liquid surface after each test (once the sample weight has reached a plateau) and then subtracting the new weight from the weight with the meniscus. This will provide a measurement of the side meniscus force, which is assumed to be constant throughout the whole test. It will be subtracted from all the data points to correct the measured mass. To evaluate the dynamic effect of this meniscus and the possible errors that it may cause, the time required to form this meniscus was measured by a high speed camera. It was ~0.02s which is much smaller than the first data points in our tests (0.5s). This effect is present in both test configurations and an example of the effect of this correction on the measured raw data for the total wicked mass measurement (configuration II) can be seen in Figure 5.3.

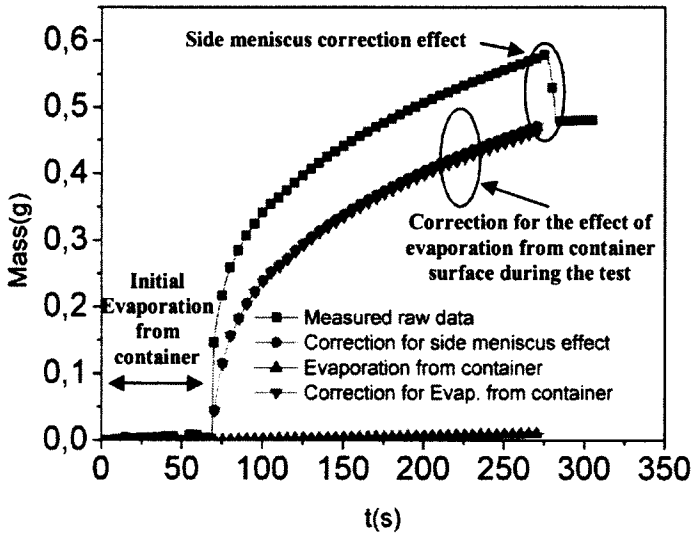

Figure 5.3. Measured raw data correction due to side meniscus, evaporation from container during the tests, and initial evaporation from the container before beginning the test.

5.5.1.2 Effect of evaporation from container

For the second experimental setup (configuration II in Figure 5.2.c), the transient total wicked mass due to both liquid storage and evaporation is measured. Hence, evaporation from the liquid in the container should be subtracted from the results to obtain the values for the foam only. To correct this additional evaporation, the foam sample was detached from the ethanol surface after each test and the mass decrease due to evaporation from the container was recorded. This provides the ethanol evaporation rate from the container. It is assumed constant throughout the test and is therefore subtracted from the balance recorded data (Figure 5.3).

5.6 Result and discussions

5.6.1 Rate of rise experimental results

Using acetone, ethanol and water as the test liquid and the stored mass measurement experimental setup (configuration I) the rate of rise test has been performed on the foam samples of 68%, 75% and 82% porosity in both open and closed ambient without any sintered wall, a wall sintered to one side (backed) and to both sides (double backed). To account for measurement and foam microstructure variations, tests were done on 2 to 3 different samples

for each porosity and repeated 3 times on each sample. Figure 5.4 shows the average of the results for all 3 porosities for acetone as the test liquid. For different foam porosities, the variations seen in rate of rise test results can be attributed to either the sintered wall or the surrounding ambient (open or closed). The capillary effect of the walls can be isolated by analyzing the results in a closed ambient, where evaporation effects are minimized. The results for bare, backed and double backed samples (Figure 5.4.b and c) in a closed ambient are found to be almost the same for each foam porosity. Although the nominal measurements suggest a slight increase in mass uptake with the number of walls, this is negligible considering the measurement uncertainty. This suggests that the presence of walls adjacent to the foam has no significant effect on the capillary wicking. In the open ambient, the presence of adjacent walls could affect the evaporation rate and therefore the mass uptake. Although the mass uptakes for the open ambient in Figure 5.4.a (68% porosity) are slightly different, they are practically identical for 75% and 82% porosity foams (Figure 5.4.b and c).

Even for the 68% foam, the effect of this difference in the values of K and r_{eff} will be shown to be negligible considering the measurement uncertainties (Table 5.4). It can be concluded that enclosing the samples with walls does not change the capillary rate of rise and also is not able to affect the evaporation rate effectively. Considering the almost identical results for different wall configurations (bare, backed and double backed) in each ambient, it can be concluded that doing tests on bare foam samples is adequate to get reliable values for K and r_{eff} by the rate of rise method.

However, the mass uptake in the closed ambient seems to be slightly higher than in the open ambient. It can be seen in Figure 5.4.a and b (68% and 75% porosities) that the highest mass uptake for the closed ambient (partially saturated container). It can be concluded that only by using a partially saturated ambient (closed ambient) can the evaporation rate be sufficiently suppressed to result in a slight change in mass uptake of the foams.

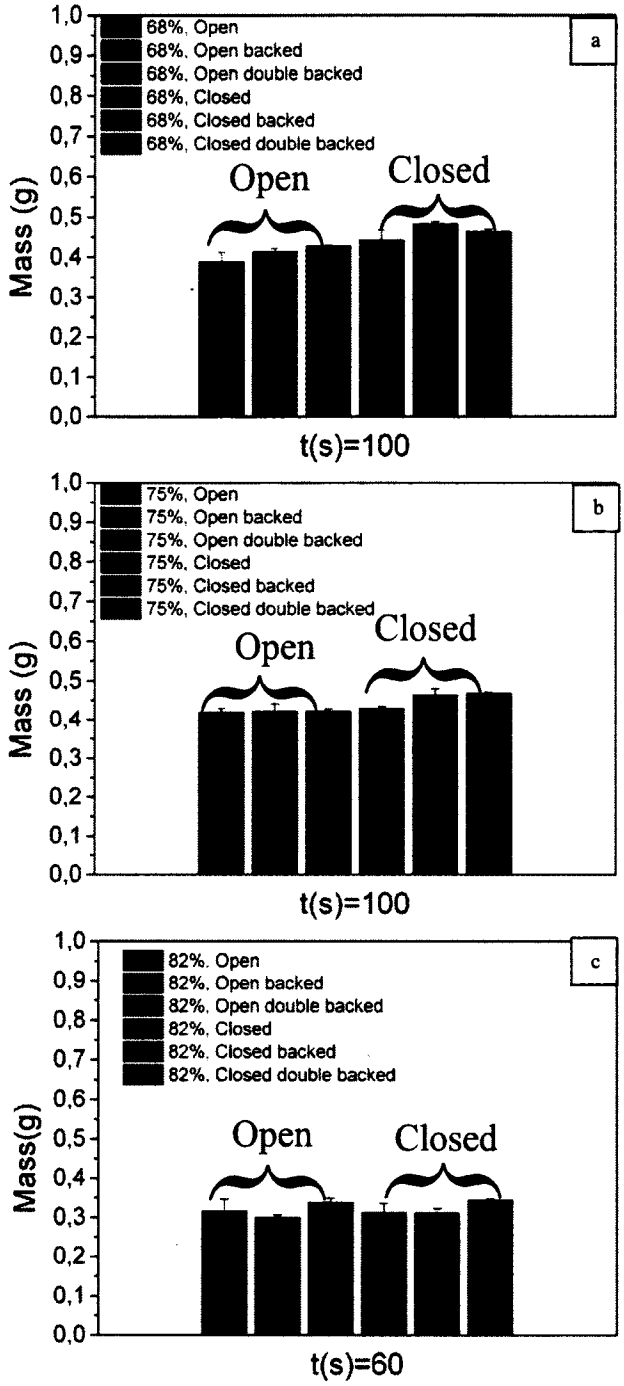

Figure 5.4. Rate of rise results for 68%, 75% and 82% porosity foams with acetone in open and closed environments, without any wall, a wall sintered to one side (backed) and to both sides (double backed).

5.6.2 Evaporation effect

5.6.2.1 Evaporation rate from stationary liquid

As it was discussed before, evaporation rate of a sample can be measured by measuring the rate of weight loss of a suspended saturated sample. In this case, liquid is stationary in the pores and no fluid dynamics are involved. To investigate the effect of evaporation, acetone and ethanol are used as the test liquids. Figure 5.5 shows the non-dimensional measured rate of evaporation of 75% porosity foam samples (16 × 50 × 0.7mm) without any sintered copper wall, with one sintered wall (backed) and two sintered walls (double backed) in an open and a closed (partially saturated) environment. It should be noted that for the sake of clarity, Figure 5.5 does not show the complete drying curve. The results are non-dimensionalized with respect to the maximum stored mass in the foams at the beginning of each test.

It can be seen in Figure 5.5.a that the rate of evaporation from the foam is significantly decreased by increasing the saturation level of the surrounding ambient of the sample. It can be observed in Figure 5.5.b that in the short time interval of the first 200s, the sample weight in the closed container is almost constant which implies a very low rate of evaporation compared with the sample left in the open environment. Given that the rate of rise test lasts around 100s, it can be concluded that the closed container has successfully decreased the evaporation rate. On the other hand, the effect of sintered walls on the evaporation rate is very small. Although first one side and then the two sides of the foam sample are covered by the copper plate, only a very slight change in evaporation rate can be observed. To make this effect more clear, Kapton® tape was used to block the uncovered parts of the copper foam (edges and top). Only in this case, the evaporation rate in the open ambient decreases significantly. This shows that in the case of high porosity materials, liquid is trapped in the inner pores during the evaporation and the vapor resulting from the evaporation of the trapped liquid is able to diffuse through the pores and exit the smallest free surface available. In this case, the mass diffusion resistance in the foam is lower than the free convection resistance between the surface and the ambient. Only when the path length required for diffusing the

vapor is larger than a characteristic length (the total length of the porous sample in the case of the Kapton® covered sample), then the diffusion rate is affected and hence, the evaporation rate is significantly decreased. Therefore, compared to using a partially saturated ambient, using external walls is not an effective method to decrease evaporation rate. Tests on other foam porosities show the same trend and the results in the form of $\dot{m}_e$ (kg/m^2 s) are presented in Table 5.3 for the open, and partially saturated ambient.

Although the measured rates of evaporation in Table 5.3 are significantly higher in the open ambient, the rates of rise of liquids between bare sample in open and closed ambient are the same (Figure 5.4). This is surprising because it is expected that the higher rate of evaporation in the open ambient should lead to a lower liquid rise rate compared to liquid rise rate in the closed ambient. This suggests that the evaporation rate from a rising liquid may not be the same as the evaporation rate measured from a stationary saturated sample. If it can be shown that the evaporation rate is lower in the dynamic case (rising liquid), then this will open path to use model 2 (Negligible evaporation) for calculating K and r_{eff}. This will be elaborated in the next section.

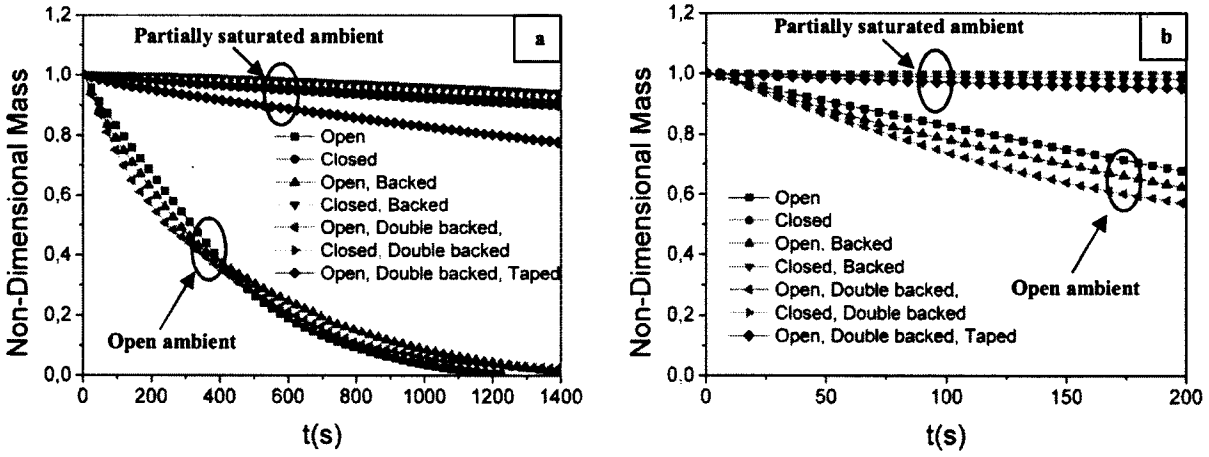

Figure 5.5. Non-dimensional evaporated mass measurement of acetone for a 75% porosity foam in open and closed environments with one sintered wall (backed) and two sintered walls (double backed) and covered edges by Kapton® tape, (b) with a close-up on the first 200s.

Table 5.3. Measured evaporation flux for bare samples, $\dot{m}_e$ (kg/m^2 s)

	Open		Closed	
	Acetone	Ethanol	Acetone	Ethanol
68%	3.9e-4	1.1e-4	1.1e-5	2.2e-6
75%	2.9e-4	1.1e-4	1.1e-5	2.9e-6
82%	2.3e-4	1.7e-4	1.2e-5	3.3e-6

5.6.2.2 Evaporation rate from rising liquid during rate of rise test

In the stored mass setup (configuration I), the balance measures the mass stored in foam at each moment (m_{st}). By employing configuration II, the sum of stored mass in the foam (m_{st}) and evaporated liquid from the foam surface (m_{evp}) is measured. Therefore, the difference between the measurements with configurations I and II provides the evaporation from the foam surface during the liquid rise (Figure 5.6). However, a theoretical mass uptake can also be calculated by using the measured evaporation flux of a suspended saturated sample (Table 5.3) and liquid height. To calculate this mass, the liquid height is visually measured at each moment, multiplied by the evaporation flux in Table 5.3, and added to the measured stored mass. It is expected that this predicted mass be equal to the measured mass by the total wicked mass setup but it can be seen in Figure 5.6 that values of predicted mass are more than the measured ones. This clearly shows that the evaporation fluxes measured for a stationary liquid in a saturated sample (Table 5.3), will lead to overestimation of the evaporation. In fact, it can be seen that in the short periods of the rate of rise test (~100s), results of configuration I and II are very close. This suggests that evaporation for this time period can be ignored even for a volatile liquid. Other authors [22] have used the evaporation rate found by measuring the weight loss of a suspended saturated sample in which liquid is stationary. They have found a 20% difference between their measured values and results of the full implicit model with the evaporation term (equation 2). This smaller evaporation rate for a rising liquid compared with stationary liquid can explain this difference.

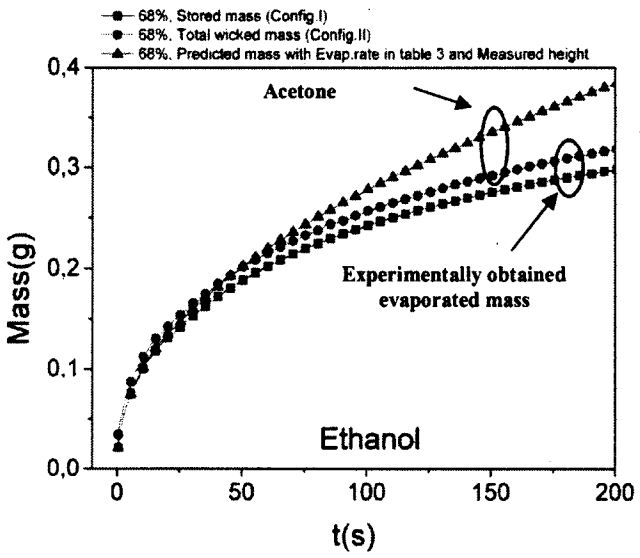

Figure 5.6. Rate of rise results for the two setup configurations: stored mass setup (configuration I), total wicked mass setup (configuration II) and predicted mass based on the stationary liquid evaporation rate and measured height for a 68% porosity foam strip.

A possible reason for the lower evaporation rate of the rising liquid compared with stationary liquid can be the difference in the capillary and disjoining pressure in the thin film interface in these two cases. The equilibrium vapor pressure at the liquid-vapor interface of a curved thin film is lower compared with a flat surface at the same saturation temperature due to the disjoining and capillary pressure effect [18]. This will lead to a lower evaporation rate from the vapor-liquid interface. However, Wang et al. [84] show that for the length scales (or wick dimensions) more than 100μm this effect is negligible. Given the two pore scales of the foam used in this study, evaporation may occur mainly from the small scale meniscuses formed on the small scale pores (less than 100 μm) in the rising liquid. When the foam is saturated and the liquid is stationary, the bigger pores contribute to the evaporation and the evaporation rate is increased. It should be noted that in a real operating heat pipe, higher evaporation rate and increased temperature may change the meniscus configuration, so this explanation may need to be revisited.

5.7 Data analysis and parameter extraction

5.7.1 Permeability and effective pore radius

In order to extract permeability K and effective pore radius r_{eff}, model 2 (negligible evaporation effect) [31] will be used along with measurements from the stored mass setup (configuration I) for the first 100 s of test. Neglecting the evaporation term, Eq. 5.3 will lead to an ordinary differential equation with two unknowns: permeability and effective pore radius. Solving this simplified equation will lead to the following expression:

$$-\left[\frac{2\sigma}{r}\ln(1-\frac{gr}{2\sigma A\phi}m)+\frac{g}{A\phi}m\right]=\frac{K\rho^2g^2}{\phi\mu}t \qquad 5.7$$

It can be seen in Eq.5.7 that t can be expressed explicitly as a function of m, liquid properties, sample geometry (assumed constant) and two unknowns: permeability K and effective pore radius r_{eff}. These unknowns can be defined by fitting Eq. 5.7 to the experimental data. After measuring liquid mass uptake versus time, test liquid properties such as surface tension, viscosity and density and foam sample geometry (width and thickness) are inserted in Eq. 5.7. The time can then be predicted for a range of K and r_{eff} values. The most representative value of K and r_{eff} is then defined as the pair that minimizes the error, in a least squares sense, between the experimental data (time for a given mass) and predicted time using Eq. 5.7. The optimization is done over a broad range of K and r_{eff} values to identify the minimum.

Using this approach with acetone, ethanol and water as test liquids, permeability K and effective pore radius r_{eff} are extracted. Results for open and closed ambient and with bare, backed and double backed samples are presented in Table 5.4. It can be seen that, generally, the results for permeability from acetone, ethanol and water as test liquids are in good agreement. This is expected because permeability is a function of the microstructure of the foams and not the liquid used. The results for effective pore radius between water, ethanol and acetone are different because, as it is shown in Eq.5.1, effective pore radius includes the contact angle of the liquid, which is different for different liquids. In fact, unlike permeability,

effective pore radius depends on the combination of the liquid and the microstructure. The highest permeability and effective pore radius belong to 82% porosity and the lowest values to 68% porosity foam samples. The impact of the lower evaporation rate in the closed ambient, on the K and r_{eff} can also be seen in this table. Due to the rather small effect of evaporation in the liquid uptake of the foams, the values of K and r_{eff} are generally close in the partially saturated and open ambient. This validates the hypothesis of neglecting the evaporation effect and will confirm the use of model 2 in Table 5.1. Mass uptake rate for four limiting cases

Table 5.4. Permeability K and effective pore radius reff for foam samples of 68%, 75% and 82% porosities

		68%				75%				82%			
		$K(\mu m^2)$		r_{eff} (µm)		$K(\mu m^2)$		r_{eff} (µm)		$K(\mu m^2)$		r_{eff} (µm)	
		mean	STDV	Mean	STDV	mean	STDV	Mean	STDV	mean	STDV	Mean	STDV
Acetone	Open	24	2	73.8	0.4	46	7	89.7	0.3	89	11	140.2	0.1
	Closed	21	3	64.6	0.2	45	5	87.7	0.2	96	13	141.1	0.1
	Open, backed	22	2	71.6	0.5	41	5	88.7	0.4	110	10	146.3	0.4
	Closed, backed	20	2	56.0	0.7	42	6	79.6	0.3	127	13	137.5	0.2
	Open, double backed	27	3	73.4	0.2	38	3	87.9	0.6	85	1	128.1	0.7
	Closed, double backed	25	4	66.0	0.4	35	1	78.3	0.9	112	8	106.0	0.2
Ethanol	Open	31	6	89.4	0.9	59	8	104.0	1.0	94	10	135.0	1.0
	Closed	23	6	65.1	0.7	60	9	93.3	0.3	104	9	132.6	0.5
	Open, backed	25	7	66.5	0.9	55	2	84.5	0.9	129	2	135.3	0.2
	Closed, backed	20	3	52.3	0.3	52	1	77.4	1.0	139	11	132.2	0.8
	Open, double backed	40	7	86.4	0.3	60	7	95.5	0.3	105	10	118.8	1.0
	Closed, double backed	32	3	69.1	0.4	45	6	82.1	0.3	104	16	118.9	0.2
Water	Open	19	5	74.8	18.9	51	24	102.0	18.1	74	42	176.0	8.9
Avg.		25	9	-	-	48	13	-	-	105	24		

Table 5.5 presents the values of K/r_{eff} for different foam samples. As discussed before, unlike permeability (K), effective pore radius depends on the liquid used for the rate of rise test therefore, the values obtained for K/r_{eff} also depend on the liquid. It can be seen that using acetone and ethanol as test fluid, the highest K/r_{eff} ratio belongs to 82% porosity foam which suggests that this foam should have the highest capillary pumping. But in the case of water, 75% foam is more effective for liquid pumping. This can be validated by results presented in

Figure 5.7 in which mass uptakes of three foam porosities for different test liquids are compared with each other. It can be seen that for acetone and ethanol, the slope of mass uptake of the 82% foam is the highest while for water, the 75% porosity foam can deliver the highest pumping rate (highest slope). It shows that for water as the working fluid, 75% foam is possibly the best foam to attain the highest capillary limit in a heat pipe. For the case of 82% foam, it should be noted that due to its bigger pores the maximum capillary pressure is smaller compared with other foams. However, due to higher permeability (less pressure drop), the initial rate of rise in the first seconds may be quicker than other foam porosities depending on the working liquid. This can be seen clearly in the case of 82% foam with acetone where the slope in the first period of the test (~10s) is sharper, representing the capillary pumping rate of this porous material with acetone.

Although values of K/r_{eff} depend on parameters such as particle size and porosity, an example in the open literature for sintered copper powder wick with 52% porosity (K/r_{eff} =0.096μm with water) [18] can be chosen for comparison. These results show a 5 times increase in K/r_{eff} for 75% porosity foam using water (K/r_{eff} =0.5μm) compared to the sintered copper powder wick. While other parameters such as thermal conductivity, wick thickness and wall contact quality are also important, this clearly shows the potential enhancement in the capillary pumping that can be obtained by using these foams.

Table 5.5. Values of K/reff (μm) for different conditions and configurations

	68%			75%			82%		
	Acetone	ethanol	Water	Acetone	ethanol	Water	Acetone	ethanol	Water
Open	0.32	0.35	0.25	0.52	0.56	0.50	0.63	0.70	0.42
Open, backed	0.31	0.37	-	0.46	0.65	-	0.75	0.96	-
Open, double backed	0.37	0.46	-	0.43	0.62	-	0.66	0.89	-

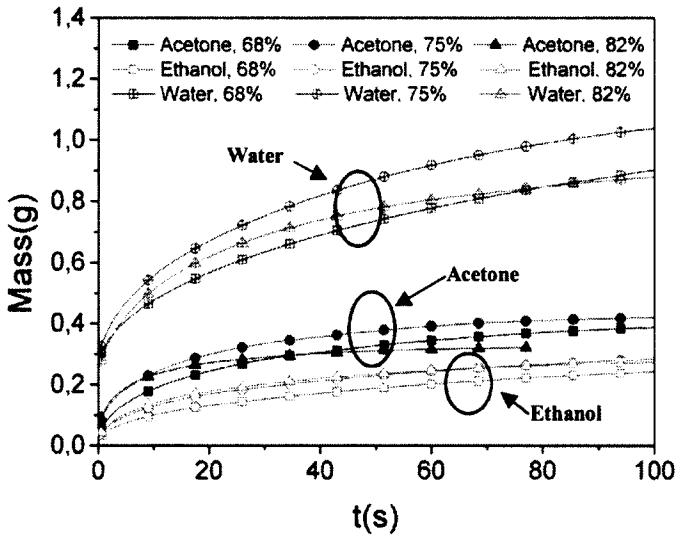

Figure 5.7. Mass uptake values for different foam porosities in a closed container with acetone, ethanol and water.

5.7.2 Internal contact angle

Water is the typical working liquid for heat pipes and knowing its internal contact angle can provide insight on the wicking behaviour. Contact angle measurements show a value of 47° for water on a hydrogen treated (hydrophilic) copper plate sample, but these may be different in porous structures. Reducing this value could potentially increase the heat pipe performance by increasing K/r_{eff}. The approach to extract the internal contact angle is to use a low surface energy liquid (near zero contact angle) to measure the effective pore radius and then calculating r in Eq. 1. The use of ethanol for this comparison was ruled out because the contact angle of 95% ethanol (employed in this study) is higher than zero. Collier and Thome [14] present the values of contact angle of 14-19° for ethanol on a copper surface. Moreover, Fan et al. [19] measure a contact angle of 10-15° for 85% ethanol in atmospheric conditions on a copper surface. Our tests in the laboratory show the same non-zero contact angle for ethanol on a copper plate. Therefore, the 'near zero' contact angle assumption would be violated. However, our measurements show that acetone has a zero contact angle on a flat copper surface, making it a good reference fluid to extract r. The cosine of the internal contact angle for water is therefore simply the ratio of the effective pore radius of acetone and water. It can

be seen in Table 5.6 that these values are smaller than the water contact angle on a flat copper surface. This is due to the morphology of the pores and the interactions of the liquid with the microstructure. Moreover, as the porosity increases, internal contact angle increases also. This can be attributed to the close to zero contact angle of the liquid in small pores [7]. As the porosity increases, the pores become larger and the effect of the microstructure becomes less dominant. It can be seen that although the hydrogen treatment is obviously able to render the surfaces hydrophilic, this hydrophilicity is not perfect (zero contact angle). Developing more effective methods for making the copper hydrophilic can increase the capillary pumping, especially for higher porosity foams (in this case 82% foam). A combination of high porosity and low liquid contact angle could increase the operating limit of the heat pipes by providing bigger paths for vapor to escape, less pressure drop and better capillary pumping.

Table 5.6. Internal contact angle of water in an open ambient

Porosity	reff, acetone ,(μm)	reff, water ,(μm)	θ water,int
68%	73.8	74.8	~9
75%	89.7	102	~28
82%	140.2	176	~37
Copper flat surface	-	-	~47

5.8 Conclusion

Permeability, effective pore radius and internal contact angle of copper metal foams are obtained by measuring the rate of mass uptake with acetone, ethanol, and water as test liquids. Specific attention was given to the role of evaporation and the presence of walls to evaluate their importance on the vertical rising of a liquid in a porous material. The following conclusions can be drawn from this study:

- Permeability and effective pore radius are obtained by doing the measurements in the open ambient and using model 2 in Table 5.1. Mass uptake rate for four limiting cases(negligible evaporation) for the foam porosities of 68%, 75% and 82%. The highest permeability and effective pore radius were found for the 82% porosity and the lowest values for 68% porosity foam samples. Using acetone and ethanol as test fluids, the highest K/r_{eff} ratio belongs to 82% porosity foam which suggests that this foam

should have the highest capillary pumping. But in the case of water, 75% porosity foam is more effective for liquid pumping. Its K/r_{eff} ratio is almost 5 times bigger than sintered copper powder, which makes it a very promising wicking material.

- The rate of evaporation of acetone and ethanol from the rising liquid is significantly lower than that measured for stationary liquid in a saturated foam sample. For a rising liquid, this may be due to lower evaporation rate from the meniscuses formed on the smaller scale pores (less than 100μm) caused by higher disjoining and capillary pressures. This allows evaporation effects to be neglected in the rate of rise test even for highly volatile liquids like acetone. This way, permeability and effective pore radius can be extracted directly by using model 2 in Table 5.1, which ignores the evaporation effect.

- Sintering copper walls to the copper metal foams has almost no effect on the capillary rise behavior and the evaporation rate. Hence, covering most of the foam surfaces does not hinder the evaporation rate. Only by putting the samples in a semi saturated ambient can a significant change in evaporation rate be observed. This suggests that the foams are very efficient mass transport media with low internal mass diffusion resistance.

- The non-zero internal contact angle of water in the copper porous foams is seen to be smaller than the water contact angle on a flat piece of copper. It is caused by the morphology of the foams and the interactions of the liquid and microstructure. Decreasing the internal contact angle can change the ratio of K/r_{eff} which would favor more porous foams.

This work has therefore not only provided capillary properties of copper metal foams for the first time, but also clarified the conditions under which the rate of rise method should be conducted to properly extract these properties. Although the effects of evaporation and the presence of an adjacent wall were found to have a negligible impact on the rate of rise

measurement, these effects may be different at high heat rates typically seen in heat pipes. In particular, evaporation during the operation of a heat pipe may be a function of its pumping rate, since this work has shown the evaporation rate to be different for wicking versus saturated foams.

5.9 Acknowledgments

This research was jointly funded by NSERC and Metafoam Technologies Inc. We are grateful for the support and guidance of Dominic Pilon. The contributions of Stéphane Gutierrez for SEM imaging and Louis-Simon Malo for testing are also greatly appreciated.

CHAPITRE 6 AVANT-PROPOS

Auteurs et affiliation:

- Mahmood R.S. Shirazy: étudiant au doctorat, Université de Sherbrooke, Faculté de génie, Département de génie mécanique.
- Luc G. Fréchette : professeur, Université de Sherbrooke, Faculté de génie, Département de génie mécanique.

Date de soumission: 28 février 2013

Revue: Proceedings of the ASME 2013 International Technical Conference and Exhibition on Packaging and Integration of Electronic and Photonic Microsystems, InterPACK2013, July 16-18, 2013, Burlingame, CA, USA **(Outstanding paper award)**

Titre français: Effet du recule du ménisque sur le rayon de pore effectif et le pompage capillaire de mousses métalliques en cuivre

Contribution au document:

Cet article contribue à la thèse en déterminant le rôle du recul du ménisque dans le pompage capillaire et le taux d'évaporation. Cet effet est caractérisé pour la première fois et un modèle est proposé pour mesurer le rayon de pore effectif de matériaux poreux dans des conditions d'opération. Cet article résume des efforts pour couvrir l'aspect d'évaporation de cette thèse et il complète l'étude de deux phonèmes importants dans les caloducs, soit la capillarité et l'évaporation.

Résumé français :

Une étude expérimentale est effectuée pour caractériser l'effet du recul du ménisque sur le rayon de pore effectif et le pompage capillaire de mousses métalliques en cuivre qui doivent être utilisés comme mèche dans les caloducs plats pour le refroidissement électronique. Connaître le rayon de pore effectif, et les paramètres influant sur elle comme la récession de ménisque, est essentielle dans la définition d'un bon matériau capillaire. Il est connu que le

ménisque recule lors de l'évaporation, mais l'impact sur le pompage capillaire selon le taux d'évaporation n'est pas clair. Des bandes de mousse avec des porosités de 68%, 75% et 82% sont testées en appliquant un flux de chaleur et en mesurant les taux d'évaporation de l'éthanol. Le profil de température le long de l'échantillon de mousse est mesuré directement avec des thermocouples. L'emplacement du front de liquide sous différents flux de chaleur est déterminé à l'aide d'une caméra infrarouge (IR) et le taux d'évaporation maximal est mesuré. Les taux d'évaporation mesurés sont corrigés pour tenir compte des pertes thermiques dont la convection naturelle, la conduction thermique directe vers le liquide, et l'évaporation à partir du récipient. Un modèle analytique est ensuite développé pour relier la masse évaporée à la pression maximale capillaire et les résultats sont présentés. Il est montré pour la première fois, que juste avant le début de l'assèchement, le ménisque reculé mènera à une baisse de 15%, 28% et 52% en rayon de pore effectif pour l'échantillon avec des porosités 68%, 75% et 82% respectivement. Cela peut avoir un impact significatif sur la prédiction de la limite capillaire de dispositifs bi phasique, tel que les caloducs.

6 EFFECT OF MENISCUS RECESSION ON THE EFFECTIVE PORE RADIUS AND CAPILLARY PUMPING OF COPPER METAL FOAMS

6.1 Abstract

An experimental study is performed to characterize the effect of meniscus recession on the effective pore radius and capillary pumping of copper metal foams which are to be used as wicks in heat pipes for electronic cooling. Knowledge of the effective pore radius is critical in defining the capillary pumping of a wicking material, but is rarely measured under operating conditions. It is known that the meniscus of a liquid recedes when evaporating from a porous media, which could impact the effective pore radius and therefore the capillary pumping capabilities of the foam. To elucidate this impact, the evaporation rate is measured from foam strips wicking ethanol from a reservoir while applying heat fluxes to the foam. Using thermocouple and IR camera measurements, the measured evaporation rates are corrected to account for different thermal losses, including natural convection, direct thermal conduction to the liquid, and evaporation from the container. An analytical model is then developed to relate the evaporated mass to the maximum capillary pressure (minimum effective pore radius) provided by the foam. It is shown for the first time, that just before the onset of dryout, the recessed meniscus will lead to 15%, 28% and 52% decrease in effective pore radius for samples with 68%, 75% and 82% porosities respectively. The capillary pumping therefore increases during evaporation. This can have significant impact on the prediction of the capillary limits in two phase capillary driven devices.

6.2 Nomenclature

A	Heated area of the foam, m^2
A_c	Cross sectional area of the wick, m^2
C_p	Specific heat, (kJ/kg K)

g	Gravity, m/s^2
h	Liquid height, m
h_{fg}	Heat of vaporization, (kJ/kg)
k	Thermal conductivity, W/m K
K	Permeability, m^2
m	Liquid mass, kg
$\dot{m}$	Liquid mass flow rate, kg/s
r	Pore radius, m
$\dot{m}_{cont}$	Container evaporation rate, kg/s
$\dot{m}_{foam}$	Foam Evaporation rate, kg/s
$\dot{m}_{tot}$	Total evaporation rate, kg/s
$P_{capillary}$	Capillary pressure, Pa
Q_{conv}	Convection heat transfer, W
Q_{cond}	Conduction heat transfer, W
Q_{evap}	Evaporation heat transfer, W
Q_{in}	Total power dissipated in the heater, W
Q_{rad}	Radiation heat transfer, W
Q_{sens}	Sensible heat transfer, W
r_{eff}	Effective pore radius, m
t	Time, s
T1-T7	Thermocouple labels
T_{amb}	Ambient temperature, °C
T_{cont}	Liquid container temperature, °C
T_{heater}	heater temperature, °C
T_{surf}	Average temperature of the heated area, °C
x	Location from liquid surface, m

Greek symbols

φ	Porosity
ε	Emissivity
μ	Viscosity, Pa s

ρ	Liquid density, kg/m^3
Θ	Contact angle, deg.

6.3 Introduction

Wicking materials are the main part of two phase cooling devices increasingly used for thermal management of electronics, such as heat pipes and heat spreaders. Due to their capillarity and open pore structure, they carry liquid from the condenser side to the evaporator side in these devices. When one end of a heat pipe is connected to a heat source, such as a hot microprocessor, heat is removed by the evaporation of the liquid enclosed in the pipe. The vapor travels to the other end of the heat pipe where it condenses [54]. The liquid is pumped back to the hot end by the capillary action of the wicking material inserted in the pipe or chamber. The operating range of heat pipes is subjected to several physical limits. For the case of a heat pipe utilizing copper metal foam as the wicking material, the dominant limit will be capillary pumping [70]. This limit is reached when the capillary pressure of the wicking material is not sufficient to supply the required rate of liquid to the evaporator and hence, the evaporator will dry out. Therefore, the pumping capacity of the wicking material is a key parameter in the performance of heat pipes. Typical wicking materials include sintered copper powders, copper meshes and more recently copper metal foams. These wicking materials are characterized by their permeability, pore size, porosity, and thermal conductivity. Copper metal foams used in this research (made by Metafoam technologies Inc.) have shown promising results in heat pipes [57] and their dryout heat fluxes are much higher than what can be predicted by available correlations for capillary limit prediction.

Evaporation is usually considered to be the dominant mode of heat transfer in capillary-driven two phase cooling devices. During their operation, heat is conducted from the substrate through the saturated wick. Due to the lower conductivity of the liquid, most of the heat is conducted through the wick structure to its surface. At the surface, heat transfer occurs mainly in the thin liquid film region of several microns in thickness [49]. The evaporative heat transfer at the surface depends on the thin film area, its thickness and also the effective conductivity of the saturated porous wick [30]. A wick with low evaporation resistance is characterized by a low thermal resistance of the saturated wick R_{wick} and the liquid-vapor

interface R_{int}. However, it is shown that R_{int} is dominant only in the case of very thin wicks (~100 μm) [62]. Sintered particle wicks have been tested by many researches [16, 30, 69] and it is shown that they can support heat fluxes up to 500 W/cm^2 in the boiling mode [86]. Higher heat fluxes of 600-1000 W/cm^2 have been achieved by using thick (3 mm) biporous wicks [68]. All these high heat fluxes were obtained by testing the samples in the horizontal position or a very short vertical wetted length (8mm). In this way, liquid pressure drop of the capillary-driven liquid flow from the reservoir to the evaporation zone was minimized. It should be noted that by increasing the sample length, the liquid pressure drop will increase and eventually decrease the maximum heat flux. A maximum heat flux of 20 W/cm^2 is obtained by using a 6-8 cm wick length [34] which shows a great difference compared with previous values. This clearly shows that the extremely high heat fluxes obtained by decreasing the sample length may not be possible in real two phase capillary devices due to excessive liquid pressure drop in the wicks which leads to dry-out or its capillary limit.

Capillary properties of a wicking material such as permeability (K) and effective pore radius (r_{eff}) are critical in defining the capillary limit of heat pipes, because their ratio (K/ r_{eff}) is a measure of pumping capacity of the wicking material [18]. Permeability can be defined as the porous material resistance against the liquid passing through it. A high permeability will result in a lower liquid pressure drop. Permeability is a pure function of the porous material microstructure and does not depend on the liquid used. Effective pore radius on the other hand, depends on the wetting properties of the liquid in the porous structure. The meniscus profile formed at the liquid-vapor interface of each pore is a function of the pore structure and also the liquid contact angle on the porous material. Therefore, *effective* pore radius is rather used instead of the geometrical pore radius to account for the effect of liquid contact angle. According to the definition of the effective pore radius, it is related to the actual pore radius of a porous material, r, and the liquid contact angle θ on that material by:

$$r_{eff} = r/\cos\theta \qquad 6.1$$

Effective pore radius is inversely proportional to the liquid contact angle on the solid surface. Hence, a lower liquid contact angle will result in a lower effective pore radius which in turn will increase the K/ r_{eff}.

For porous media, a series of methods are available to measure capillary parameters, such as pressure drop measurement for permeability [4, 59], or bubble test and rising meniscus for the effective pore radius [18]. The rate of rise method which is based on the transient rise of liquid in the capillary structures can also provide K and r_{eff} simultaneously [72]. An overlooked aspect in these methods is the meniscus recession in the heated wick, and its impact on r_{eff}. In an operating wick, as the heat flux increases, the meniscus formed at the liquid-vapor interface recedes into the wick due to higher evaporation rate [18]. The receded meniscus provides a thinner liquid film, which is shown to result in lower wick thermal resistance in multi-layer mesh wicks or sintered powder wicks [36, 43, 73-75, 88]. It should be expected that the capillary pressure will also be affected when the meniscus recedes and deforms. Therefore, the current methods to measure r_{eff} may not represent the real minimum effective pore radius as they do not consider meniscus recession due to evaporation. This is especially important because the widely used models predicting dryout or capillary limit [18, 54] are all based on comparing the pressure drop in wick and vapor core with the maximum available capillary pressure calculated by

$$P_{capillary} = 2\sigma/r_{eff} \qquad 6.2$$

in which σ is the surface tension (N/m). An underestimation of the r_{eff} will result in an under predicted capillary limit or dryout.

This work therefore aims, for the first time to characterize the impact of meniscus recession on the effective pore radius and capillary pumping performance of copper metal foams. Copper metal foams with porosities of 68%, 75% and 82%, with ethanol as the test fluid are used. An experimental setup is used to measure temperature profile along the length of the foam samples and the capillary-driven evaporation rate in ambient air. Using IR pictures of the foam surface at each steady state heat flux, the liquid front height is measured. An analytical model based on first principles that relates capillary flow to evaporation rate is developed and used to calculate the modified r_{eff}. It will be shown that meniscus recession has a significant effect on r_{eff} and evaporation rate from the foam.

6.4 Governing equations and models

A momentum equation for rise of liquid in a wick should include the capillary pressure, hydrostatic force of the liquid column and viscous friction force in the porous media. Applying force balance on the volume averaged flow, the momentum equation can be written as [22]:

$$\frac{2\sigma}{r_{eff}} = \frac{g}{A_c\phi}.m + \frac{\mu}{K\phi(A_c\rho)^2}.m.\frac{dm}{dt} \qquad 6.3$$

The term on the left-hand side is the capillary pressure. Capillary pressure is generated by the curvature of the meniscus formed in the pore at the liquid-vapor interface. On the right-hand side, the first term is the hydrostatic pressure of the liquid column in the foam strip in which g is the gravity (m/s^2), A_c is the cross sectional area of the wick (m^2), φ is foam porosity, and m is liquid mass in the foam (kg). Friction in the form of a pressure drop is expressed by Darcy's law, as shown by the second term, expressed here in terms of mass. It is a function of viscosity, μ (Pa s), liquid density, ρ (kg/m^3), permeability, K (m^2), and time, t (s). By relating mass to the wicking height according to the following equation:

$$m = hA_c\phi\rho \qquad 6.4$$

The existing liquid mass m at each moment inside the foam can be calculated.

6.5 Experimental methods

6.5.1 Sample properties

The copper metal foams used in this study consist of 15 × 45 × 0.7 mm strips with 68%, 75% and 82% porosity, provided by Metafoam Technologies, Inc (Figure 6.1.a). As it can be seen in Figure 6.1.b and c, the foams have a spherical cluster structure (SCS) with the approximate particle diameter of 10-50μm, and unlike other types of metal foams, no ligaments can be observed. This morphology is also different than other types of foams which usually have cells shaped as polygons. Instead, the small particles join each other to form clusters that are separated from each other to provide a large-scale porosity in the foam. Within the clusters,

we can observe a second smaller scale porosity formed between the particles. The microstructure formed by the small particles and their clusters is therefore characterized by two pore scales and a high surface area.

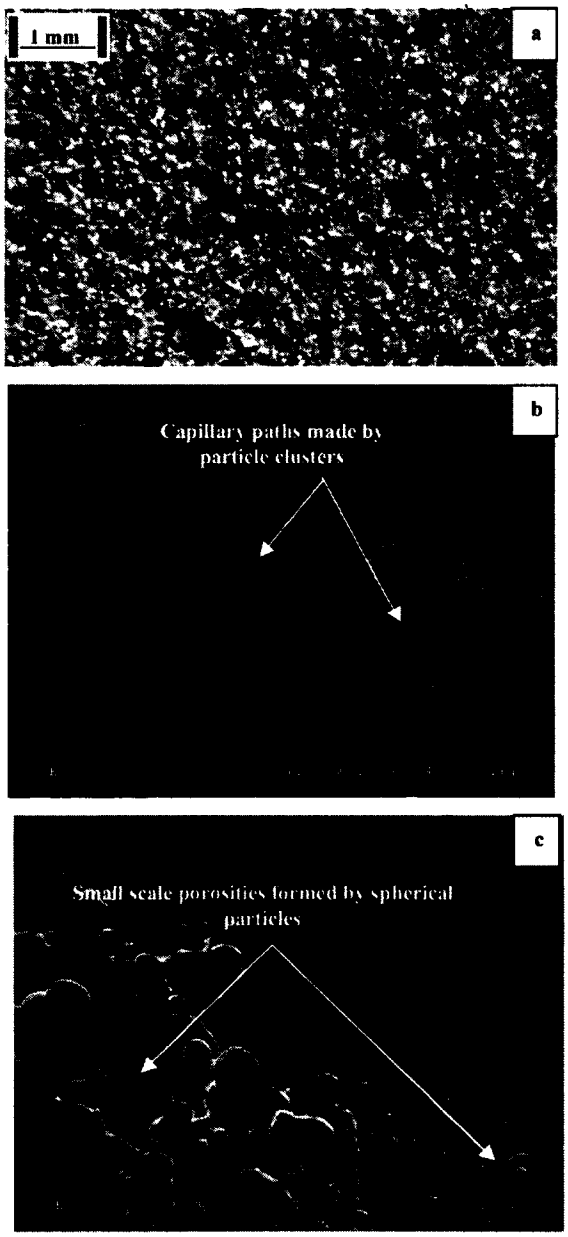

Figure 6.1. Morphology of the 75% porosity copper metal foams: (a) a macroscopic view of the copper metal foam (b) capillary paths made by clusters of the spherical particles; (c) small scale porosities formed between the spherical particles

Ethanol is chosen as a working fluid. Copper based porous materials become hydrophobic when exposed to ambient air and a time consuming hydrogen treatment is required to make them hydrophilic again. But unlike water, a low surface energy liquid like ethanol imbibes readily in the copper foams without hydrogen treatment. Table 6.1 shows the properties of ethanol used in the experiments. When liquids are heated, non-condensable gases trapped in the liquid are released. In actual heat pipe operation, non-condensable gases can block the phase change in the condenser section. It is therefore important that the operating liquid in a real heat pipe is degassed completely. Moreover, dissolved gases in liquid can be mistaken for actual boiling upon heating, which can lead to wrong interpretations. But ethanol is not degassed in this work because neither condensation nor boiling is studied. Dissolved gases have no important effect on capillary and evaporation, which are the focus of this work.

Table 6.1 Properties of the ethanol, 20 °C [2]

Viscosity (Pa s)	**1.17e-3**
Surface Tension (N/m)	**0.022**
Density (kg/m^3)	**788.8**
Heat of vaporization (kJ/kg)	**846**
Specific heat (kJ/kg K)	**2.44**

6.5.2 Experimental setup

The experimental approach consists of measuring the mass of ethanol evaporated when a heated foam strip is dipped in the liquid container. As shown in Figure 6.2, heat is provided on one side of the foam strip by a heater block, allowing evaporation from the exposed surface. The heater block (Figure 6.2a) is made of Delrin® as an insulation material. Due to the relatively low melting temperature of the Delrin® (~175 °C), the inner part of the insulation block is filled with 20 mm of glass fiber (Pyrogel® XT) so that the copper block and heater are not touching the Delrin® walls directly. This increases the maximum operating temperature of the setup to much higher than the Delrin® melting temperature. The heat input is generated by a 580 W, 25×15 mm rectangular Watlow Ultramic 600® heater which is then transferred to a copper block. The gap between the copper block and heater is filled with a Tpli™ 200 thermal pad (k = 6 W/m K), covering an area of 25×15 mm. The sample is then attached to the copper block using thermal paste (OMEGA-OT-201, k = 2.3 W/m K). Due to the small size and

weight of the foam samples, the bonding force of the thermal paste is enough to hold them in place.

Seven Type-K thermocouples (OMEGA®, 0.25 mm diameter tip) are used to measure the temperature at different locations of the setup. These are the heater surface (T1), in the copper block (T2), along the foam surface (T3-T6) and inside the liquid (T7). The copper block temperature (T2) is measured by a thermocouple inserted in a small hole (0.3 mm diameter) machined 2.5 mm from the copper-foam interface. T1 and T2 are attached using thermal paste, while thermocouples T3 to T6 are brought in direct contact with the exposed foam surface at the locations shown in Figure 6.2a. T7 is directly immersed in the liquid at the depth of ~5 mm from the liquid surface. The whole heater block with thermocouples is attached to a stage allowing motion in the Z direction. The thermocouples are connected to a data acquisition system (Agilent® 34970A). A 120W power supply (Anatek®) feeds the heater with the power being determined from current and voltage measurements (Fluke® 4S and Extech® EX530 multimeters).

A high precision analytical balance (A&D® model HR-120) with a precision of 0.1mg is connected to a computer and is used to measure liquid mass uptake in the foam due to evaporation. A high performance IR camera (Flir® SC620) with a resolution of 640×480 pixels is used to capture the liquid front. The liquid front location is also confirmed visually by using a high magnification zoom lens (Navitar® model zoom 6000) connected to a microscopic camera (Infinity® 3).

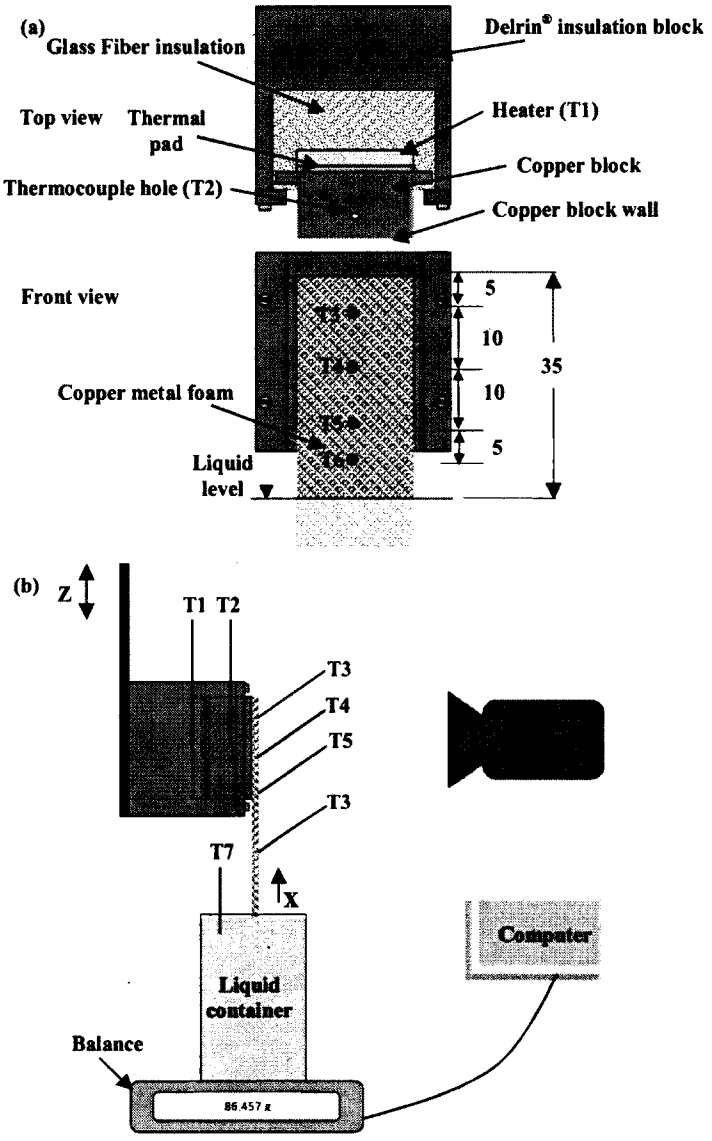

Figure 6.2 Schematic drawing of a) the heater block and thermocouple locations (dimensions in mm) b) measurement setup with IR camera

6.5.3 Test procedure

At the start of each set of tests, the heater block height is adjusted in a way that the distance from the top of the sample to the liquid surface in the full container is 35 mm and 10 mm of the sample length is immersed in the liquid. The length of the samples is chosen so that liquid imbibes its entire length and wets the whole surface. Then the tips of the thermocouples are carefully placed on the foam surface to measure surface temperature. Our extensive tests showed that this method is reliable when the surface is wet with liquid due to better surface

contact of the tip and saturated wick. The results are less reliable when the surface is dry (dryout mode). The temperature values for a dry surface are calibrated with IR measurements.

The mass and temperature are measured in 2s intervals. The voltage is increased by 5V increments to acquire different test data points. Steady state operation is achieved over a period of 15 min which is defined by temperature changes at a rate of less than 0.1 °C/min, time-averaged over a period of 5 min. At the end of each steady state period, the IR camera is used to capture the liquid front on the foam surface.

During evaporation, the liquid height in the container is constantly decreasing due to capillary pumping of the liquid to the foam. By measuring the internal diameter of the container, the allowable minimum weight of the liquid is calculated so that the liquid level is never less than 3 mm from the full level in the container. Fresh liquid is added to the container as soon as the liquid weight reaches the allowable minimum value so that the liquid surface is kept in the acceptable range. Three samples are tested 3 times each for each porosity.

6.6 Data reduction and parameter extraction

6.6.1 Mass measurements

The evaporation rate is calculated by fitting a line through the data points of the mass vs. time at the end of each steady state period. The selected data points include a time period showing a mass decrease of no more than 1g. This will guaranty that the liquid height change during this period is less than 1 mm and the associated error is negligible. The measured evaporation rate $\dot{m}_{mes}$ is the sum of the foam evaporation rate $\dot{m}_{foam}$ and evaporation rate from container $\dot{m}_{cont}$. Therefore, this measured evaporation rate should be corrected to obtain $\dot{m}_{foam}$. In order to obtain $\dot{m}_{cont}$, a series of tests were conducted with a heater submerged in the container. Liquid temperature in the container, T_{cont}, was also measured at the depth of ~5 mm from the surface for each power level. A relationship between evaporated mass and liquid surface temperature was then obtained by curve fitting (R=0.99) the following relation:

$$\dot{m}_{cont} = 3.5e^{-7}\left(1+\exp(\frac{T_{cont}-21.6}{12.55})\right) \qquad 6.5$$

By measuring the liquid temperature at each steady state period, a good estimate of the evaporated mass from the container can be obtained. This value is then subtracted from $\dot{m}_{mes}$ to obtain $\dot{m}_{foam}$.

6.6.2 Heat loss measurements

All the recorded temperatures are averaged over the final 30 data points (1min) of the acquired steady state data. Assuming 1-D conduction from the heater to the copper block surface, including the thermal pad and thermal paste resistances, the wall temperature, T_{wall}, of the copper block (Figure 6.2a) can be calculated. Due to the difficulty in estimating the thermal pad and paste thicknesses, separate natural convection tests were done on the copper block without the foam. By measuring the copper wall temperature with thermal paste on the surface, in different heat fluxes and assuming 1-D conduction, thermal pad and paste thicknesses are estimated to be 350 μm and 200 μm respectively. It is noted that due to much higher thermal resistances of the heater block insulation, all the heat is assumed to go towards the copper block.

Foam surface temperature T_{surf} is defined as the average temperature of the foam area touching the copper block wall (25×15) measured by thermocouples T3 to T5. It will be shown that prior to the onset of dryout; these temperatures are almost the same which implies a constant temperature phase change. Moreover, due to the low thermal conductivity of copper metal foams (k = 4.8 W/m K), a sharp temperature drop below the lower edge of the heated area is observed which clearly shows that most of the heat transfer occurs right on the heated area.

To calculate the energy balance and different heat losses through the setup, it is assumed that all the power produced by the power supply is converted to heat and the resistance in the wiring is negligible. The total power dissipated in the heater Q_{in} is lost to the ambient through the following mechanisms:

$$Q_{in} = Q_{evap} + Q_{conv} + Q_{rad} + Q_{cond} + Q_{sens} \qquad 6.6$$

The heat transfer by evaporation Q_{evap} is determined according to

$$Q_{evap} = \dot{m}_{foam} h_{fg} \tag{6.7}$$

In which h_{fg} for ethanol is 846 kJ/kg.

An empirical approach is employed to calculate the convective heat loss Q_{conv} from all surfaces of the test apparatus A foam sample of the same length as those used in the experiments was tested without contacting the liquid container. A series of tests at different power levels were performed for this configuration and the average steady-state heater temperature was recorded at each power level. A relationship between input power and heater temperature was then obtained as a curve fit, with the results:

$$Q_{conv} = 0.037 T_{heater} - 0.95 \tag{6.8}$$

By substituting the measured average heater temperature into the curve-fit relationship, the heat loss through convection can be estimated. This approach is suitable because of the short length of the foam samples in this research (3.5 cm exposed to ambient) and therefore, no other correlation was used to calculate the convection heat loss.

The radiation heat loss in wick region is obtained by

$$Q_{rad} = \varepsilon \sigma A \left(T_{surf}^4 - T_{amb}^4 \right) \tag{6.9}$$

in which T_{surf} is the average temperature of the heated area (measured by T3-T5) and A is the heated area of the foam. The radiation from the unheated part of the foam is estimated to be negligible due to much lower average temperature. T_{amb} is the ambient temperature and emissivity is assumed to be unity.

Heat conduction down the length of the wick into the liquid container Q_{cond} is determined from the temperature gradient in the wick near the surface of the liquid container according to:

$$Q_{cond} = kA\left(\frac{T_5 - T_6}{x_5 - x_6}\right) \tag{6.10}$$

Where T_5 and T_6 are the closet thermocouples to the liquid surface and k is the measured thermal conductivity of the foams (k = 4.8 W/m K).

Part of the applied heat rate is used to increase the liquid temperature as it rises from the container to the heated zone. The maximum temperature reached by the liquid will be the ethanol saturation temperature in 1 bar pressure (T_{sat} = 78.8 °C), even if the foam surface temperature is higher. This heat rate can be expressed as:

$$Q_{sens} = \dot{m}_{foam} C_p \left(\min\{T_{surf}, T_{sat}\} - T_{cont} \right) \qquad 6.11$$

where C_p for ethanol is 2.44 kJ/kg K. The surface temperature will rise to much higher temperatures than ethanol saturation temperature in high heat fluxes. Therefore, in those cases, T_{surf} is replaced by ethanol saturation temperature (78.8 °C).

6.7 Results and discussion

6.7.1 Heat loss

Figure 6.3 shows a comparison of the input power and individual contribution of each heat transfer mode to the overall heat transfer for 68% porosity foam. The values for other porosities are similar and not shown here. Q_{in} is measured directly by multimeters and all other terms are calculated indirectly based on the heat and mass transport analysis provided in the previous section. A linear increase in evaporation rate is seen with an increase in applied input power, as expected. Quantification of the other possible heat transport modes reveals that approximately 45–50% of the applied power is dissipated by evaporation of the working fluid; 35-40% is dissipated by convection and the rest by the combined effect of radiation, conduction and sensible heating of the working liquid (~10%). The high percentage of convection can be attributed to the condition in which tests were conducted which is in ambient room. It is expected that if the tests are done in a more confined environment then the contribution of the convection decreases accordingly. Due to the relatively low surface temperature, very low thermal conductivity and small liquid mass fluxes, the contribution of all other heat transfer modes are small. Comparison of the values of the input power and measured heat flow shows that values agree to within 10% for all cases except for two cases

where the difference is 20%. The comparison demonstrated in Figure 6.3 demonstrates the accuracy of the measurement technique developed.

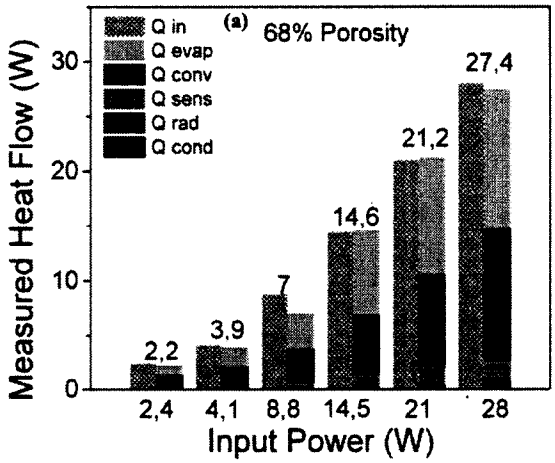

Figure 6.3 Comparison of input power and individual contribution of each heat transfer mode to the measured heat flow of 68% porosity foam

6.7.2 Wick Temperature

Axial temperature distribution in different foam porosities and power levels can be seen in Figure 6.4. The location x = 0 mm is at the liquid surface temperature. Data points shown here are measured by the thermocouples T6 to T3 respectively (Figure 6.4a). It can be seen that as it is expected, there is an increase in surface temperatures at higher applied heat fluxes. The dryout heat fluxes can be identified by the surface temperatures higher than 78.8 °C (ethanol saturation temperature in 1 bar). It can also be seen that the surface temperature before dryout is relatively constant which is consistent with the liquid phase change occurring on the surface. Table 6.2 shows the onset of dryout for different foam porosities. The temperature shown by T5 (located at the lower edge of the heater area) is relatively constant and does not change much in different heat fluxes. It can be explained by the vaporization of working fluid at a constant temperature which limits the temperature increase along this length.

Table 6.2 Onset of dryout for different foam porosities

Porosity	68%	75%	82%
Input power (W)	4.5	10.5	19.5

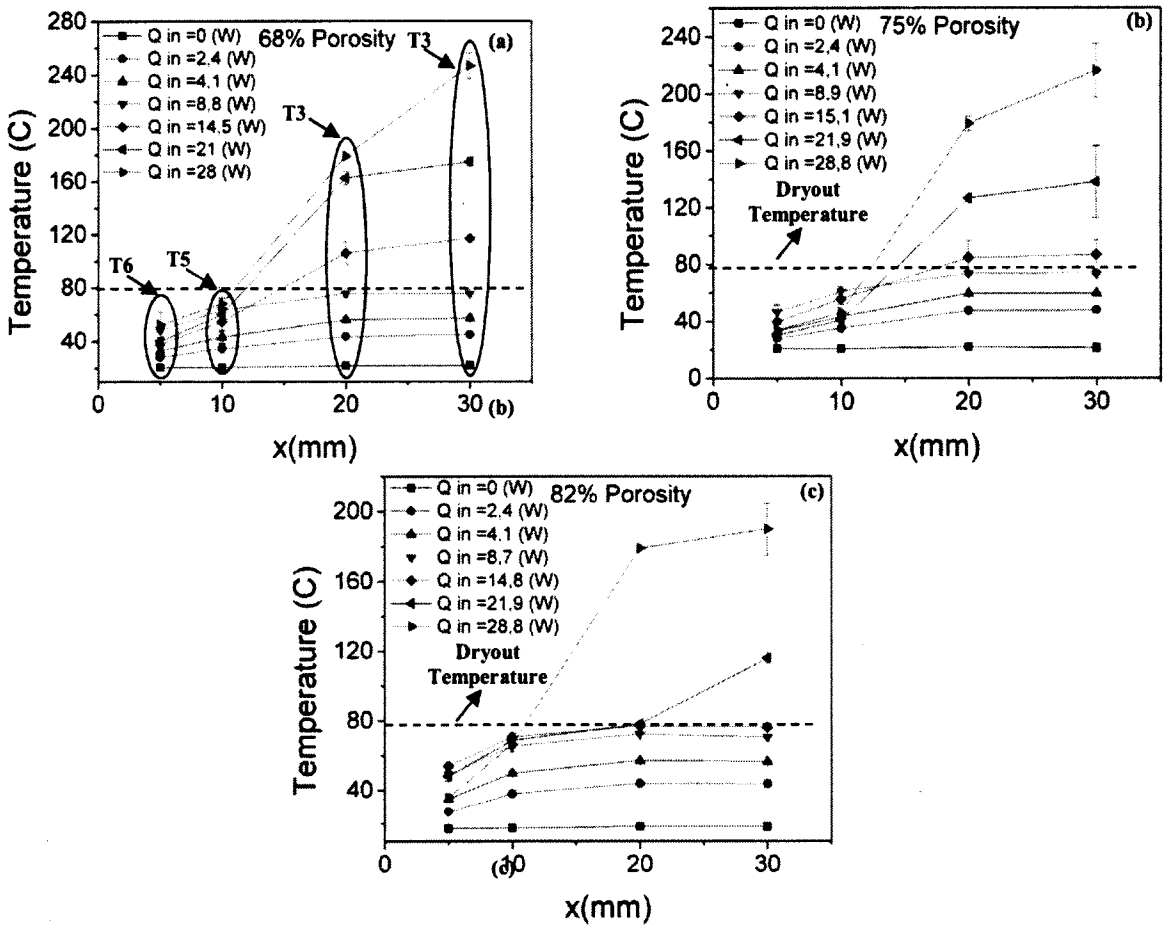

Figure 6.4 Axial temperature distribution in metal foams of a) 68% porosity b) 75% porosity and c) 82% porosity. x = 0 is in the liquid container

6.7.3 Evaporation rate

Figure 6.5 shows the foam evaporation rate in different calculated wall temperatures and measured heat fluxes. As it is expected, the evaporated liquid flow rate increases with heat flux increase. This evaporation rate keeps increasing even after the onset of dryout at the top of the foam surface. This shows that the evaporation limit is much higher than the capillary limit and much higher vaporization rates can be obtained if the capillary limit is bypassed by choosing a short length sample. Furthermore, the evaporation rates are the same for the first 4 data points (for different foam porosities with the same input heat flux). This shows that the evaporation rate is a strong function of the macro effects such as availability of liquid to evaporate and higher effective thermal conductivity. In fact, the microstructures on the foam

surface provide enough evaporation sites for thin film evaporation and the main resistance then becomes the pumping liquid capacity and thermal conductivity of the foams.

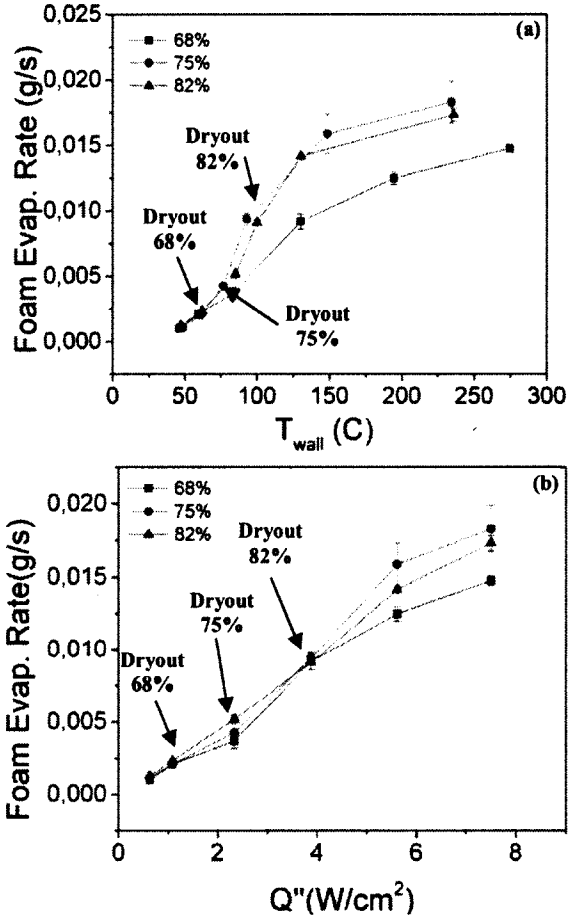

Figure 6.5 Effect of (a) wall temperature and (b) heat flux on the evaporation rates of the different foam porosities

6.7.4 Effect of temperature on the effective pore radius

Figure 6.6 shows the effect of temperature on the liquid front in 75% porosity foam for three different heat fluxes. The location of liquid front and its vertical displacement can be identified in this figure. Up to Qin = 8.7 W, no dryout is observed and the whole surface is wet and contributes to the evaporation Figure 6.6a). The relatively uniform temperature of the heated area foam surface shows the effect of evaporation. The gradual increase of the heat flux up this point leads to higher vaporization rate and therefore, more liquid should be pumped to the heated area. The required pressure should be provided by capillary pressure produced by

the meniscus curvature at the vapor-liquid interface. As the heat flux increases, the intensified vaporization of the liquid leads to a point where the maximum capillary pressure produced by the recessed meniscus cannot maintain the liquid in the whole length of the foam sample. Therefore, as can be seen in Figure 6.6b, the liquid front will displace and adjust itself to a lower height to face lower liquid pressure drop.

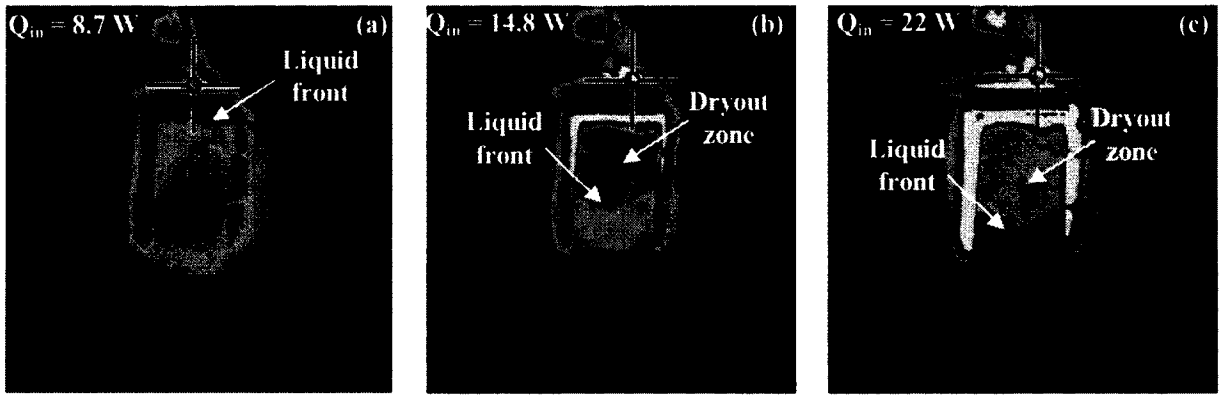

Figure 6.6 IR profile of the 75% porosity foam (a) the whole surface is wet (wetted length, x = 35 mm) (b) liquid front decreased to x = 23 mm from liquid surface (c) liquid front in x = 13 mm from liquid surface

Figure 6.7 shows the effect of the increased heat flux on the effective pore radius of the copper metal foams and its ratio to permeability. As the heat flux increases the liquid pumping rate increases accordingly to replenish the evaporated liquid mass. By measuring this liquid mass (the foam evaporation rate), the liquid front height, foam geometrical properties and liquid properties and by employing Equations 6.3 and 6.4 we can obtain the required effective pore radius for different heat fluxes. Permeability and effective pore radius of these foams are already measured by the rate of rise method [72] and the results are presented in Table 6.3. Permeability is only a function of the porous material resistance and can be considered to be constant regardless of the applied heat flux.

It can be seen in Figure 6.7a that the increased evaporation rate leads to a meniscus recession and accordingly to a decreased effective pore radius. For the case of 75% and 82% porosity, the meniscus recession reaches its minimum just before the onset of dryout. After dryout, the liquid front moves towards a lower position and the effective pore radius increases. Generally, with further increase in heat flux, the meniscus recesses again and adjusts its curvature so that

the maximum liquid is pumped to the meniscus region for evaporation. For the case of 68% porosity, the heat flux where dryout occurs is not exactly where the maximum meniscus recession occurs. In this foam, the location of the liquid front is difficult to identify due to denser structures and smaller pores. This may be the reason for this discrepancy. Our results show that the recessed meniscus will lead to 15%, 28% and 52% decrease in r_{eff} for 68%, 75% and 82% sample porosities respectively, compared with the values obtained by the rate of rise method. This clearly shows the importance of the meniscus recession phenomena in the capillary pumping of the porous materials.

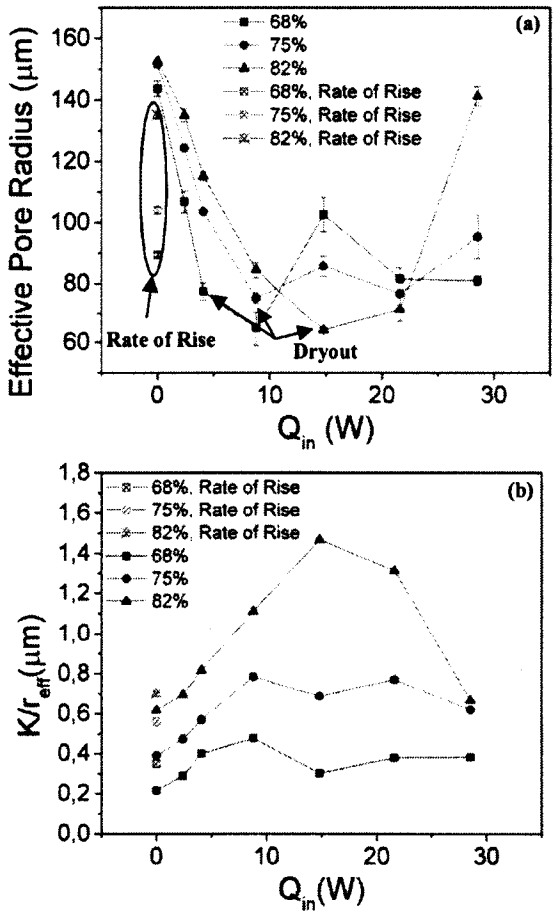

Figure 6.7 (a)Values of calculated effective pore radius for different heat fluxes (b) Values of K/reff for different heat fluxes

Table 6.3. Permeability K and effective pore radius r_{eff} for foam samples of 68%, 75% and 82% porosities measured by the rate of rise method (no applied heat flux) [72]

	68%				75%				82%			
	K(μm2)		reff (μm)		K(μm2)		reff (μm)		K(μm2)		reff (μm)	
	mean	STDV	Mean	STDV	mean	STDV	Mean	STDV	mean	STDV	Mean	STDV
Open	31	6	89.4	0.9	59	8	104.0	1.0	94	10	135.0	1.0

6.7.5 Conclusion

Effect of meniscus recession on the effective pore radius and capillary pumping of copper metal foams is obtained using an in-situ heated capillarity test method. IR imaging along with mass and temperature measurements are used to characterize the impact of meniscus recession on the effective pore radius and capillary pumping of copper metal foams. Results show that the effective pore radius decreases at higher heat fluxes. Furthermore, it reaches a minimum value at the onset of dryout. The recessed meniscus will lead to 15%, 28% and 52% decrease in r_{eff} for 68%, 75% and 82% sample porosities respectively. This shows a significant improvement compared with the maximum capillarity measured by the rate of rise method which does not include the effect of forced evaporation, hence the role of meniscus recession. The results of this study can lead to a better prediction of the capillary limits in two-phase capillary-driven devices such as heat pipes and heat spreaders.

6.8 Acknowledgements

This research was jointly funded by NSERC and Metafoam Technologies Inc. We are grateful for the support and guidance of Dominic Pilon. The contribution of Stéphane Gutierrez for SEM imaging is also greatly appreciated.

7 CONCLUSIONS AND FUTURE WORK

The principal objective of this work was to understand the mechanisms governing the heat and mass transport in the capillary-driven phase change heat transfer in Metafoam's biporous metal foams used as wick in heat pipes. This will help to improve modeling and performance capabilities of heat pipes utilizing these foams. Characterizing the capillary driven phase change heat transfer performance in these copper metal foams opens a way for enhancing the future materials by recognizing the specifications of an effective media for heat pipe wicking materials. This work investigated wicking and capillary properties as well as phase change transport in capillary-fed copper metal foams. In the following, a summary of the primary conclusions resulting from each of these investigations, along with several suggestions for future work will be presented.

7.1 Conclusions

Here are the important results of this research:

- The results of parametric study on transport limits for a circular heat pipe confirm that capillary and boiling limits are the dominant ones in the temperature ranges used in electronics cooling. Entrainment may however become limiting in lower temperature ranges. However, for the typical dimensions and wick properties, capillary limit will be the first limit to occur. This required studying the transport phenomena related to this limit i.e. capillarity and evaporation.

- Wettability of the foams was investigated and it was shown that contrary to a common belief in the heat pipe community, the adsorption of volatile organic compounds (VOC) and not the oxidation is the reason for the loss of hydrophilicity in metal foams. It is believed that the same phenomenon is responsible for the wetting transition in other copper based porous materials such as copper powder or wire mesh.

- Capillary properties such as permeability, effective pore radius and internal contact angle of copper metal foams are obtained by measuring the rate of mass uptake with acetone, ethanol, and water as test liquids with a specific attention to the evaporation role and the presence of walls. It was found that the rate of evaporation of acetone and ethanol from the rising liquid is significantly lower than that measured for stationary liquid in a saturated foam sample. This shows the coupled nature of evaporation and capillarity in these porous materials.

- Sintering copper walls attached to the copper metal foams has almost no effect on the capillary rise behavior and the evaporation rate. Hence, covering most of the foam surfaces does not hinder the evaporation rate. Only by putting the samples in a semi saturated ambient can a significant change in evaporation rate be observed. This suggests that the foams are very efficient mass transport media with low internal mass diffusion resistance.

- The non-zero internal contact angle of water in the copper porous foams is seen to be smaller than the water contact angle on a flat piece of copper. It is caused by the morphology of the foams and the interactions of the liquid and microstructure. Decreasing the internal contact angle can change the ratio of K/r_{eff} which would favor more porous foams.

- The effective pore radius decreases at higher heat fluxes. Furthermore, it reaches a minimum value at the onset of dryout. The recessed meniscus will lead to up to 50% decrease of r_{eff} in different foam porosities. This shows a significant improvement compared with the maximum capillarity measured by the rate of rise method which does not include the effect of forced evaporation, hence the role of meniscus recession. Moreover, the meniscus recession leads to a minimum wick thermal resistance. Coupling of evaporation and capillarity can best be seen by considering that both minimum effective pore radius and minimum wick thermal resistance occur at the same heat flux.

- Although this research was specifically performed on the bi-porous copper metal foams, some findings in this thesis can be applicable to other types of wicking materails. The 1-D model developed to characterize the heat pipe operation can be used to evaluate the performance of heat pipes with other types of wicking materials if their permeability and effective pore radius are know. Moreover, the mechanism of wettability transition and the reason for the hydrophilicity loss of the copper metal foams when exposed to ambient air, can be used to explain the same phenomena in other copper based wicking materails. The novel experimental methods including the rate of spreading and the recessed meniscus effective pore radius measurement with forced evaporation can also be employed to characterize other porous wicking materials.

7.2 Suggested future work

1. An overlooked aspect in the previous investigations on the capillary driven evaporation in porous wicks has been the coupling and interconnection between evaporation and capillarity. By separating the evaporation and capillarity and studying each one separately, the impact of the coupling between the two is ignored and this may lead to unrealistic results. As it was done here in this thesis, it is suggested that in the future works, research methodologies and more specifically experiments are designed to consider this effect.

2. In chapter 6, the effect of meniscus recession on capillary pumping was studied by choosing a relatively long wetted sample length. By changing the wetted length of the sample, effect of capillary pumping can be varied. Therefore, by decreasing the sample length, the evaporation rate can be increased substantially. This will have an impact on the overall thermal resistance of the foam sample. In this way, the extreme values of thermal resistance associated with evaporation dominant and capillary dominant mode can be evaluated.

3. The results show that the pumping capacity of the foams is critical in designing high performance wicking materials. Therefore, methods to increase K/r_{eff} which is a function of capillary pumping are important. Increasing the wettability of a surface has a direct effect on capillary pumping through decreasing r_{eff}. The current method to make the foam surface hydrophilic and decrease the water contact angle is hydrogen treatment. If other methods can be used to further increase the wettability, higher pumping rates will be achieved. Therefore, more research in this regard is required.

4. The conditions occurring inside an operating heat pipe are different from those used in this research because of saturated ambient and higher vapor core pressure drop. Hence, all the parameters found by methods in this thesis should be eventually tested in conditions similar to that of an operating heat pipe to confirm the findings. Therefore, developing test setup with typical specifications of a heat pipe is valuable.

7.3 Conclusions (en français)

Voici les principaux résultats de cette recherche:

- Les résultats de l'étude paramétrique sur les limites de transport pour un caloduc circulaire confirment que les limites capillaires et d'ébullition sont les limites dominantes dans les plages de température utilisés pour le refroidissement de l'électronique. L'entraînement peut cependant devenir limitant dans les gammes inférieures de température. Toutefois, pour les dimensions typiques et les propriétés de mèche, limite capillaire sera la première limite de se produire. Il a fallu étudier les phénomènes de transport liés à cette limite soit capillarité et l'évaporation.

- Mouillabilité des mousses a été étudiée et il a été montré que, contrairement à une croyance commune dans la communauté de caloduc, l'adsorption de composés organiques volatils (COV) et non l'oxydation est la raison de la perte d'hydrophilicité dans les mousses métalliques. On pense que le même phénomène est responsable de la transition de mouillage dans d'autres matériaux poreux à base de cuivre tels que la poudre de cuivre ou de treillis métallique.

- Propriétés capillaires telles que la perméabilité, le rayon de pore effectif et de l'angle de contact interne de mousses métalliques de cuivre sont obtenus en mesurant la vitesse d'absorption de la masse avec de l'acétone, de l'éthanol et de l'eau comme liquide d'essai avec une attention particulière au rôle de l'évaporation et de la présence de parois. Il a été constaté que le taux d'évaporation de l'acétone et d'éthanol à partir de la montée du liquide est nettement inférieur à celle mesurée pour le liquide stationnaire dans un échantillon de mousse saturée. Cela montre le caractère couplé de l'évaporation et la capillarité dans ces matériaux poreux.

- Murs de cuivre de frittage attachés aux mousses métalliques en cuivre n'a presque aucun effet sur le comportement de la remontée capillaire et le taux d'évaporation. Ainsi, couvrant la plupart des surfaces de mousse n'empêche pas le taux d'évaporation.

Seulement en mettant les échantillons dans une ambiance semi-saturée, un changement important dans la vitesse d'évaporation peut être observé. Ceci suggère que les mousses sont des moyens de transport de masse très efficaces avec une faible résistance à la diffusion de masse interne.

- L'angle de contact interne non nul de l'eau dans les mousses poreuses en cuivre est considéré comme étant plus petit que l'angle de contact de l'eau sur un morceau plat de cuivre. Elle est causée par la morphologie des mousses et les interactions du liquide et de la microstructure. Diminuant l'angle de contact interne peut changer le rapport K / r_{eff} qui favoriserait les mousses plus poreuses.

- Le rayon de pore efficace diminue au flux thermique élevé. De plus, il atteint une valeur minimale au début de l'assèchement. Le ménisque reculé va mènera à un maximum de 50% de diminution de r_{eff} dans différentes porosités de mousse. Cela montre une amélioration significative par rapport à la capillarité maximale mesurée par la méthode du taux d'augmentation qui n'inclut pas l'effet de l'évaporation forcée, d'où le rôle du ménisque récession. De plus, la récession du ménisque mène à une résistance thermique minimum de mèche. Couplage de l'évaporation et de capillarité est plus visible en considérant que tous les deux du rayon de pore efficace minimum et de la résistance thermique minimum de la mèche se produisent au même flux thermique.

- Cette recherche a été spécifiquement réalisée sur les mousses métalliques cuivre biporeux cependant, certaines conclusions de cette thèse peuvent être applicables à d'autres types de matériaux de mèches. Le modèle 1-D développé pour caractériser le fonctionnement du caloduc peut être utilisée pour évaluer la performance des caloducs avec d'autres types de matériaux mèches si leur perméabilité et le rayon de pore effectif sont connus. En outre, le mécanisme de transition de mouillabilité et la raison de la perte d'hydrophilicité des mousses métalliques en cuivre lorsqu'ils sont exposés à l'air atmosphère peut être utilisé pour expliquer le même phénomène dans d'autres matériaux de mèche à base de cuivre. Les nouvelles méthodes expérimentales, dont le

taux de propagation et la mesure de ménisque reculé avec l'évaporation forcée peuvent également être utilisés pour caractériser d'autres matériaux de mèche poreux.

7.4 Travaux futurs

1. Un aspect négligé dans les études précédentes sur l'évaporation et la capillarité dans les mèches poreuses a été le couplage et l'interconnexion entre l'évaporation et la capillarité. En séparant l'évaporation et la capillarité et l'étude de chacun d'eux séparément, l'impact du couplage entre les deux est ignoré et cela peut mène à des résultats irréalistes. Comme cela a été fait ici, dans cette thèse, il est suggéré que, dans les travaux futurs, les méthodes de recherche et plus particulièrement les expériences sont conçues pour examiner cet effet.
2. Dans le chapitre 6, l'effet de la récession du ménisque capillaire de pompage a été étudié par le choix d'une longueur relativement importante de l'échantillon mouillé. En modifiant la longueur mouillée de l'échantillon, l'effet de pompage capillaire peut être modifié. Par conséquent, en réduisant la longueur de l'échantillon, le taux d'évaporation peut être augmenté en grande partie. Cela aura un impact sur la résistance thermique totale de l'échantillon de mousse. De cette façon, les valeurs extrêmes de résistance thermique associée avec le mode de capillaire dominant et d'évaporation dominante peuvent être évaluées.

3. Les résultats montrent que la capacité de pompage des mousses est essentielle dans la conception de matériaux de mèche haute performance. Par conséquent, les méthodes pour augmenter K/r_{eff} qui est une fonction de pompage capillaire sont importants. L'augmentation de la mouillabilité d'une surface a un effet direct sur le pompage capillaire en diminuant Reff. La méthode actuelle de rendre la surface de la mousse hydrophile et de diminuer l'angle de contact de l'eau est le traitement de l'hydrogène. Si d'autres méthodes peuvent être utilisées pour augmenter la mouillabilité davantage, les taux de pompage élevés seront atteints. Par conséquent, plus de recherche dans ce domaine est nécessaire.

4. Les conditions qui se produisent à l'intérieur d'un caloduc fonctionnel sont différentes de ceux utilisés dans cette étude en raison d'ambiant saturé et perte de charge plus élevée de vapeur. Par conséquent, tous les paramètres trouvés par les méthodes de cette thèse devraient être finalement testés dans des conditions similaires à celles d'un caloduc fonctionnel pour confirmer les résultats. Par conséquent, le développement d'un montage de test avec les conditions typiques d'un caloduc est très utile.

APPENDIX A

A.1 Solving the differential Eqautuins in chapter 3

From the mathematical point of view, the pressure distribution in the liquid and vapor phase of a heat pipe can be expressed by second order ordinary differential eqautions:

$$\frac{d^2P}{dx^2} = Aq_d \qquad \text{A.1}$$

Where A and q_d are constants. An analytical solution can be obtained for this equation based on the different zones of the heat pipe (evaporator, adiabatic zone and condenser)

In the evaporator zone:

$0 \le x \le L_e$

$$\frac{d^2P}{dx^2} = Aq_{d,evp}$$

$$\frac{dP}{dx} = Aq_{d,evp}x + C_1$$

$$B.C: \left.\frac{dP}{dx}\right|_{x=0} = 0 \rightarrow C_1 = 0$$

$$P = \frac{1}{2}Aq_{d,evp}x^2 + C_2$$

In the adiabatic zone:

$L_e \le x \le L_e + L_a$

$$\frac{d^2P}{dx^2} = 0$$

$$\frac{dP}{dx} = C_3$$

$$B.C: \left.\frac{dP}{dx}\right|_{x=L_e} = \left.\frac{dP}{dx}\right|_{x=L_e+L_a} \rightarrow C3 = Aq_{d,evp}L_e$$

$$P = (Aq_{d,evp}L_e)x + C_4$$

In the condesner zone:

$$L_e + L_a \le x \le L_e + L_a + L_c$$

$$\frac{d^2P}{dx^2} = Aq_{d.con}$$

$$\frac{dP}{dx} = Aq_{d.con}x + C_5$$

$$B.C: \left.\frac{dP}{dx}\right|_{x=L_e+L_a+L_c} = 0 \rightarrow C_5 = -Aq_{d.con}(L_e + L_a + L_c)$$

$$P = \frac{1}{2}Aq_{d.con}x^2 - Aq_{d.con}(L_e + L_a + L_c)x + C_6$$

Tofind the equation constants C_2, C_4, and C_6 it is assumed that the pressure at the end of the condenser zone is equal to the saturatuion pressure at the operating temperature. Therefore, all constants can be found.

APPENDIX B

B.1 Effect of meniscus recession on wick thermal resistance

This appendix is a complement to the material presented in chapter 6 and was not included in that chapter because of the page limit of the corresponding conference. As it was explained before in that chapter, the copper wall temperature T_{wall} can be calculated by measuring the copper block temperature in different heat fluxes, taking into account the effect of thermal paste and thermal pad and assuming 1-D conduction. It is noted that due to the much higher thermal resistances of the surrounding insulation, all the heat is assumed to go towards the copper block. The calculated thermal resistance for wick samples is defined as:

$$R_{wick} = \frac{T_{wall} - T_{surf}}{Q_{in}} \qquad \text{B.1}$$

in which T_{wall} is the copper block wall temperature, T_{surf} is the average temperature of the foam area in line with the copper block wall (25×15) measured by the thermocouples T3 to T5. The calculated thermal resistances of different foam porosities are presented in Figure B.1 as a function of wall superheat and heat flux. A lower thermal resistance corresponds to a more favorable overall heat transfer coefficient from the surface to the wick. It can be seen in Figure B.1a that at a certain wall superheat, 75% foam porosity has the highest transferred heat flux which corresponds to a lower thermal resistance. Figure B.1b shows the thermal resistance of different foam porosities vs. heat flux. It can be seen that at lower heat inputs, the wick thermal resistance is higher and decreases as the heat input increases up to the point where dryout occurs. Once dryout commences and liquid level starts to displace to a lower height, the surface temperature in the dried region increases drastically. This dryout will lead to a higher average surface which in turn will increase the overall wick thermal resistance. It can also be seen that 75% foam has the lowest thermal resistance which can be attributed to an optimum value of wick thermal conductivity and capillary pumping to maintain evaporation on the surface. Given the lower porosity of the 68% foam and hence the highest thermal conductivity, it is expected that the 68% foams would have a lower thermal resistance

compared with 75% porosity foam. But the lower thermal resistance of the 75% foams clearly demonstrates the role of effective capillary fed evaporation on the overall heat transfer. In fact, the higher permeability of 75% porosity foams permits better capillary pumping to the evaporation sites on the foam surface which will eventually lead to lower thermal resistance. It should also be noted that while 82% foam has the highest dryout limit (highest dryout heat flux), it has a poor thermal performance (higher wall temperature) by having a high thermal resistance.

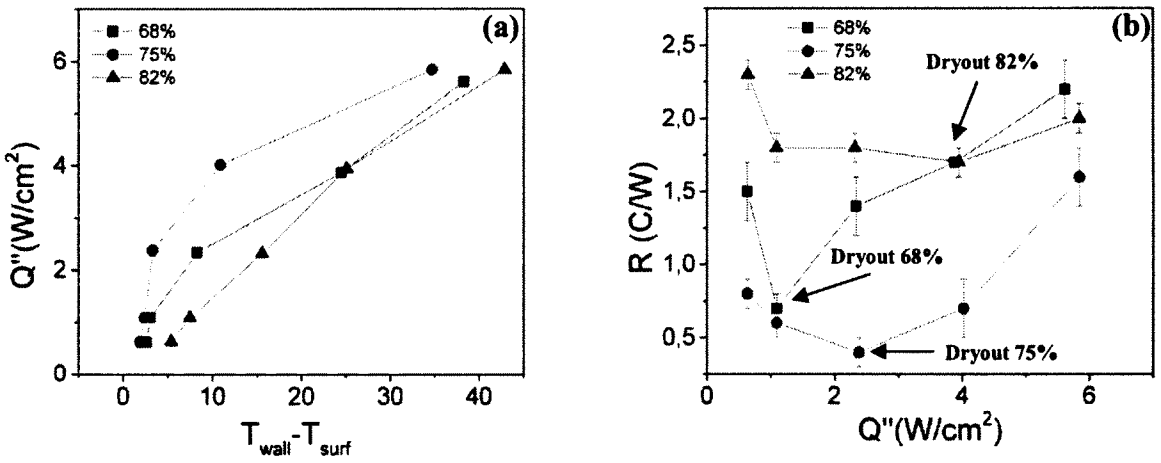

Figure B.1 Steady-state thermal performance results for different foam porosities: (a) evaporation curves; (b) calculated wick thermal resistances as a function of heat flux.

Variation of the effective pore radius and the wick thermal resistance as a function of heat flux are shown in Figure B.2 . It can be seen that wick thermal resistance reaches a minimum value at the onset of dryout for all foam porosities. Wick minimum thermal resistance coincides with the minimum effective pore radius for the foam porosities of 75% and 82%. However, it is not clearly the case for the 68% porosity foam. Further research is required to explain this phenomenon.

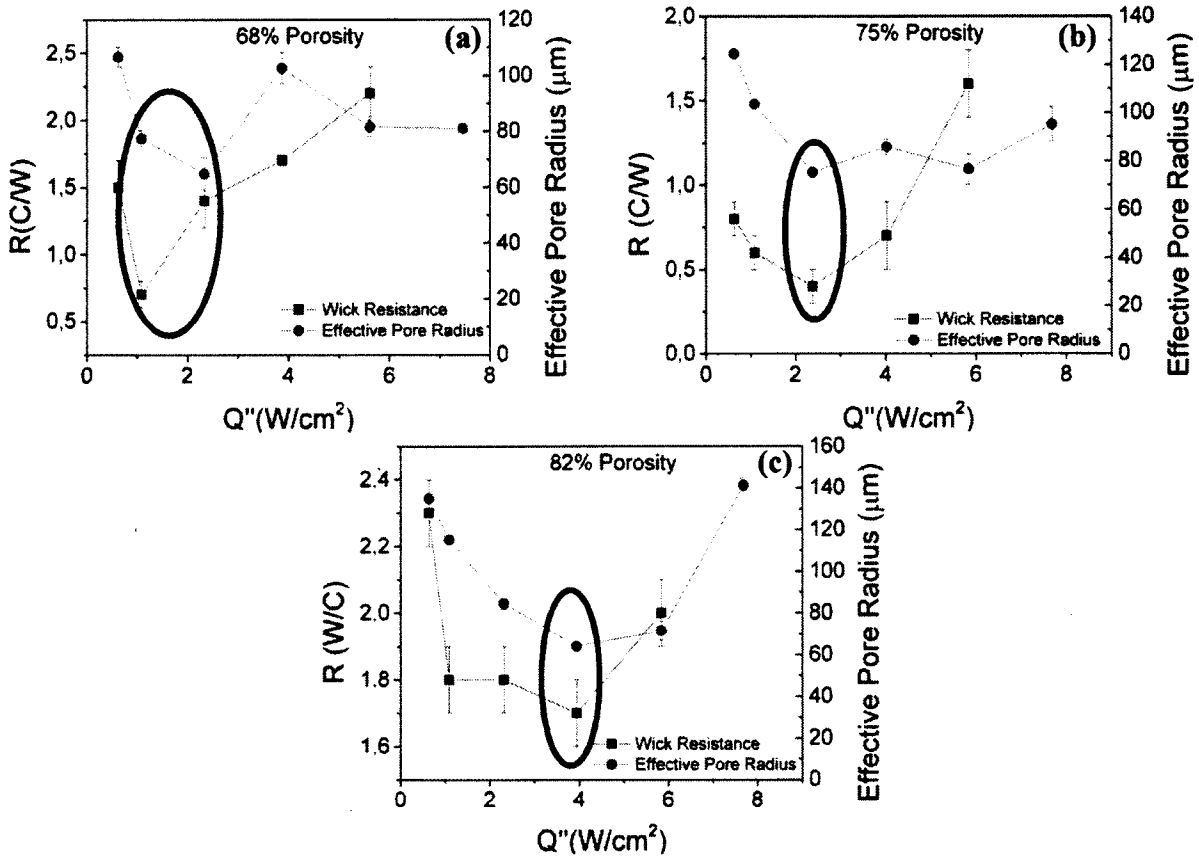

Figure B.2 Variation of effective pore radius and wick thermal resistance with input heat flux for different foam porosities

REFERENCES

[1] Adam, N. K. (1968). *The Physics and Chemistry of Surfaces* . Dover Publications, Inc., Canada, 402 p.

[2] Adamson, A.W., Gast, A.P. (1997). *Physical Chemistry of Surfaces*, 6th edition . Wiley-Interscience, United states of America, 808 p.

[3] Agostini, B., Fabbri, M., Park, J. E., Wojtan, L., Thome, J. R. and Michel, B. (2007). State of the art of high heat flux cooling technologies. *Heat Transfer Engineering,* volume 28, number 4, p. 258-281.

[4] Berti, L. F., Santos, P. H. D., Bazzo, E., Janssen, R., Hotza, D. and Rambo, C. R. (2011). Evaluation of permeability of ceramic wick structures for two phase heat transfer devices. *Applied Thermal Engineering,* volume 31, number 6-7, p. 1076-81.

[5] Biesinger, M. C., Lau, L. W. M., Gerson, A. R. and Smart, R. S. C. (2010). Resolving surface chemical states in XPS analysis of first row transition metals, oxides and hydroxides: Sc, Ti, V, Cu and Zn. *Applied Surface Science,* volume 257, number 3, p. 887-898.

[6] Boomsma, K., Poulikakos, D. and Zwick, F. (2003). Metal foams as compact high performance heat exchangers. *Mechanics of Materials,* volume 35, number 12, p. 1161-1176.

[7] Byon, C. and Kim, S. J. (2012). Capillary performance of bi-porous sintered metal wicks. *International Journal of Heat and Mass Transfer,* volume 55, number 15-16, p. 4096-4103.

[8] Carbajal, G., Sobhan, C. B., Bud Peterson, G. P., Queheillalt, D. T. and Wadley, H. N. G. (2007). A quasi-3D analysis of the thermal performance of a flat heat pipe. *International Journal of Heat and Mass Transfer,* volume 50, number 21-22, p. 4286-4296.

[9] Chavez, K. L. and Hess, D. W. (2001). A novel method of etching copper oxide using acetic acid. *Journal of the Electrochemical Society,* volume 148, number 11, p. 640-3.

[10] Chen, S., Hsieh, J., Chou, C., Lin, H., Shen, S. and Tsai, M. (2007). Experimental investigation and visualization on capillary and boiling limits of micro-grooves made by different processes. *Sensors and Actuators, A: Physical,* volume 139, number 1-2, p. 78-87.

[11] Chen, X., Kong, L., Dong, D., Yang, G., Yu, L., Chen, J. and Zhang, P. (2009). Fabrication of functionalized copper compound hierarchical structure with bionic superhydrophobic properties. *Journal of Physical Chemistry C,* volume 113, number 14, p. 5396-401.

[12] Chen, X., Kong, L., Dong, D., Yang, G., Yu, L., Chen, J. and Zhang, P. (2009). Synthesis and characterization of superhydrophobic functionalized $Cu(OH)_2$ nanotube arrays on copper foil. *Applied Surface Science,* volume 255, number 7, p. 4015-4019.

[13] Chu, R. C., Simons, R. E., Ellsworth, M. J., Schmidt, R. R. and Cozzolino, V. (2004). Review of cooling technologies for computer products. *IEEE Transactions on Device and Materials Reliability,* volume 4, number 4, p. 568-85.

[14] Collier, J. G. et Thome, J. R. (2001). *Convective Boiling and Condensation*, third edition . Oxford University Press, United states, 640 p.

[15] Coursey, J. S., Kim, J. and Boudreaux, P. J. (2005). Performance of graphite foam evaporator for use in thermal management. *Transactions of the ASME.Journal of Electronic Packaging,* volume 127, number 2, p. 127-34.

[16] Davis, T. W. and Garimella, S. V. (2008). Thermal resistance measurement across a wick structure using a novel thermosyphon test chamber. *Experimental Heat Transfer,* volume 21, number 2, p. 143-54.

[17] Elayiaraja, P., Harish, S., Wilson, L., Bensely, A. and Lal, D. M. (2010). Experimental investigation on pressure drop and heat transfer characteristics of copper metal foam heat sink. *Experimental Heat Transfer,* volume 23, number 3, p. 185-195.

[18] Faghri, A. (1995). *Heat Pipe Science and Technology*, first edition . Taylor & Francis Group, Great Britain, 854 p.

[19] Fan, L., Yuan, X., Zhou, C., Zeng, A., Yu, K., Kalbassi, M. and Porter, K. (2011). Contact angle of ethanol and n-propanol aqueous solutions on metal surfaces. *Chemical Engineering and Technology,* volume 34, number 9, p. 1535-1542.

[20] Feng, X. and Jiang, L. (2006). Design and creation of superwetting/antiwetting surfaces. *Advanced Materials,* volume 18, number 23, p. 3063-3078.

[21] Fries, N. and Dreyer, M. (2008). An analytic solution of capillary rise restrained by gravity. *Journal of colloid and interface science,* volume 320, number 1, p. 259-263.

[22] Fries, N., Odic, K., Conrath, M. and Dreyer, M. (2008). The effect of evaporation on the wicking of liquids into a metallic weave. *Journal of colloid and interface science,* volume 321, number 1, p. 118-129.

[23] Friess, B. R. and Hoorfar, M. (2010). Measurement of internal wettability of gas diffusion porous media of proton exchange membrane fuel cells. *Journal of Power Sources,* volume 195, number 15, p. 4736-42.

[24] Ganesan, G. S., Lewis, G. L., Anderson, T.andBerg, H. M. (1996). Organic contamination in IC package assembly and it's impact on interfacial integrity. In *Proceedings 46th Electronic Components and Technology Conference.* IEEE, New York, NY, USA, p. 68-70.

[25] Garimella, S. V. (2006). Advances in mesoscale thermal management technologies for microelectronics. *Microelectronics Journal,* volume 37, number 11, p. 1165-1185.

[26] Gennes, P. d., Brochard-Wyard, F. et Quere, D. (2004). *Capillarity and Wetting Phenomena: Drops, Bubbles, Pearls, Waves*. Springer, United states, 291 p.

[27] Gros, E. (2006). *Caractérisation thermique des mousses métalliques.* M.Sc.A., Université de Sherbrooke, Sherbrooke, Canada.

[28] Gurau, V., Bluemle, M. J., De Castro, E. S., Tsou, Y., Mann Jr., J. A. and Zawodzinski Jr., T. A. (2006). Characterization of transport properties in gas diffusion layers for proton exchange membrane fuel cells. 1. Wettability (internal contact angle to water and surface energy of GDL fibers). *Journal of Power Sources,* volume 160, number 2, p. 1156-1162.

[29] Gurau, V. and Mann, J. A. (2010). Technique for characterization of the wettability properties of gas diffusion media for proton exchange membrane fuel cells. *Journal of colloid and interface science,* volume 350, number 2, p. 577-580.

[30] Hanlon, M. A. and Ma, H. B. (2003). Evaporation heat transfer in sintered porous media. *Journal of Heat Transfer,* volume 125, number 4, p. 644-652.

[31] Holley, B. and Faghri, A. (2006). Permeability and effective pore radius measurements for heat pipe and fuel cell applications. *Applied Thermal Engineering,* volume 26, number 4, p. 448-462.

[32] Hong, K. T., Imadojemu, H. and Webb, R. L. (1994). Effects of oxidation and surface roughness on contact angle. *Experimental Thermal and Fluid Science,* volume 8, number 4, p. 279-285.

[33] Hwang, G. S., Nam, Y., Fleming, E., Dussinger, P., Ju, Y. S. and Kaviany, M. (2010). Multi-artery heat pipe spreader: experiment. *International Journal of Heat and Mass Transfer,* volume 53, number 13-14, p. 2662-9.

[34] Iverson, B. D., Davis, T. W., Garimella, S. V., North, M. T. and Kang, S. S. (2007). Heat and mass transport in heat pipe wick structures. *Journal of Thermophysics and Heat Transfer,* volume 21, number 2, p. 392-404.

[35] Iwamoto, T., Morita, M.andOhmi, T. (1996). Highly-reliable ultra thin gate oxide formation process. In*Technical Digest.* International Electron Devices Meeting. IEEE, New York, NY, USA, p. 751-4.

[36] Jhan-Hong Liou, Chia-Wei Chang, Chao, C. and Shwin-Chung Wong (2010). Visualization and thermal resistance measurement for the sintered mesh-wick evaporator in operating flat-plate heat pipes. *International Journal of Heat and Mass Transfer,* volume 53, number 7-8, p. 1498-506.

[37] Kamenova, L., Avenas, Y., Tzanova, S., Popova, N.andSchaeffer, C. (2006). 2D numerical modeling of the thermal and hydraulic performances of a very thin sintered powder copper flat heat pipe. In *37th IEEE Power Electronics Specialists Conference 2006, PESC'06,* June 18 - 22, Jeju, Korea.

[38] Kandlikar, S. G. and Bapat, A. V. (2007). Evaluation of jet impingement, spray and microchannel chip cooling options for high heat flux removal. *Heat Transfer Engineering,* volume 28, number 11, p. 911-923.

[39] Labajos-Broncano, L., Gonzalez-Martin, M., Bruque, J. M. and Gonzalez-Garcia, C. (2001). Comparison of the use of Washburn's equation in the distance-time and weight-time imbibition techniques. *Journal of colloid and interface science,* volume 233, number 2, p. 356-360.

[40] Lefevre, F. and Lallemand, M. (2006). Coupled thermal and hydrodynamic models of flat micro heat pipes for the cooling of multiple electronic components. *International Journal of Heat and Mass Transfer,* volume 49, number 7-8, p. 1375-83.

[41] Leong, K. C. and Jin, L. W. (2008). Study of highly conductive graphite foams in thermal management applications. *Advanced Engineering Materials,* volume 10, number 4, p. 338-45.

[42] Leong, K. C., Jin, L. W., Li, H. Y.andChai, J. C. (2008). Forced convection air cooling in porous graphite foam for thermal management applications. In *11th IEEE Intersociety*

Conference on Thermal and Thermomechanical Phenomena in Electronic Systems, I-THERM, May 28, 2008 - May 31. Inst. of Elec. and Elec. Eng. Computer Society, Orlando, FL, United states, p. 57-64.

[43] Li, C. and Peterson, G. P. (2006). Evaporation/boiling in thin capillary wicks (II)-effects of volumetric porosity and mesh size. *Transactions of the ASME.Journal of Heat Transfer,* volume 128, number 12, p. 1320-8.

[44] Lips, S., Lefevre, F. and Bonjour, J. (2009). Nucleate boiling in a flat grooved heat pipe. *International Journal of Thermal Sciences,* volume 48, number 7, p. 1273-1278.

[45] Liu, J., Huang, X., Li, Y., Li, Z., Chi, Q. and Li, G. (2008). Formation of hierarchical CuO microcabbages as stable bionic superhydrophobic materials via a room-temperature solution-immersion process. *Solid State Sciences,* volume 10, number 11, p. 1568-76.

[46] Liu, J., Huang, X., Li, Y., Sulieman, K. M., He, X. and Sun, F. (2006). Hierarchical nanostructures of cupric oxide on a copper substrate: controllable morphology and wettability. *Journal of Materials Chemistry,* volume 16, number 45, p. 4427-34.

[47] Lu, M., Mok, L. and Bezama, R. J. (2006). A graphite foams based vapor chamber for chip heat spreading. *Transactions of the ASME.Journal of Electronic Packaging,* volume 128, number 4, p. 427-31.

[48] Metafoam Technologies Inc. (2009). Copper Foam Properties. In http://www.metafoam.com/,(page consulted on 2009/07/12).

[49] Migliaccio, C. P. and Garimella, S. V. (2011). Evaporative heat and mass transfer from the free surface of a liquid wicked into a bed of spheres. *International Journal of Heat and Mass Transfer,* volume 54, number 15-16, p. 3440-3447.

[50] Mochizuki, M., Nguyen, T., Mashiko, K., Saito, Y., Xiao, P. W., Nguyen, T.andWuttijumnong, V. (2009). Thermal management in high performance computers by use of heat pipes and vapor chambers, and the challenges of global warming and

environment. In *4th International Microsystems, Packaging, Assembly and Circuits Technology Conference (IMPACT)*. IEEE, Piscataway, NJ, USA, p. 191-4.

[51] Mohseni, M. and Allen, D. G. (2000). Biofiltration of mixtures of hydrophilic and hydrophobic volatile organic compounds. *Chemical Engineering Science,* volume 55, number 9, p. 1545-1558.

[52] Nam, Y. andJu, Y. S. (2009). Comparative study of copper oxidation schemes and their effects on surface wettability. In *ASME International Mechanical Engineering Congress and Exposition, IMECE 2008, October 31, 2008 - November 6*, volume 10. American Society of Mechanical Engineers, Boston, MA, United states, p. 1833-1838.

[53] Nam, Y., Sharratt, S., Byon, C., Sung, J. K. and Ju, Y. S. (2010). Fabrication and Characterization of the Capillary Performance of Superhydrophilic Cu Micropost Arrays. *Journal of Microelectromechanical Systems,* volume 19, number 3, p. 581-8.

[54] Peterson, G. P. (1994). *An Introduction to Heat Pipes: Modeling, Testing, and Applications*. Wiley-Interscience, United states, 368 p.

[55] Peterson, G. P., Carbajal, G., Sobhan, C. B., Queheillalt, D. T. and Wadley, H. N. G. (2006). Thermal response of a flat heat pipe sandwich structure to a localized heat flux. *International Journal of Heat and Mass Transfer,* volume 49, number 21-22, p. 4070-81.

[56] Phillips, E. C. (1969). *Low-temperature heat pipe research program* (technical report). NASA, United states, 116 p.

[57] Pilon, D. (2009). High Heat Load Capacity Copper Foam Wick structures. In *AMD Technical Forum and Exposition,* Taipei, Taiwan.

[58] Pilon, D. (2009). *Metafoam's foam performance in industrial tests.* Personal communications, Sherbrooke. QC, Canada,

[59] Pilon, D., Labbe, S., Touzin, J., Marsan, B., Panneton, R., Frechette, L.andGros, E. (2008). Characterization of high surface area open-cell metal foams and application to

thermal management and electrochemistry. In*5th International Conference on Porous Metals and Metallic Foams, MetFoam 2007, September 5, 2008 - September 7.* DEStech Publications Inc, Montreal, QC, Canada, p. 501-504.

[60] Popova, N., Schaeffer, C., Avenas, Y.andKapelski, G. (2006). Fabrication and thermal performance of a thin flat heat pipe with innovative sintered copper wick structure. In *2006 IEEE Industry Applications Conference - Forty-First IAS Annual Meeting*, volume 2. Institute of Electrical and Electronics Engineers Inc, Piscataway, NJ 08855-1331, United States, p. 791-796.

[61] Queheillalt, D. T., Carbajal, G., Peterson, G. P. and Wadley, H. N. G. (2008). A multifunctional heat pipe sandwich panel structure. *International Journal of Heat and Mass Transfer,* volume 51, number 1-2, p. 312-326.

[62] Ranjan, R., Murthy, J. Y., Garimella, S. V. and Vadakkan, U. (2011). A numerical model for transport in flat heat pipes considering wick microstructure effects. *International Journal of Heat and Mass Transfer,* volume 54, number 1-3, p. 153-68.

[63] Reinhardt, K. A. (2008). *handbook of silicon wafer cleaning technology.* William Andrew Inc., United States of America, 660 p.

[64] Rogacs, A., Steinbrenner, J. E., Rowlette, J. A., Weisse, J. M., Zheng, X. L. and Goodson, K. E. (2010). Characterization of the wettability of thin nanostructured films in the presence of evaporation. *Journal of colloid and interface science,* volume 349, number 1, p. 354-360.

[65] Saga, K. and Hattori, T. (2005). Analysis of organic contamination adsorbed on a silicon surface in a vacuum chamber in electron beam lithography. *Journal of the Electrochemical Society,* volume 152, number 6, p. 494-9.

[66] Salmeron, M., Bluhm, H., Tatarkhanov, M., Ketteler, G., Shimizu, T. K., Mugarza, A., Deng, X., Herranz, T., Yamamoto, S. and Nilsson, A. (2009). Water growth on metals

and oxides: binding, dissociation and role of hydroxyl groups. *Faraday discussions,* volume 141, p. 221-9.

[67] Schoelkopf, J., Gane, P. A. C., Ridgway, C. J.andMatthews, G. P. (2002). Practical observation of deviation from Lucas-Washburn scaling in porous media. In, volume 206. Elsevier, p. 445-454.

[68] Semenic, T. and Catton, I. (2009). Experimental study of biporous wicks for high heat flux applications. *International Journal of Heat and Mass Transfer,* volume 52, number 21-22, p. 5113-21.

[69] Semenic, T., Lin, Y. Y., Catton, I. and Sarraf, D. B. (2008). Use of biporous wicks to remove high heat fluxes. *Applied Thermal Engineering,* volume 28, number 4, p. 278-83.

[70] Shirazy, M. R. S. andFréchette, L. G. (2010). A parametric investigation of operating limits in heat pipes using novel metal foams as wicks. In *ASME 2010 3rd Joint US-European Fluids Engineering Summer Meeting and 8th International Conference on Nanochannels, Microchannels, and Minichannels FEDSM2010-ICNMM2010.*

[71] Shirazy, M. R. S., Blais, S. and Frechette, L. G. (2012). Mechanism of wettability transition in copper metal foams: from superhydrophilic to hydrophobic. *Applied Surface Science,* volume 258, number 17, p. 6416-24.

[72] Shirazy, M. R. S. and Frechette, L. G. (2013). Capillary and wetting properties of copper metal foams in the presence of evaporation and sintered walls. *International Journal of Heat and Mass Transfer,* volume 58, number 1-2, p. 282-291.

[73] Shwin-Chung Wong and Chung-Wei Chen (2012). Visualization and evaporator resistance measurement for a groove-wicked flat-plate heat pipe. *International Journal of Heat and Mass Transfer,* volume 55, number 9-10, p. 2229-34.

[74] Shwin-Chung Wong, Jhan-Hong LiouandChia-Wei Chang (2009). Evaporation resistance measurement with visualization for sintered copper-powder evaporator in operating flat-

plate heat pipes. In*2009 4th International Microsystems, Packaging, Assembly and Circuits Technology Conference (IMPACT)*. IEEE, Piscataway, NJ, USA, p. 336-9.

[75] Shwin-Chung Wong and Yi-Huan Kao (2008). Visualization and performance measurement of operating mesh-wicked heat pipes. *International Journal of Heat and Mass Transfer,* volume 51, number 17-18, p. 4249-59.

[76] Singh, R., Akbarzadeh, A. and Mochizuki, M. (2009). Effect of wick characteristics on the thermal performance of the miniature loop heat pipe. *Journal of Heat Transfer,* volume 131, number 8, p. 082601 (10 pp.).

[77] Smith, T. (1980). The hydrophilic nature of a clean gold surface. *Journal of colloid and interface science,* volume 75, number 1, p. 51-5.

[78] Sonan, R., Harmand, S., Pelle, J., Leger, D. and Fakes, M. (2008). Transient thermal and hydrodynamic model of flat heat pipe for the cooling of electronics components. *International Journal of Heat and Mass Transfer,* volume 51, number 25-26, p. 6006-6017.

[79] Stephan, P. and Brandt, C. (2004). Advanced Capillary Structures for High Performance Heat Pipes. *Heat Transfer Engineering,* volume 25, number 3, p. 78-85.

[80] Suman, B. and Kumar, P. (2005). An analytical model for fluid flow and heat transfer in a micro-heat pipe of polygonal shape. *International Journal of Heat and Mass Transfer,* volume 48, number 21-22, p. 4498-509.

[81] Taborelli, M. and Scheuerlein, C. (2006). The assessment of metal surface cleanliness by XPS. *Applied Surface Science,* volume 252, number 12, p. 4279-88.

[82] Tang, K., Wang, X., Yan, W., Yu, J. and Xu, R. (2006). Fabrication of superhydrophilic Cu2O and CuO membranes. *Journal of Membrane Science,* volume 286, number 1-2, p. 279-284.

[83] Vasiliev, L. L. (2008). Micro and miniature heat pipes - Electronic component coolers. *Applied Thermal Engineering,* volume 28, number 4, p. 266-273.

[84] Wang, H., Garimella, S. V. and Murthy, J. Y. (2007). Characteristics of an evaporating thin film in a microchannel. *International Journal of Heat and Mass Transfer,* volume 50, number 19-20, p. 3933-3942.

[85] Wang, Y., Luo, Q.andChen, X. (2009). Advanced electronic cooling technologies. In*2009 Asia Pacific Conference on Postgraduate Research in Microelectronics & Electronics (PrimeAsia)*. IEEE, Piscataway, NJ, USA, p. 149-52.

[86] Weibel, J. A., Garimella, S. V. and North, M. T. (2010). Characterization of evaporation and boiling from sintered powder wicks fed by capillary action. *International Journal of Heat and Mass Transfer,* volume 53, number 19-20, p. 4204-4215.

[87] Williams, R. R. and Harris, D. K. (2006). A device and technique to measure the heat transfer limit of a planar heat pipe wick. *Experimental Thermal and Fluid Science,* volume 30, number 3, p. 277-284.

[88] Wong, S. and Lin, Y. (2011). Effect of copper surface wettability on the evaporation performance: Tests in a flat-plate heat pipe with visualization. *International Journal of Heat and Mass Transfer,* volume 54, number 17-18, p. 3921-3926.

[89] Xiao, J., Chu, Y., Zhuo, Y. and Dong, L. (2009). Amphiphilic molecule controlled synthesis of CuO nano/micro-superstructure film with hydrophilicity and superhydrophilicity surface. *Colloids and Surfaces A: Physicochemical and Engineering Aspects,* volume 352, number 1-3, p. 18-23.

[90] Yin, H., Jin, Z., Zhang, S., Wang, S. and Zhang, Z. (2002). Reason for the loss of hydrophilicity of TiO2 film and its photocatalytic regeneration. *Science in China, Series B: Chemistry,* volume 45, number 6, p. 625-632.

[91] Zhang, H. Y., Pinjala, D.andPoi-Siong Teo (2003). Thermal management of high power dissipation electronic packages: from air cooling to liquid cooling. In *Proceedings of the 5th Electronics Packaging Technology Conference (EPTC 2003)*. IEEE, Piscataway, NJ, USA, p. 620-5.

[92] Zhang, H. Y., Pinjala, D., Joshi, Y. K., Wong, T. N., Toh, K. C. and Iyer, M. K. (2005). Fluid flow and heat transfer in liquid cooled foam heat sinks for electronic packages. *IEEE Transactions on Components and Packaging Technologies,* volume 28, number 2, p. 272-280.

[93] Zhao, C. Y., Tassou, S. A. and Lu, T. J. (2008). Analytical considerations of thermal radiation in cellular metal foams with open cells. *International Journal of Heat and Mass Transfer,* volume 51, number 3-4, p. 929-40.

[94] Zhou, D. and Zhao, C. Y. (2011). Experimental investigations on heat transfer in phase change materials (PCMs) embedded in porous materials. *Applied Thermal Engineering,* volume 31, number 5, p. 970-7.

[95] Zorba, V., Persano, L., Pisignano, D., Athanassiou, A., Stratakis, E., Cingolani, R., Tzanetakis, P. and Fotakis, C. (2006). Making silicon hydrophobic: Wettability control by two-lengthscale simultaneous patterning with femtosecond laser irradiation. *Nanotechnology,* volume 17, number 13, p. 3234-3238.